การสังเคราะห์ซีโอไลต์เอกซ์ ซีโอไลต์วายและเอสบีเอ-15 ด้วยไมโครเวฟเพื่อการผลิตไบโอดีเซล

นางสาวพิจาริน รักเมือง

วิทยานิพนธ์นี้เป็นส่วนหนึ่งของการศึกษาตามหลักสูตรปริญญาวิทยาศาสตรมหาบัณฑิต
สาขาวิชาปิโตรเคมีและวิทยาศาสตร์พอลิเมอร์
คณะวิทยาศาสตร์ จุฬาลงกรณ์มหาวิทยาลัย
ปีการศึกษา 2553

SYNTHESIS OF X-ZEOLITE, Y-ZEOLITE AND SBA-15 VIA MICROWAVE FOR BIODIESEL PRODUCTION

Miss Pijarin Rakmuang

A Thesis Submitted in Partial Fulfillment of the Requirements
for the Degree of Master of Science Program in Petrochemistry and Polymer Science
Faculty of Science
Chulalongkorn University
Academic Year 2010

Thesis Title	SYNTHESIS OF X-ZEOLITE, Y-ZEOLITE AND SBA-15 VIA MICROWAVE FOR BIODIESEL PRODUCTION
By	Miss Pijarin Rakmuang
Field of Study	Petrochemistry and Polymer Science
Thesis Advisor	Duangamol Nuntasri, Ph.D.
Thesis Co-advisor	Rewadee Anuwattana, Ph.D.

Accepted by the Faculty of Science, Chulalongkorn University in Partial Fulfillment of the Requirements for the Master's Degree

……..Dean of the Faculty of Science

(Professor Supot Hannongbua, Dr. rer. nat.)

THESIS COMMITTEE

……..Chairman

(Professor Pattarapan Prasassarakich , Ph.D.)

……..Thesis Advisor

(Duangamol Nuntasri, Ph.D.)

……. Thesis Co-advisor

(Rewadee Anuwattana, Ph.D.)

……..Examiner

(Associate Professor Wimonrat Trakarnpruk, Ph.D.)

……..External Examiner

(Gamolwan Tumcharern, Ph.D)

พิจาริน รักเมือง : การสังเคราะห์ซีโอไลต์เอกซ์ ซีโอไลต์วายและเอสบีเอ-15 ด้วยไมโครเวฟเพื่อการผลิตไบโอดีเซล (SYNTHESIS OF X-ZEOLITE, Y-ZEOLITE AND SBA-15 VIA MICROWAVE FOR BIODIESEL PRODUCTION) อ.ที่ปรึกษาวิทยานิพนธ์หลัก: อ. ดร. ดวงกมล นันทศรี, อ.ที่ปรึกษาวิทยานิพนธ์ร่วม: ดร.เรวดี อนุวัฒนา, 146 หน้า

ได้สังเคราะห์ตัวเร่งปฏิกิริยาซีโอไลต์เอกซ์ ซีโอไลต์วาย และเอสบีเอ-15 ด้วยวิธีไมโครเวฟ ได้ศึกษาผลของเวลาที่ใช้ในการสังเคราะห์ 0.5 ถึง 4 ชั่วโมง เพื่อเปรียบเทียบกับการสังเคราะห์ด้วยวิธีทางความร้อน องค์ประกอบของเจลของซีโอไลต์วายเป็น 13.41 SiO_2: 5.41 Na_2O: Al_2O_3: 171 H_2O ในกรณีของซีโอไลต์เอกซ์อัตราส่วนซิลิกาต่ออะลูมินาถูกเปลี่ยนเป็น 1.5 ถึง 2.5 ซึ่งองค์ประกอบอื่นเหมือนกับซีโอไลต์วาย นอกจากนี้องค์ประกอบของเจลของเอสบีเอ-15 เป็น 1.0 TEOS: 0.0165 P123: 6.95 HCl: 140 H_2O จากผลการทดลองรังสีไมโครเวฟสามารถลดระยะเวลาการสังเคราะห์ซึ่งเร็วกว่าการสังเคราะห์ด้วยวิธีทางความร้อน หลังจากนั้นตัวเร่งปฏิกิริยาที่สังเคราะห์ได้สามารถดัดแปรด้วยกรดโดยวิธีการเชื่อมต่อกับหมู่โพรพิลซัลโฟนิก ตัวอย่างรูพรุนกรดถูกตรวจสอบลักษณะเฉพาะด้วยเทคนิคการเลี้ยวเบนของรังสีเอกซ์ การดูดซับแก๊สไนโตรเจน กล้องจุลทรรศน์แบบส่องกราด การวิเคราะห์ปริมาณซัลเฟอร์ และการคายแอมโมเนียด้วยการเพิ่มอุณหภูมิแบบตั้งโปรแกรม ตัวเร่งปฏิกิริยาที่สังเคราะห์ทั้งหมดถูกนำไปประยุกต์กับปฏิกิริยาเอส เทอริฟิเคชันของกรดไขมันอิสระโอเลอิก และปาล์มิติกกับเมทานอล เพื่อผลิตเมทิลเอสเทอร์ของกรดไขมันอิสระ (ไบโอดีเซล) ได้ศึกษาผลของภาวะปฏิกิริยาต่างๆ ได้แก่ ปริมาณของตัวเร่งปฏิกิริยา อัตราส่วนโดยโมลของเมทานอลต่อกรดไขมันอิสระ เวลาและอุณหภูมิ จากผลการทดลองภาวะที่เหมาะสมของเอสบีเอ-15 ที่มีหมู่โพรพิลซัลโฟนิกคืออัตราส่วนโมลของเมทานอลเท่ากับ 12 ปริมาณตัวเร่งปฏิกิริยา 3 เปอร์เซ็นต์โดยน้ำหนัก ที่อุณหภูมิ 60 องศาเซลเซียส เวลา 1 ชั่วโมง ได้ปริผลได้สูงสุดที่ 98.14 เปอร์เซ็นต์ ในทางตรงกันข้ามวัสดุที่มีรูพรุนขนาดเล็กที่เป็นกรดต้องการภาวะที่รุนแรงซึ่งได้ปริมาณเมทิลโอลิเอต 80 เปอร์เซ็นต์และ 76.72 เปอร์เซ็นต์ สำหรับซีโอไลต์วายและซีโอไลต์เอกซ์ที่มีหมู่โพรพิลซัลโฟนิก ตามลำดับ

สาขาวิชา ปิโตรเคมีและวิทยาศาสตร์พอลิเมอร์ ลายมือชื่อนิสิต .....

ปีการศึกษา 2553 ลายมือชื่อ อ.ที่ปรึกษาวิทยานิพนธ์หลัก .....

ลายมือชื่อ อ.ที่ปรึกษาวิทยานิพนธ์ร่วม .....

5172383723: MAJOR PETROCHEMISTRY AND POLYMER SCIENCE
KEYWORDS: X ZEOLITE / Y ZEOLITE / SBA-15 / MICROWAVE/ ESTERIFICATION / BIODIESEL

PIJARIN RAKMUANG: SYNTHESIS OF X-ZEOLITE, Y-ZEOLITE AND SBA-15 VIA MICROWAVE FOR BIODIESEL PRODUCTION. ADVISOR: DUANGAMOL NUNTASRI, Ph.D., CO-ADVISOR: REWADEE ANUWATTANA, Ph.D., 146 pp.

X zeolite, Y zeolite and SBA-15 were synthesized via microwave method. The influence of synthesis time on catalyst formation was varied from 0.5 to 4.0 hrs to compare with hydrothermal method. The gel molar composition of Y zeolite was 13.41 SiO_2: 5.41 Na_2O: Al_2O_3: 171 H_2O. In case of X zeolite Si/Al molar ratio was changed to 1.5-2.5 with constant for other compositions as Y zeolite synthesis. In addition, the gel molar composition of SBA-15 was 1.0 TEOS: 0.0165 P123: 6.95 HCl: 140 H_2O. From the experimental results, the microwave irradiation could reduce synthesis time which was faster than synthesized by hydrothermal method. After that, synthesized materials could be acid-modified by propyl sulfonic grafting. The acidic porous samples were characterized by X-ray powder diffraction, nitrogen sorption analysis, scanning electron microscopy, sulfur elemental analysis and ammonia temperature programmed desorption techniques. All synthesized catalysts were applied in esterification of oleic and palmitic acid with methanol to produce fatty acid methyl ester (biodiesel). The various reaction conditions such as catalyst amount, methanol to free fatty acid mole ratio, reaction time and temperature were studied. From the results, the optimum conditions for SBA-15-SO_3H catalyst were methanol to oleic acid molar ratio of 12, amount of catalyst to reactant weight ratio of 3 wt% at 60°C for 1 hr which gave the maximum methyl oleate yield as 98.14%. On the other hand, acidic microporous materials were required more vigorous condition which gave methyl oleate yield as 80% and 76.72% for the sulfonic functionalized Y and X zeolite, respectively.

Field of Study: Petrochemistry and Polymer Science Student's Signature .....
Academic Year: 2010 Advisor's Signature .....
Co-Advisor's Signature .....

ACKNOWLEDGEMENTS

The accomplishment of this thesis can be attributed to the extensive support and assistance from Dr. Duangamol Nuntasri, her thesis advisor and Dr. Rewadee Anuwattana, her thesis co-advisor. The author would like to sincere gratitude to their for valuable advice and guidance in this research as well as extraordinary experiences throughout the work.

The author would like to give her gratitude to the chairman and the examiners of this thesis committee for all of their comment and useful suggestion about this research.

The author would like to gratefully thank to the financial support Thailand Institute of Scientific and Technology Research under Ministry of Science and Technology. The author would like to gratefully thank Department of Chemistry and Program of Petrochemistry and Polymer Science, Faculty of Science, Chulalongkorn University for the valuable knowledge and experience. Moreover, the author would like to thank Thailand Japan Technology Transfer Project for supporting instruments.

Many thanks go in particular to the members of Materials Chemistry and Catalysis Research Unit and her friends for their sincere help and kindness. Finally, the author would like to express her deepest gratitude to her family for their entirely care and understanding during her graduate study.

CONTENTS

CHAPTER **Page**

CHAPTER **Page**

CHAPTER **Page**

CHAPTER **Page**

LIST OF TABLES

Table **Page**

Table **Page**

LIST OF FIGURES

Figure Page

Figure **Page**

Figure **Page**

Figure **Page**

LIST OF SCHEMES

LIST OF ABBREVIATIONS

Å	Angstrom
a.u.	Arbitrary unit
BET	Brunauer-Emmett-Teller
BJH	Barret, Joyner, and Halenda
^{o}C	Degree Celsius
CMC	critical micelle concentration
MO	Methyl oleate
MP	Methyl palmitate
GC	Gas chromatography
g	Gram (s)
hr	Hour
MPTMS	(3-mercaptopropyl)trimethoxysilane
μm	Micrometer (s)
ml	Milliliter (s)
min	Minute (s)
M	Molarity
nm	Nanometer (s)
%	Percentage
SEM	Scanning electron microscopy
TEOS	Tetraethyl orthosilicate
XRD	X-ray diffraction

CHAPTER I

INTRODUCTION

1.1 Background

World energy consumption is projected to increase by 49 percent per year, from 495 guadrillion Btu in 2007 to 739 guadrillion Btu in 2035.

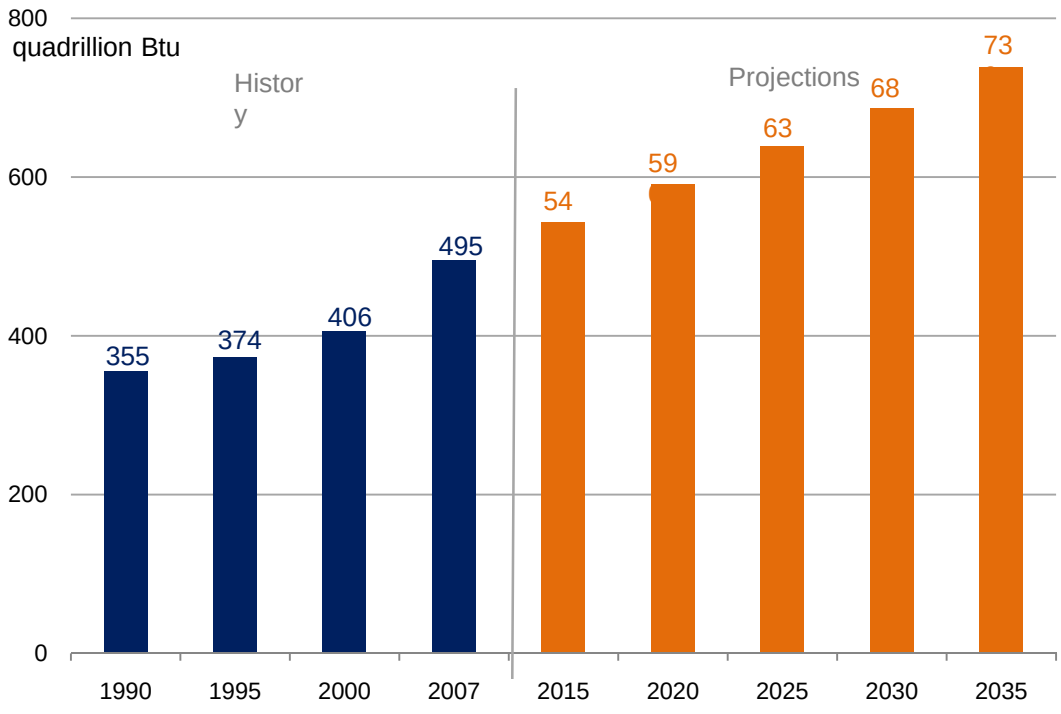

Figure 1.1 World marketed energy consumption, 1990-2035 [1].

Majority of the world energy needs are supplied through petrochemical sources. Coal and natural gases, with in exception of hydroelectricity and nuclear energy, of all, these sources are finite and at current usage rates will be consumed shortly. Diesel fuels have an essential function in the industrial economy of a developing country and are used for transport of industrial and agricultural goods, operation of diesel tractor and pump sets in agricultural sector. Economic growth is

always accompanied by commensurate increase in the transport. The high energy demand in the industrialized world as well as in the domestic sector, the increase in diesel prices and environmental concerns causes the widespread use of fossil fuels. It is increasingly necessary to develop the renewable sources of limitless duration and smaller environmental impact than the traditional one.

Thailand is a country that imports crude oil up 79 percent of all commercial energy. When world oil prices increase the Thailand economy has been affected, which mean the campaign has to produce and use biodiesel fuel, instead To replace the current diesel which can be produced from raw materials in various countries, including vegetable oil and used oil from the food industry. Apart from energy and perspective use of biodiesel which produced from agricultural products, it can encourage in farmer's occupation as well. Moreover, it also reduces environmental problems and global warming phenomenon.

Mostly, biodiesel is prepared by the transesterification and esterification, whereby triglycerides and free fatty acid react with low molecular weight alcohols, typically methanol or ethanol in the presence catalyst to produce a complex mixture of fatty acid alkyl esters (biodiesel). Catalysts used for the esterification of free fatty acid are classified as homogenous catalyst, enzyme [2, 3] or heterogeneous catalyst, but conventional processing mostly involves an alkali catalyzed process. Because base catalyzed process is less corrosive than the homogeneous acid catalyzed one and proceeds at higher rate. The alkali catalysts including sodium hydroxide, sodium methoxide, potassium hydroxide and potassium methoxide, etc. are effective [4]. However, when oil with high amounts of free fatty acid is used, these catalysts are not recommendable due to the formation of soap. Pretreatment processes using strong acid catalysts have been shown to provide good conversion yields and high quality final products. These techniques have even been extended to allow biodiesel production from feedstocks like soapstock that are often considered to be waste. Even though, homogeneous catalyzed biodiesel production processes are relatively fast and show high conversions with minimal side reactions, they are still not very cost competitive with petrodiesel ones because the catalyst cannot be recovered and must be neutralized at the end of the reaction. Moreover, the processes are very sensitive to the presence of water and FFAs (Free Fatty Acids). In this research, focus on

heterogeneous catalysts type Y zeolite, X zeolite and SBA-15 due to the distribution of pore size uniformity, high surface area and high thermal stability. Furthermore, it can be easily separated from product and reusable. In general, these materials have multi-step and long time for preparation. Thus, microwave energy was alternative energy for synthesis of catalyst. Moreover, the synthesized material was increased acidity by grafting sufonic acid group on the catalyst surface to provide more efficiency.

In this study, the modified household microwave oven was used as an energy source to reduce time for synthesis Y zeolite, X zeolite and SBA-15 under various synthetic parameters. The synthesized materials from optimal condition was grafting with sulfonic group for using in esterification of oleic acid with methanol.

1.2 Literature reviews

In 2007, Kim *et al.* [5] have studied the synthesis of zeolite X and found that the optimum conditions is the ratio of silica to alumina from 2.1 to 2.4 and using seed gel to accelerates the synthesis pathway. The synthesized zeolite X has a particle of 50 μm and surface area 542.36 m^2/g.

In 2001, large zeolite Y was synthesized from gels ($4.76Na_2O$: $1.0Al_2O_3$: $xSiO_2$: $454H_2O$: 5TEA, x = 5.25 – 8.75) reported by Albert Sacco *et al.* [6]. Sieving of products grown from gels with x = 8.75 aged for 7 days resulted in nearly pure zeolite Y in the 50–125 mm particle size range.

After that, Zhongmin *et al.* [7] studied the synthesis of zeolite Y by using two steps crystallization at 40^{o}C for 24 hrs and 60^{o}C for 48 hrs, respectively. The result indicated small particle and exhibited no others phase. The results indicated a narrow distribution of particle size, with an average crystal size of 0.4 μm.

Because of longer crystallization time for material synthesis, the microwave energy contributed the decreasing period of catalyst preparation. In addition, this method provided rapid heating to crystallization temperature because of volumetric heating, homogenous heating throughout the reaction vessel, the

possibility of selective heating of desired material, homogeneous nucleation compared to conventional method. In 2008, Komarneni *et al* [8] studied the synthesis of zeolite A from metakaolinite by using both conventional and microwave-assisted heats. The effects of reaction conditions on the rate of formation, crystallinity and actual % yield of zeolite A were investigated. The result exhibited zeolite A pattern over 4 hrs in conventional heating treatment and increase with increasing time, reflecting the nearly complete crystallization after 8 h of treatment with 82% solid yield, while the microwave heating samples showed a complete zeolite A crystal development after only 2 hrs with 80% solid product yield.

In 2009, Xao Lin *et al.* [9] investigated the synthesis of zeolite T which has structure of erionite mixing with offrelite. The crystallization of zeolite T using conventional refluxing heating (CR), conventional hydrothermal heating (CH), microwave refluxing heating (MR) and microwave hydrothermal heating (MH) techniques was investigated. The CR and CH technique obtained pure zeolite T. The MR gave the product in the shorter synthesis time and higher surface area, whereas the MH gave zeolite T with other phase.

In 2007, Borges *et al.* [10] studied the transesterification of used vegetable oil with methanol using zeolite Y as catalyst. They investigated that the Y zeolite catalyst with the Al_2O_3 of 5.6% showed the best catalytic performance in the methyl ester synthesis process which decrease viscosity of the product obtained until values close to biodiesel specification.

In 2007, Xie *et al.* [11] studied the transesterification of soybean oil with methanol to methyl ester by using NaX zolite loaded with KOH as a solid base catalyst. The best result was obtained with NaX zeolite loaded with 10% KOH, 10:1 molar ratio of methanol to soybean oil, temperature of 65^{o}C, reaction time of 8 hrs and a catalyst amount of 3 wt.%, the conversion of soybean oil was 85.6%.

In 2009, Apanee *et al*. [12] prepared methyl ester (biodiesel) from transesterification of palm oil and methanol over KOH/NaY. The optimum condition

was 3 hrs reaction time, 10 wt% KOH/NaY, 60^{o}C and 15:1 methanol to oil molar ratio. At the optimum conditions, a biodiesel yield of 91.07% was obtained.

In part of mesoporous material, Stucky *et al.* [13] synthesized well-ordered hexagonal mesoporous silica structure (SBA-15) which was synthesized in acidic media. SBA-15 exhibited pore size from 50 to 300 angstroms pore volume fractions up to 0.85 and wall thickness of 31 to 64 angstroms. SBA-15 used a variety poly(alkylene oxide) triblock copolymers and addition of co-solvent organic molecules.

In general, the hydrothermal method has longer time for synthesis of SBA-15. Therefore, Jaroniec *et al*. [14] studied the synthesis of SBA-15 compared the hydrothermal method with microwave method. This study showed that microwave method synthesis of SBA-15 several advantages which have larger pore widths suitable for large molecule, shorter crystallization time and better thermal stability than those obtained under conventional condition.

Because the SBA-15 has less acidity. In 2005, Luo *et al*. [15] studied the increasing acidity of SBA-15 by grafting sulfonic acid group on the surface using post-synthesis method. The effects of time and amount of oxidizing agent were investigated. The resultant material showed the highest acidity when oxidized with 30% H_2O_2 for 24 hrs. Moreover, SBA-15-SO_3H exhibited a good long-range order, high specific surface areas (*ca.* 600 m^2/g) and uniform pore sizes (*ca.* 6 nm).

In 2008, Park *et al*. [16] studied the synthesis of SBA-15-SO_3H under hydrothermal method and microwave method. It was found that the catalysts synthesized under microwave offered hexagonal type whereas catalysts synthesized under hydrothermal offered cubic type (Ia3d) as well as hexagonal. The sulfonic acid functionalized SBA-15 catalysts were applied to the liquid-phase reaction of 20-hydroxyacetophenone and benzaldehyde under both microwave and thermal reaction. In the case of synthesized catalyst by microwave method, gave higher conversion of 20-hydroxyacetophenone with higher selectivity to substituted flavanone than thermal reaction owing to the strong absorption of reactant in microwave irradiation.

From the research data, there is a few studies of synthesis X zeolite, Y zeolite and SBA-15 via microwave. Therefore, this research aims to study the catalyst synthesis via microwave which may reduce the synthesis time. Moreover, the difference between microporous and mesoporous materials in catalyst performance is also investigated. In addition, the catalysts are grafting with sulfonic acid to increase their acidity and then use in the esterification of free fatty acid.

1.3 Objective

To investigate the optimum condition for preparation of biodiesel using sulfonic functionalized X Zeolite, Y Zeolite and SBA-15 synthesis by the hydrothermal and microwave techniques.

1.4 Scopes of work

1. Synthesis of X Zeolite, Y Zeolite and SBA-15 by the hydrothermal and microwave methods.
2. Functionalized synthesis catalysts with sulfonic group.
3. Characterization all prepared catalysts.
4. Determination the optimum condition of biodiesel production by studying the effect of reaction time, mole ratio of methanol to oleic acid, the weight ratio to catalyst and reaction temperature.

CHAPTER II

THEORY

2.1 Catalysts

A catalyst is a substance that increased the rate of a chemical reaction by reducing the activation energy (E_a) as shown in Figure 2.1. The highest peak position performing the highest energy refers to the transition state. In typically reaction, the energy required to enter the transition state is high, whereas the energy to transition state decreases in catalytic reaction. In addition, the catalyst may participate in multiple chemical transformations and is not consumed by the reaction.

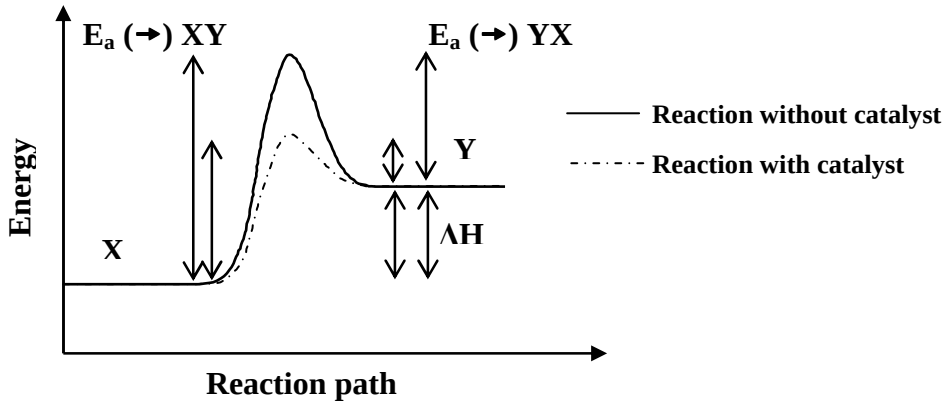

Figure 2.1 The relationship between activation energy (E_a) and enthalpy (ΔH) of the reaction with and without a catalyst [17].

2.2 Properties of industrial catalysts

In general, the suitable catalysts for industrial processes are considered mainly on the three properties [18]:

a) Activity is a measure of how fast one or more reactions proceed which can be defined in terms of kinetics. A high activity catalyst will be given high productivity

when the less amount of the catalyst is utilized or the reaction is performed in mild operating condition, particularly temperature, which enhances selectivity and stability if the thermodynamic is more favorable. It is appropriate to measure reaction rates in the temperature that will be occurred in the reactor.

b) Selectivity of a reaction is the fraction of the starting material that is converted to the expected product. High selectivity catalyst produces high yield of a desired product, whereas undesirable competitive and consecutive reactions are suppressed. This means that the texture of the catalyst (in particular pore size and pore volume) should be improved toward reducing limitation by internal diffusion, which in case of consecutive reactions rapidly reduces selectivity.

c) Stability of a catalyst determines its lifetime in industrial processes. Catalyst stability is influenced by various factors such as decomposition, coking and poisoning. Catalyst deactivation can be followed by measuring activity or selectivity as a function of time. Deactivated catalysts can often be regenerated before they ultimately have to be replaced. The catalyst lifetime is a crucial importance for the economics of process.

Nowadays, the efficient use of raw materials and energy is of major importance, and it is preferable to optimize existing processes than to develop new ones. For various reasons, the target quantities should be given the following order of priority:

Selectivity > Stability > Activity

2.3 Type of the catalysts

Catalysts can be classified into two main types by the boundary of the catalyst and the reactant. Heterogeneous reaction, the catalyst is in a different phase from the reactants, whereas the catalyst in the same phase of reactant is called homogeneous reaction. Thus, the solid catalysts are identified as heterogeneous catalysts, and the liquid catalysts are specified as homogeneous catalysts when assume reactant is liquid.

Homogeneous catalysts have a higher degree of dispersion than heterogeneous catalysts only the surface atoms are active [18]. Summary of the advantage and disadvantage of two-type catalyst is presented in Table 2.1.

Table 2.1 Comparison of homogeneous and heterogeneous catalysts

Consideration	**Homogeneous catalyst**	**Heterogeneous catalyst**
1. Active centers	All metal atoms	Only surface atoms
2. Concentration	Low	High
3. Selectivity	High	Low
4. Diffusion problems	Practically absent	Present (mass-transfer-controlled reaction)
5. Reaction conditions	Mild (50-200°C)	Severe (often >250°C)
6. Applicability	Limited	Wide
7. Activity loss	Irreversible reaction with product (cluster formation), poisoning	Sintering of the metal crystallites, poisoning
8. Structure/ Stoichiometry	Defined	Undefined
9. Modification possibility	High	Low
10. Thermal stability	Low	High
11. Catalyst separation	Sometimes laborious (chemical decomposition, distillation, extraction)	Fixed-bed: unnecessary Suspension: filtration
12. Catalyst recycling	Possible	Unnecessary (fixed-bed) or easy (suspension)
13. Cost of catalyst losses	High	Low

The major disadvantage of homogeneous catalyst is the difficulty of separating the catalyst from the product. Heterogeneous catalysts are either automatically removed in the process (*e.g.* vapor-phase reaction in fixed bed reactor) or separated by simple methods such as filtration or centrifugation. However, in more complicated

processes, distillation, liquid-liquid extraction and ion exchange are necessarily used homogeneous catalysts.

2.4 Porous molecular sieves

Molecular sieves are porous materials that exhibit selective adsorption properties which can be classified on the IUPAC definitions into three main types depending on their pore sizes that are microporous materials, mesoporous materials, and macroporous materials. Properties and examples of these materials are shown in Table 2.2.

Table 2.2 IUPAC classification of porous materials

Type of porous molecular sieve	Pore size (Å)	Examples
Microporous materials	< 20	Zeolites, Activated carbon
Mesoporous materials	20 – 500	M41s, SBA-15, Pillared clays
Macroporous materials	> 500	Glasses

2.4.1 Zeolites

Zeolites are crystalline aluminosilicates that contain uniform pores and cavities with molecular dimentions. The structures of zeolites consist of an extensive three-dimensional network of SiO_4 and AlO_4 tetrahedral. The tetrahedral are cross-linked by the sharing of oxygen atoms as shown in Figure 2.2

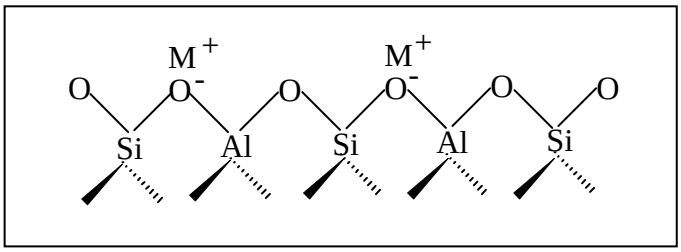

Figure 2.2 The structure of zeolites [19].

The AlO_2^- tetrahedral in the structure determines the framework charge. This is balanced by cations that occupy nonframework positions. The structure formula of a zeolite is best expressed for the crystallographic unit cell as:

$$M_{x/n}\,[(AlO_2)_x\,(SiO_2)_y].\ w\ H_2O$$

Where M is the cation of valence n, generally from the group I or II ions, although other metals, nonmetals, and organic cations are also possible, w is the number of water molecules. Water molecules presented are located in the channels and cavities, as the cations that neutralize the negative charge created by the presence of the AlO_2^- tetrahedral unit in the structure.

2.4.1.1 Zeolite structures

The structure of zeolite consisted of a three-dimension framework of the tetrahedral primary building units when tetrahedral atoms are silicon or aluminum as shown in Figure 2.3.

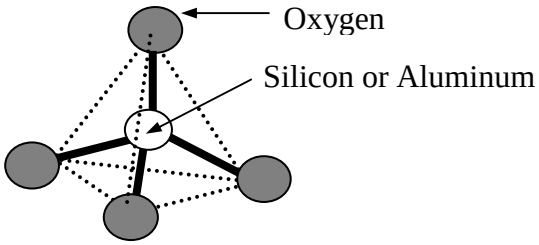

Figure 2.3 A primary building unit of zeolites [19].

Zeolites have a common subunit of structure so called primary building units of $(Al,Si)O_4$ tetrahedral, therein the Si or Al distribution is neglected. A secondary building unit (SBU) consists of selected geometric groupings of those tetrahedral. There are sixteen such building units, which can be used to describe all of the known zeolite structures; for example, 4, 5, 6 and 8-membered single rings, 4-4, 6-6, and 8-8-member double rings, and 4-1,5-1 and 4-4-1 branched rings. The secondary building units (SBU) are shown in Figure 2.3. Most zeolite framework can be generated from different SBU.

A secondary building unit (SBU) consists of selected geometric groupings of those tetrahedral. There are sixteen such building units, which can be used to describe all of the known porous materials structures; for example, 4, 5, 6 and 8-member single rings, 4-4, 6-6, and 8-8-member double rings, and 4-1, 5-1 and 4-4-1 branched rings. The secondary building units (SBU) are illustrated in Figure 2.4.

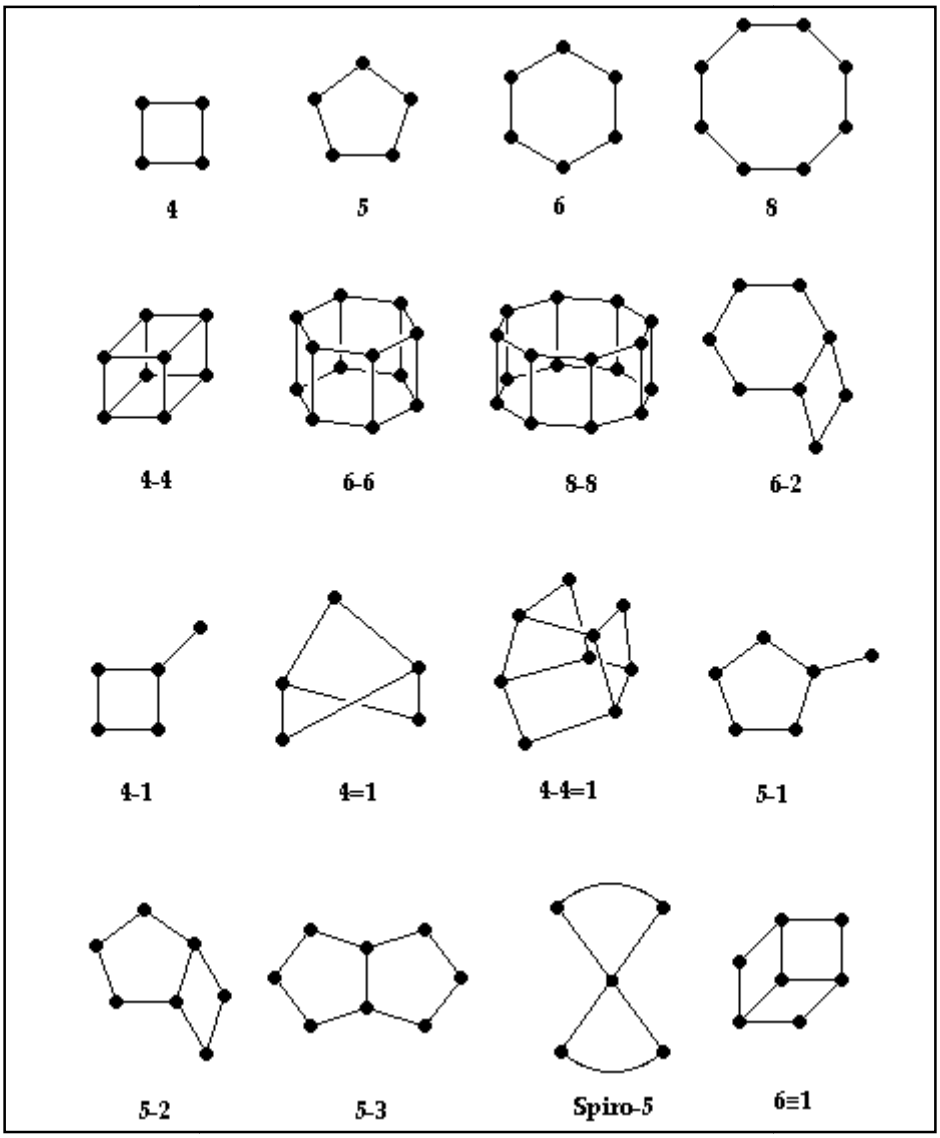

Figure 2.4 Secondary building units (SBUs) in zeolites [20].

Most zeolite frameworks can be generated from several different SBUs. For example, the sodalite framework can be build from either the single 6-member ring or the single 4-member ring. Some of them are shown in Figure 2.5

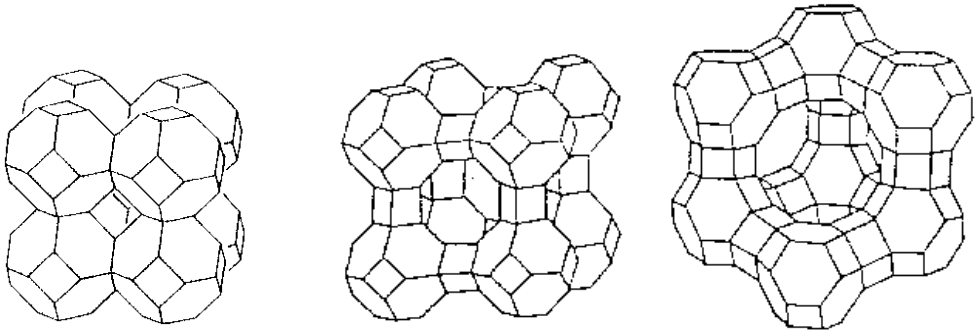

zeolite A faujasite

Figure 2.5 The structure of sodalite, zeolite A and faujasite-type zeolites.

The different ring sizes found in zeolites, based on the different number of tetrahedral atoms defining the opening, are shown in Figure 2.6. The ring sizes are often mentioned as the number of oxygen atoms which are equal to the number of tetrahedral atoms.

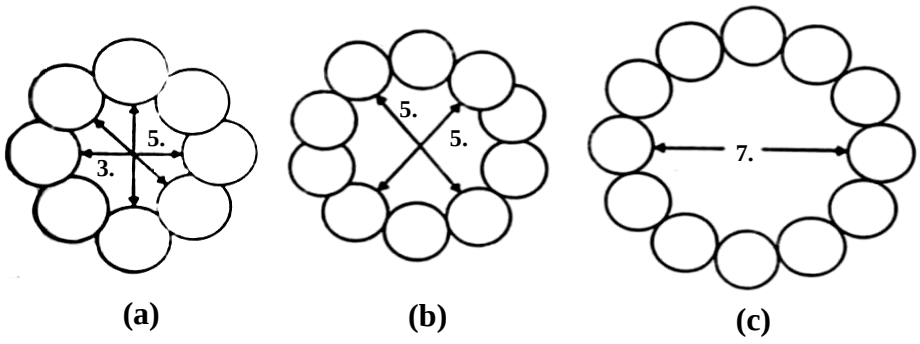

Figure 2.6 Examples of the three types of pore openings in the porous material molecular sieves (a) an 8 ring pore opening (small pore), (b) a 10 ring pore opening (medium pore) and (c) a 12 ring pore opening (large pore) [19].

2.4.1.2 Shape and size selectivity of porous materials

Shape and size selectivity presents a very important role in catalysis. Highly crystalline and regular channel structures are among the principal features that porous material used as catalysts offer over other materials. Shape selectivity is divided into 3 types: reactant shape selectivity, product shape selectivity and transition-state shape selectivity. These types of selectivity are shown in Figure 2.7. Reactant shape selectivity results from the limited diffusivity of some reactants, which cannot effectively enter and diffuse inside the porous materials. Product shape selectivity occurs when diffusing product molecules cannot rapidly escape from the crystal, and undergo secondary reactions. Restricted transition-state shape selectivity is a kinetic effect arising from the local environment around the active site: the rate steady for a certain reaction mechanism is reduced if the necessary transition state is too bulky to form readily.

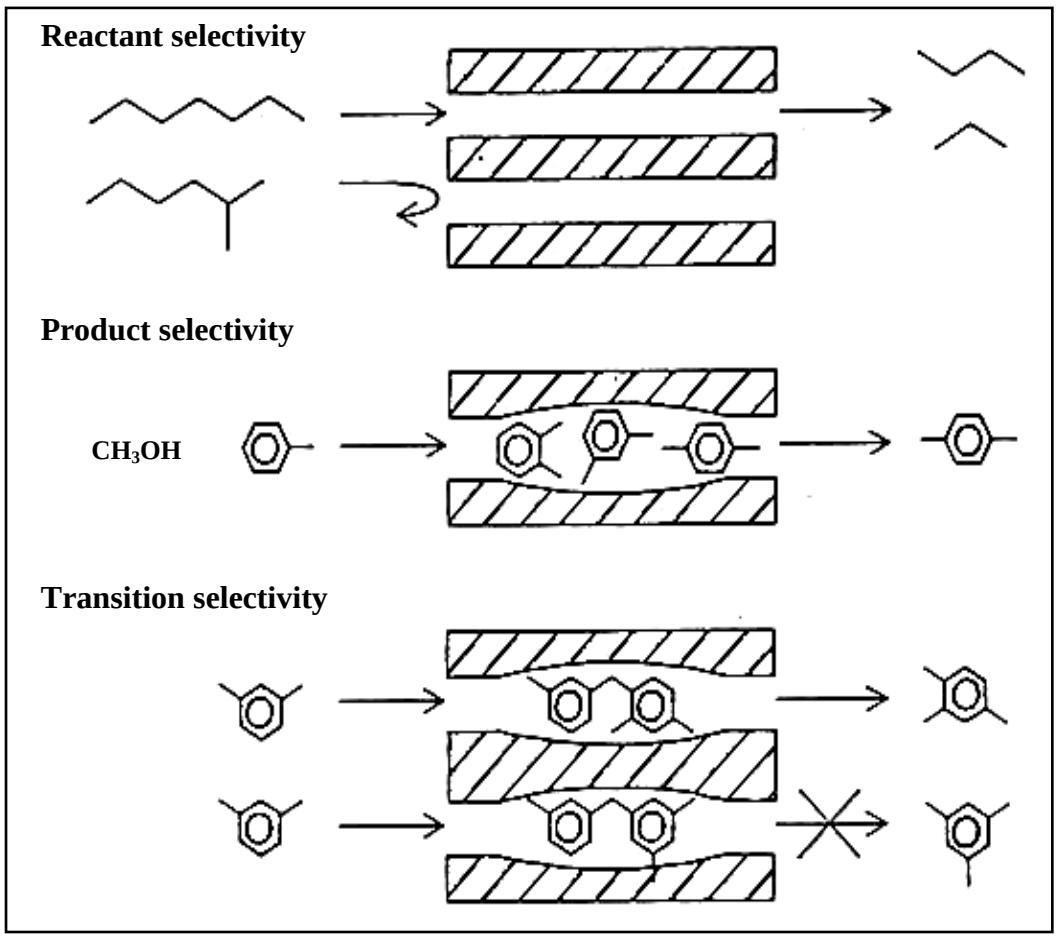

Figure 2.7 Three types of selectivity in porous materials: reactant, product and transition-state shape selectivity [21].

2.4.1.3 Acid sites of zeolites

In addition to the shape and size selective catalysis, the generation of acidic sites in the zeolite pores leads to a high efficiency in solid-acidic catalysis. The isomorphous replacement of silicon atom with aluminum atom in a tetrahedral site gives rise to a charge imbalance because aluminum atom has lower coordination ability than silicon atom and must be neutralized. This is achieved in two ways in natural zeolites:

- The length of Al-O bond becomes slightly longer.
- A coordination site is made profit for cation to counter the excess negative charge.

In natural zeolites, the excess negative charge is balanced by various cations are present in the neighboring environment *e.g.* K^+, Na^+, Mg^{2+} and Ca^{2+} as exhibited in Figure 2.8 and Figure 2.9. The type of counter ion used to balance the charge plays an important part in the use of the zeolite. For uncomplicated understanding, the cation is replaced with a proton by hydrothermal treatment to form a hydroxyl group at the sharing oxygen atom. The acid site formed behaves as a classic Brønsted, proton donating acidic site as shown in Figure 2.10.

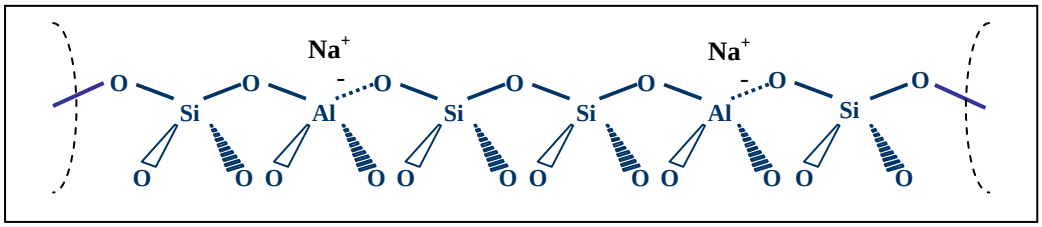

Figure 2.8 Sodium balanced zeolite framework [22].

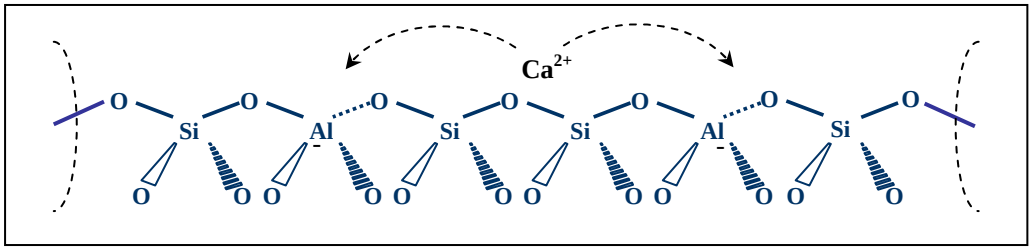

Figure 2.9 Calcium balanced zeolite framework [22].

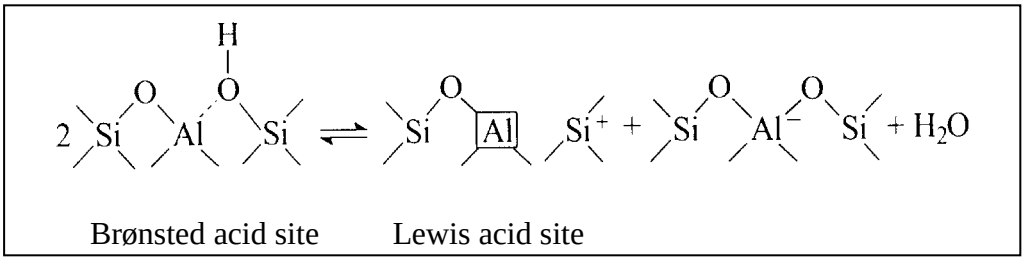

Figure 2.10 Brønsted and Lewis acid sites in zeolites [18].

The highly acidic sites combined with the high selectivity arising from shape selectivity and large internal surface area makes the zeolite as an ideal industrial catalyst. The significance of this acidic proton can be shown easily by comparisons of the experiments in H^+-exchanged zeolites and their equivalent cations from zeolite. For example, the methanol-to-gasoline (MTG) process is highly depended on the presence of the Brønsted proton. If the H-ZSM-5 catalyst is replaced by the purely siliceous analogue of ZSM-5, it has no Brønsted protons; the reaction does not take place at all. Therefore, the modification of zeolite structure could be increased their activity, which are very economically important step for industry.

2.4.2 Faujasite (X and Y Zeolites)

In faujasite structure, the diameter of supercage is 12.5 Å while the diameters of the sodalite cage and the double 6-ring are 6.6 and 2.6 Å, respectively. Each supercage contains four windows of 12-membered Al or Si rings with a diameter of 7.4 Å. X and Y Zeolite have similar structure but difference Si/Al ratio. The Si/Al ratio varies from 1 to 1.5 for X zeolite and from greater than 1.5 to 3 for Y zeolite.

The cation sites of fuajasite are illustrated in Figure 2.11. Type I sites are located at the centers of the hexagonal prisms, type I' sites are located in the sodalite cages across the hexagonal faces from type I sites, type II sites are located in the supercages near the unjoined hexanol faces, and type II' sites are located in the sodalite across the type II sites. Type III sites are located in the supercage, further from the hexagonal faces than the type II site [23].

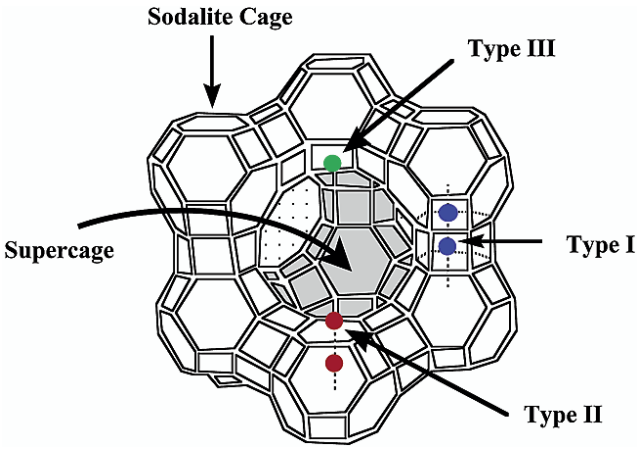

Figure 2.11 Location of cation in faujasite.

2.4.3 Process of zeolite formation

In a four component system Na_2O-Al_2O_3-SiO_2-H_2O, zeolite is commonly crystallized from a molecularly in homogeneous system referred to as a gel. The gel is defined as a hydrous metal aluminosilicate which is formed by a process of copolymerization of the silicate and aluminate ions in a basic environment. The gel preparation and crystallization is represented in Scheme 2.1

$$NaOH_{(aq)} + NaAl(OH)_{4(aq)} + Na_2SiO_{3(aq)}$$

$$\downarrow \quad T_1 \approx 25^{\circ}C$$

$$[Na_a(AlO_2)_b(SiO_2)_c].NaOH.H_2O] \text{ gel}$$

$$\downarrow \quad T_2 \approx 25 \text{ to } 175^{\circ}C$$

$$Na_x[AlO_2)_x.(SiO_2)_y].mH_2O + \text{solution}$$

$$\downarrow$$

Zeolite crystals

Scheme 2.1 Gel preparation and crystallization in the $Na_2O.Al_2O_3.SiO_2.H_2O$ system.

The gel materials dissolve continuously and are transported to the nuclei crystals in the liquid phase. A schematic representation of the crystallization of an aluminosilicate gel to a zeolite is given in Figure 2.12. The gel structure, represented hereby in two dimensions, is depolymerized by the hydroxyl ions which produce soluble aluminosilicate species that may regroup to from the nuclei of the ordered zeolite structure. In this version the hydrate cation acts as a template. The size and charge of the hydrate cation species which serve as a nucleation site for the polyhedral structural unit.

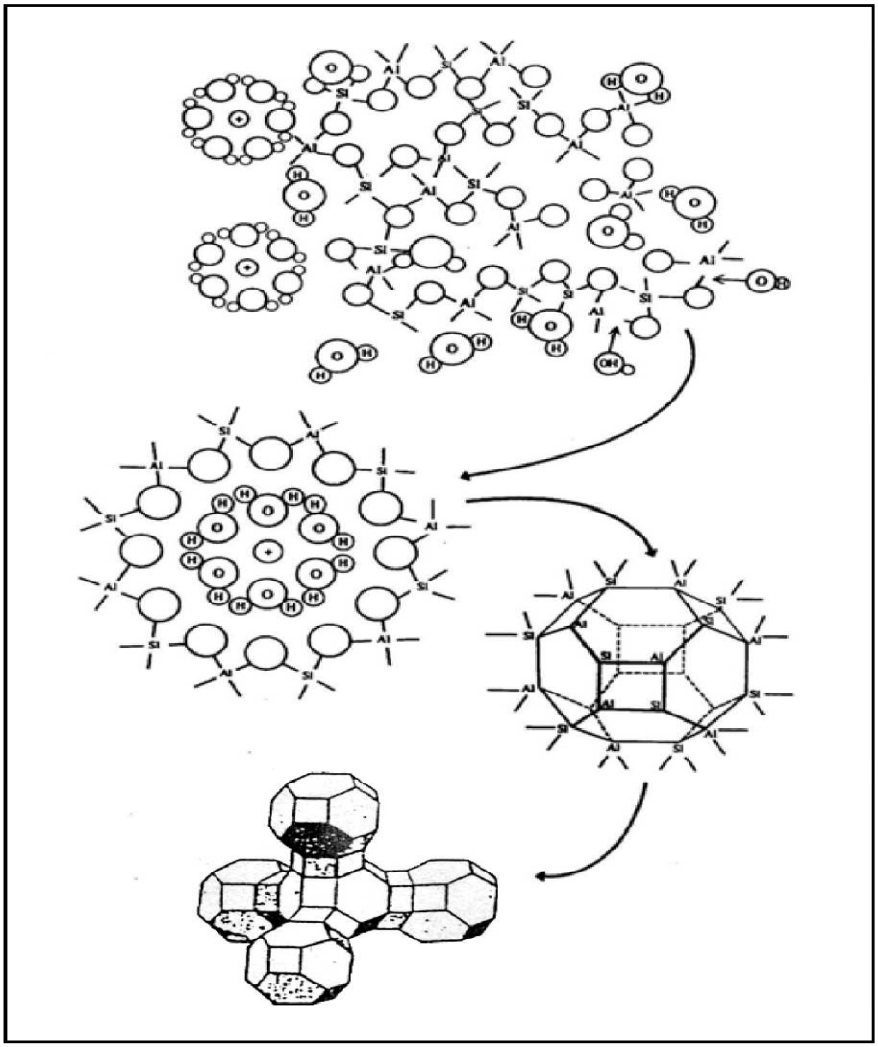

Figure 2.12 Representation of the formation of zeolite crystals in a hydrous gel.

2.4.4 Factors influence zeolite formation

Three variables have a major influence on crystallized zeolite structures [24-26]: the gross composition of the reaction mixture, temperature, and time. There are also history-dependent factors such as digestion or aging period, and order of mixing. A list of individual factors contributing to the synthesis of zeolite structure is provided below:

(a) Gross composition

1. SiO_2/Al_2O_3
2. $[OH^-]$
3. Cations (Inorganic, Organic)
4. Anions (other than $[OH^-]$)
5. H_2O content

(b) Time

(c) Temperature

(d) History-dependent factors

1. Aging
2. Stirring
3. Nature of mixture
4. Order of mixing

2.4.4.1 Reaction mixture components

Each component in the reactant mixture contributes to specific characteristic of the gel and to the final material obtained [26-27]. Table 2.3 provides

a broad listing of individual components of the mixture and the primary influence within that reaction mixture.

Table 2.3 The effect of selected variables on the final crystalline products of zeolite crystallization.

Reaction mixture composition (mole ratio)	**Primary influence**
SiO_2/Al_2O_3	Framework composition
H_2O/SiO_2	Rate, crystallization mechanism
OH^-/SiO_2	silicate molecular weight, OH^- concentration
Inorganic cation(s)/SiO_2	Structure, cation distribution
Organic additives/SiO_2	Structure , framework aluminum content

The SiO_2/Al_2O_3 ratio, the hydroxide content of the gel, and the presence of inorganic cations will also contribute to determine which structure will finally crystallize. The crystallization of a particular zeolite structure from the gel system containing these components strongly depends on the SiO_2/Al_2O_3 ratio of the starting gel mixture. The inorganic or organic cations not only influence the crystal structure, but they may also influence other features of the final crystalline products, such as morphology and crystal size. The hydroxide content enhances the formation of soluble silicate but too much hydroxide concentration catalyzes the formation of dense material such as quartz. The latter inhibits zeolite formation.

2.4.4.2 Temperature

Temperature influences several factors in zeolite synthesis; it can alter the obtained zeolite phase and can change the induction period before the start of crystallization [26-28]. This induction period decreased with increasing temperature. Also, for any mixture as the increasing temperature, the rate of crystallization increased. However, as the temperature change, conditions may favor formation of other phase.

2.4.4.3 Time

Time, as a parameter, can be optimized in the synthesis of many zeolites [26-29]. Many of interesting zeolites are metastable phase, and can recrystallize to other more stable structures which can be observed under certain conditions with prolonged reaction time. Crystallization parameters must be adjusted to minimizing the time needed to obtain the desired crystalline phase.

2.5 Mesoporous materials

Mesoporous materials are a type of molecular sieves, such as silicas or transitional aluminas or modified layered materials such as pillared clays and silicates. Mesoporous silica has uniform pore sizes from 20 to 500 Å and has found great utility as catalysts and sorption media because of the regular arrays of uniform channels. Larger surface area is desired for enhancing of the efficient in the reactions [30].

2.5.1 Classification of mesoporous materials

Mesoporous materials can be classified by different synthetic methods. By varying different types of templates used and pH of gel, synthesizing hexagonal mesoporous materials can be obtained. The interaction of various types of template with inorganic species for assembling these materials are different as summarized in Table 2.4, together with the condition typically employed for a synthesis [30-32].

Table 2.4 Various synthesis conditions of hexagonal mesoporous materials and the types of interaction between templates and inorganic species

Materials	Template	Assembly	Solution
MCM-41	Quaternary ammonium salt	Electrostatic	base or acid
FSM-16	Quaternary ammonium salt	Electrostatic	base
SBA-15	Amphiphilic triblock copolymer	H- bonding	acid (pH<2)
HMS	Primary amine	H- bonding	neutral

MCM-41 and FSM-16 can be synthesized using quaternary ammonium salt as a template. In case of SBA-15, amphiphilic tribock copolymer can be modified as a template and must be synthesized in acidic condition of hydrochloric acid. On the other hand, HMS can be prepared in neutral and environmentally benign condition using primary amine as a template. Although these materials have the same hexagonal structure, some properties are different as shown in Table 2.5.

Table 2.5 Properties of some hexagonal mesoporous materials

Material	Pore size (Å)	Wall thickness (nm)	BET specific surface area (m^2/g)	Framework structure
MCM-41	15-100	1	>1000	Honey comb
FSM-16	15-32	-	680-1000	Folded sheet
SBA-15	46-300	3-6	630-1000	Rope-like
HMS	29-41	1-2	640-1000	Wormhole

2.5.2 Synthesis schemes of mesoporous materials

Crystalline molecular sieves are generally obtained by hydrothermal crystallization. The reaction gel, usually, contains cations (*e.g.* Si^{4+} for silicate materials, Al^{3+} for aluminate materials) to form the framework; anionic species (*e.g.* OH^- and F^-); organic template and solvent (generally water). Typically, the nature of template can be considered into two parts that are hydrophobic tail on the alkyl chain side and hydrophilic head on the other side. The examples of templates used are primary, secondary tertiary and quaternary amines, alcohols, crown or linear ethers, and as well as polymers. An understanding of how organic molecules interact with each other and with the inorganic frameworks would increase the ability to design rational routes to molecular sieve materials. The organic templates are frequently occluded in the pores of the synthesized material, contributing to the stability of mineral backbone.

2.5.2.1 The behavior of surfactant molecules in an aqueous solution

In a simple binary system of water-surfactant, surfactant molecules can aggregate to form micelles in various types at a particular concentration. The shapes of micelle depend on the concentrations as shown in Figure 2.13.

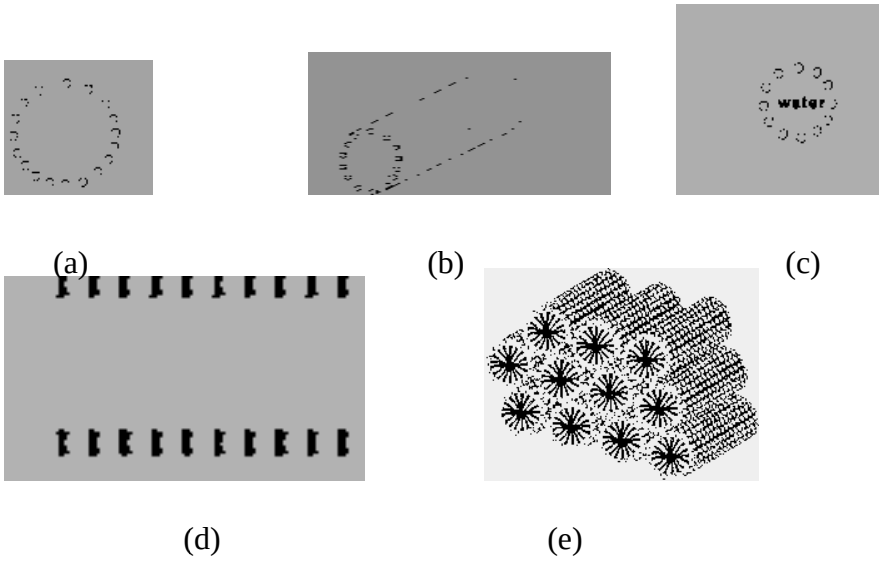

Figure 2.13 Phase sequence of the surfactant-water binary system (a) spherical micelle, (b) rod-shaped micelle, (c) reverse micelle, (d) lamellar phase, and (e) hexagonal phase [33].

At low concentration, they energetically exist as isolated molecules. With increasing concentration, surfactant molecules aggregate together to form isotropic spherical and rod shaped micelles by directing the hydrophobic tails inside and turning the hydrophilic heads outside in order to decrease the system entropy. The initial concentration threshold at which those molecules aggregate to form isotropic micelle is called critical micelle concentration (CMC). The CMC determines thermodynamic stability of the micelles. When the concentration is continuously increased, the micellar shape changes from sphere or rod shapes to hexagonal, lamellar, and inverse micelles. The particular phase present in a surfactant aqueous solution depends not only on the concentrations but also on the natural of surfactant

molecules such as its length of the hydrophobic carbon chain, hydrophilic head group, and counter ion. Besides the ionic strength, pH value, and temperature including other additives are the factors determining the shape of micelles.

2.5.2.2 Interaction between inorganic species and surfactant micelles

A number of models have been proposed to explain the formation of mesoporous materials and to provide a rational basis for synthesis routes [33]. On the common level, these models are predicted upon the presence of surfactants in a solution to direct the formation of inorganic mesostructure from stabilized inorganic precursors. The type of interaction between the surfactant and the inorganic species is significantly different depending on the various synthesis routes as shown in Table 2.6.

Table 2.6 Example routes for interactions between the surfactant and the inorganic soluble species

Surfactant type	Inorganic type	Interaction type	Example materials
Cationic (S^+)	I^-	S^+I^-	MCM-41, MCM-48
	I^+X^-	$S^+X^-I^+$	SBA-1, SBA-2, zinc phosphate
	I^0F^-	$S^+F^-I^0$	silica
Anionic (S^-)	I^+	S^-I^+	Al, Mg, Mn, Ga
	I^-M^+	$S^-M^+ I^-$	alumina, zinc oxide
Neutral S^0 or N^0	I^0	S^0I^0 or N^0I^0	HMS, MSU-X, aluminum oxide
	I^+X^-	$S^0X^-I^+$	SBA-15

Where S^x or N^x : surfactant with charge of X

I^x : inorganic species with charge of X

X^- : halogenide anions

F^- : fluoride anion

M^{n+} : with charge of X

Using ionic surfactant (S^+ and S^-), the hydrophilic head mainly binds with inorganic species through electrostatic interactions. There are two possible formation routes. Firstly, direct pathway: surfactant and inorganic species of which charges are opposite interact together directly (S^+I^- and S^-I^+). Another is the indirect pathway, occurring when the charges of surfactant and inorganic species are the same, so the counter ions in solution get involved as charge compensating species for example the $S^+X^-I^+$ path takes place under acidic conditions, in the present of halogenide anions (X^- = Cl^- or Br^-) and the S^-M^+ I^- route is the characteristic of basic media, in the existence of alkaline cation (M^+ = Na^+ or K^+). Figure 2.14 shows the possible hybrid inorganic-organic interfaces.

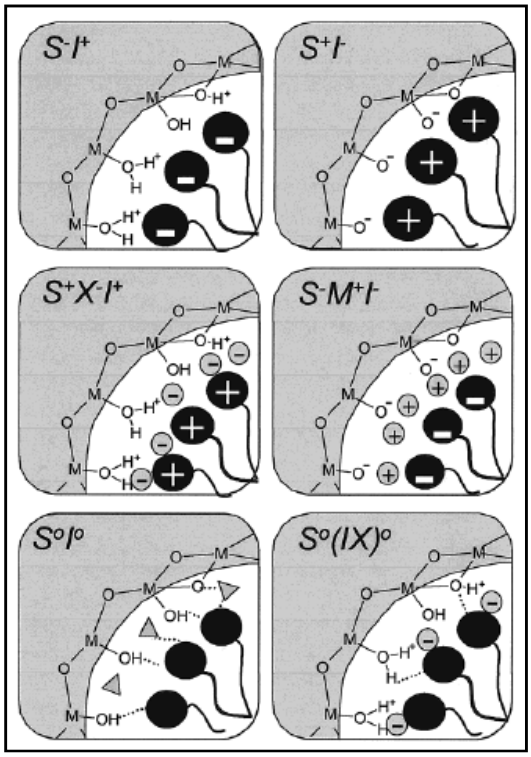

Figure 2.14 Schematic representation of the different types of silica-surfactant interfaces. Dashed line corresponded to H-bonding interactions [33].

In case of non-ionic surfactant (S^0 or N^0), the main interaction between template and inorganic species is hydrogen bonding or dipolar, which is called neutral path i.e. S^0I^0 and $S^0F^-I^+$. Nowadays, non-ionic surfactants give important commercial

advantages in comparison to ionic surfactants because they are easily removable, nontoxic, biodegradable and relatively cheap.

2.5.2.3 Formation mechanism of mesoporous materials

(a) Liquid crystal templating mechanism

A liquid crystal templating (LCT) mechanism was proposed by the Mobil researchers that firstly reported for M41S material. The variation of surfactant concentration plays a significant role to control the structure. Figure 2.15 shows two possible way of the LCT mechanism for hexagonal MCM-41.

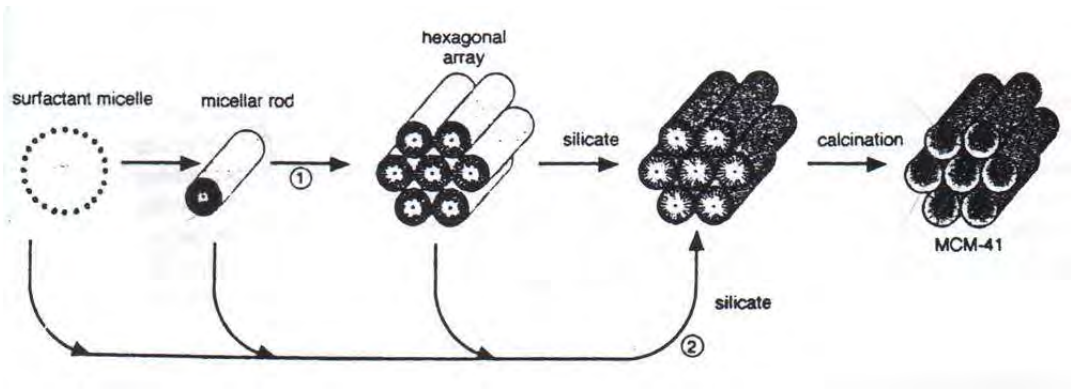

Figure 2.15 Two possible ways for the LCT mechanism [33].

There are two main pathways, in which either the liquid-crystal phase was intact before the silicate species were added (pathway 1), or the addition of the silicate results in the ordering of the subsequent silicate-encased surfactant micelles (pathway 2).

(b) Folding sheet formation

The intercalation of ammonium surfactant into hydrated sodium silicate, which composed of singled-layered silica sheet called kanemite, produces the lamellar-to-hexagonal phase in FSM-16. After surfactants were ion-exchanged into the layered structure, the silicate sheets were folded around the surfactants and condensed into hexagonal mesostructure. The final product was claimed to be very

similar to MCM-41. However, Vartuli *et al*. found that the layered structures were still retained in the kanemite-derived mesoporous materials [34]. Folding sheet formation is illustrated in Figure 2.16.

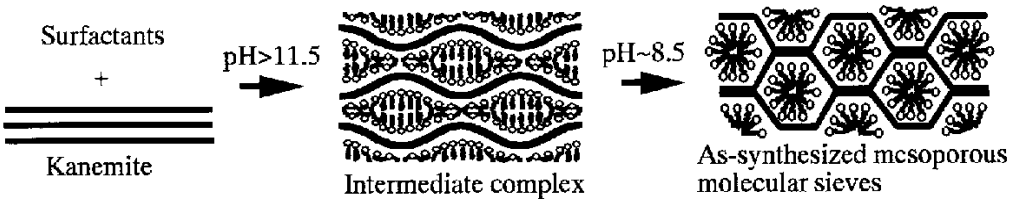

Figure 2.16 Schematic models representing "folding sheets" mechanism [33].

(c) Hydrogen bonding interaction

Tanev *et al.* [35] showed that mesoporous silica could be prepared by the hydrogen-bonding interaction of alkylamine (S°) head group and hydroxylated tetraethyl orthosilicate (I^{o}) as shown in Figure 2.17. The materials lacked long-range order of pore, but had higher amounts of interparticle of mesoporosity, because the long-range effects of the electrostatic interaction that would normally control the packering of micellar rods were absent. This neutral templating synthesis route produced mesoporous silicates with thicker walls and higher thermal stability compared to the LCT-derived silicates. The silicate framework in the resulting mesophase was neutrally charged. From this reason, the surfactant can be easily removed by solvent extraction.

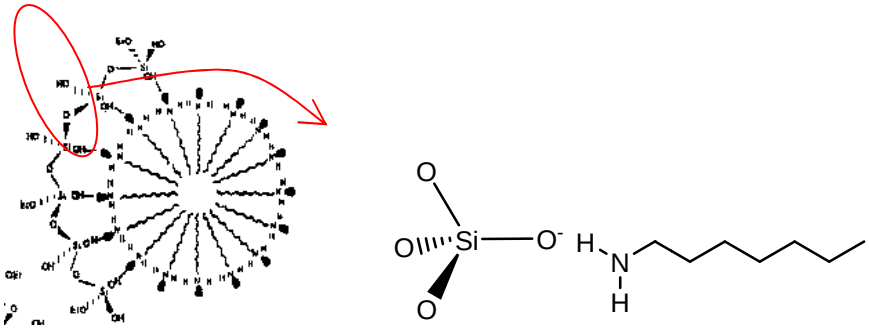

Figure 2.17 Schematic representation of the S^{o} I^{o} templating mechanism of formation of HMS [34].

2.5.3 Synthesis strategy of mesoporous material using block-copolymer as structure directing agent

In the synthesis of mesoporous materials such as MCM-41, FSM-16 ionic surfactant *i.e.* the cationic, alkyltrimethyl ammonium (C_nTA^+, $8<n<18$), and anionic surfactant, tertiary amine ($C_nH_{2n+1}N^+(CH_3)_3$) are used as template, respectively. These syntheses are done in extreme (alkaline) pH condition and the obtained materials have pore size in the range of 15 to 100 Å only. However, by this mean, two limitations occur:

(1) The lower stability of the obtained materials: due to the thinner pore wall of materials (8-13 Å).

(2) Difficult to expanding the pore size: the ionic surfactants give a limited pore size. The only way to expand the pore size is in employing swelling agents such as 1,3,5-trimethyl benzene, involving complicate synthesis.

Thus, the block copolymer has been used to solve these problems. Generally, amphiphilic block copolymer has been used in the field of surfactants, detergent manufacturing, emulsifying, coating, etc. The properties of block copolymer can be continuously tuned by adjusting solvent composition, molecular weight, or type of polymers. Figure 2.18 shows typical block copolymer used as templates.

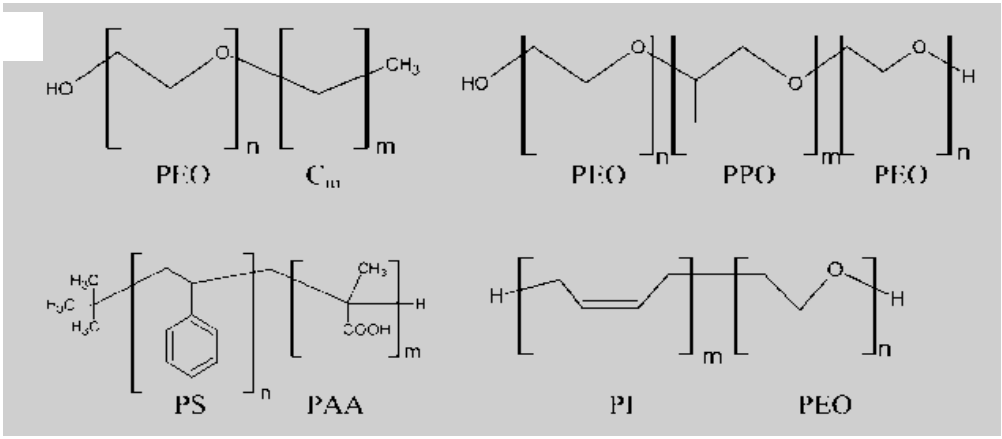

Figure 2.18 Block copolymer used in mesostructured generation [33].

Some advantages of using these block copolymer are:

(1) *The thicker wall thickness* (about 15-40 Å), enhancing hydrothermal and thermal stability of materials.

(2) *Ease to tunable pore diameter* by varying type or concentration of polymer.

(3) *Ease to remove from mineral framework* by thermal treatment or solvent extraction.

Interaction between block copolymer template and inorganic species, calls hybrid interphase (HI), is particularly important, and especially in PEO-PPO based one. Different possible interactions take place at the HI are schematized in Figure 2.19. Most of the fine HI characterization has been performed on PEO-based (di or triblock) templates. Melosh *et al*. [36] determined that in F127-templated silica monoliths, organization arose for polymer weight fractions higher than 40%. For lower polymeric silica ratios, non-ordered gels were formed. This lack of order was due to a relatively strong interaction (probably of H-bonding type) of the (Si-–O–Si) polymers forming the inorganic skeleton with both PEO and PPO blocks.

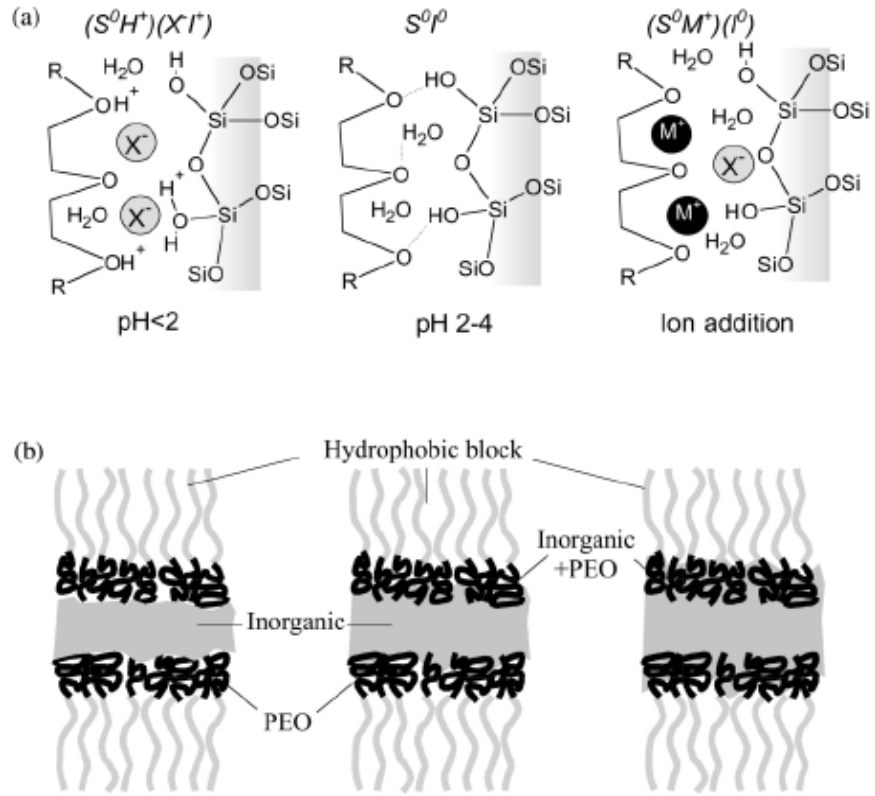

Figure 2.19 (a) Schematic view of the $(S^0H^+)(X^-I^-)$, S^0I^0, and $(S^0M^+)(X^-I^0)$ hybrid interphases (HIs) (b) Three possible structures of a HI composed by a nonionic polymer and an inorganic framework [36].

2.6 SBA-15

2.6.1 Structure and properties of SBA-15

SBA-15 mesoporous material has been synthesized under acidic condition using triblock copolymer as a structure directing agent. This mesoporous material has shown higher hydrothermal stability as compared to MCM-41 due to its thicker pore walls (3.1-6.4 nm). They also pose uniform and hexagonal-structured channel similar to MCM-41 with larger pore size which make them more desirable to deal with bulky molecule. Some properties of MCM-41 and SBA-15 are compared as described in Table 2.7. According to the properties listed in Table 2.7, SBA-15 shows better properties than MCM-41.

Table 2.7 Comparison of two well-known mesoporous materials, MCM-41 and SBA-15 in their characteristic properties [13, 37]

Properties	MCM-41	SBA-15
Pore size (Å)	20-100	46-300
Pore volume (mL/g)	>0.7	0.8-1.23
Surface area (m^2/g)	>1000	690-1040
Wall thickness (Å)	10-15	31-64

2.6.2 Synthesis of SBA-15 and formation mechanism

For SBA-15 materials, aging time and temperature are particularly important. Some research found that mesoporous SBA-15 prepared from calcination of an 'as-prepared' hybrid precursor contained a significant fraction of microporosity; further aging of the precursor in the mother liquors leads to an improvement on the pore size distribution (Figure 2.20), in agreement with the first work by Stucky *et al*. [13].

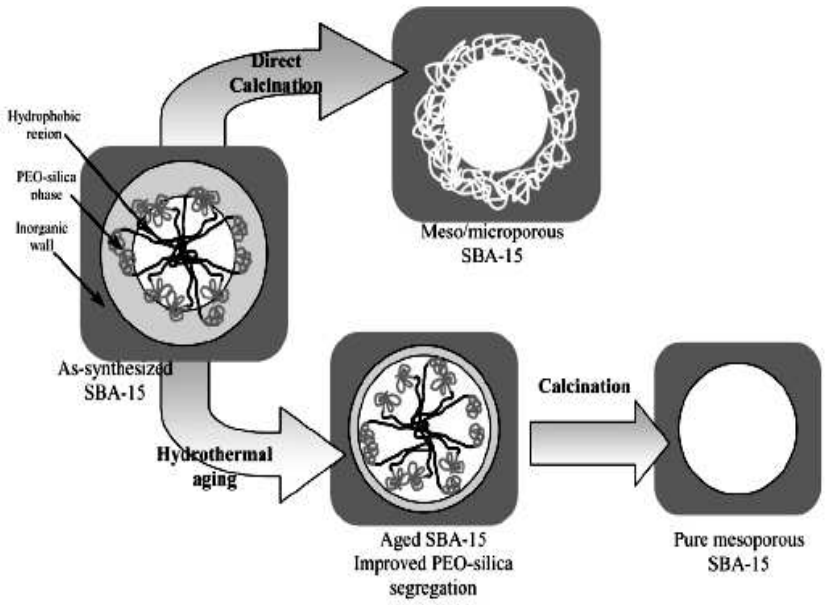

Figure 2.20 Pore evolution upon thermal treatment, depending on pre-treatment and aging [13].

Aging of an as-prepared precipitate at 80–100°C seems to help segregation of the PEO blocks and the inorganic framework, by promoting condensation of the latter. High temperatures also change the polymer behavior. It is known that for T >60°C, PEO blocks become less hydrophilic and expel water similar to PPO blocks when the temperature is higher than 40°C [38]. For a mechanism, firstly alkoxysilane species (TMOS or TEOS) are hydrolyzed as:

$$Si(OEt)_4 + nH_3O^+ \xrightarrow[pH<2]{\text{hydrolysis}} Si(OEt)_{4-n}(H_2O^+)_n + n\ EtOH$$

This is followed by partial oligomerization at the silica. Furthermore, at this condition, the PEO parts of surfactant associate with hydronium ions as followed:

$$\text{-}PEO_m\text{-} + yHX \xrightarrow{H_2O} \text{-}PEO_{m-y}[(EO)\cdot 3H_2O^+]_y \text{---}X_y^-$$

Next, coordination sphere expansion around the silicon atom by anion coordination of the form $X^-SiO_2^+$ may play an important role. The hydrophilic PEO blocks are expected to interact with the protonated silica and thus be closely associated with the inorganic wall. During the hydrolysis and condensation of the silica species, intermediate mesophase is sometimes observed and further condensation of silica species and organization of the surfactant and inorganic species result in the formation of the lowest energy silica-surfactant mesophase structure allowed by solidifying network.

2.7 Modification of catalysts

Nowadays, the attachment of organic functionalities such as sulfonic acid groups to the surface of siliceous SBA-15 mesoporous material is an interesting research area in heterogeneous catalysis and green chemistry. Basically, two strategies have been generally used to anchor organic groups onto a mesostructured silica surface.

2.7.1 Direct synthesis

Direct synthesis consists of the co-condensation of siloxane and organosiloxane precursors in the presence of the corresponding structure-directing agent.

The preparation of sulfonic-acid modified mesostructured materials is illustrated in Figure 2.21. This method is simplicity, because the incorporation of the organic precursor and the formation of the mesoporous material occur in a single synthetic step. To have a useful catalyst after synthesis, one must be able to extract the template from within the pores to create porosity. Calcination the synthetic material will destroy the incorporated organic functional groups. Extraction technique can be most effectively accomplished by ethanol solution [39-41].

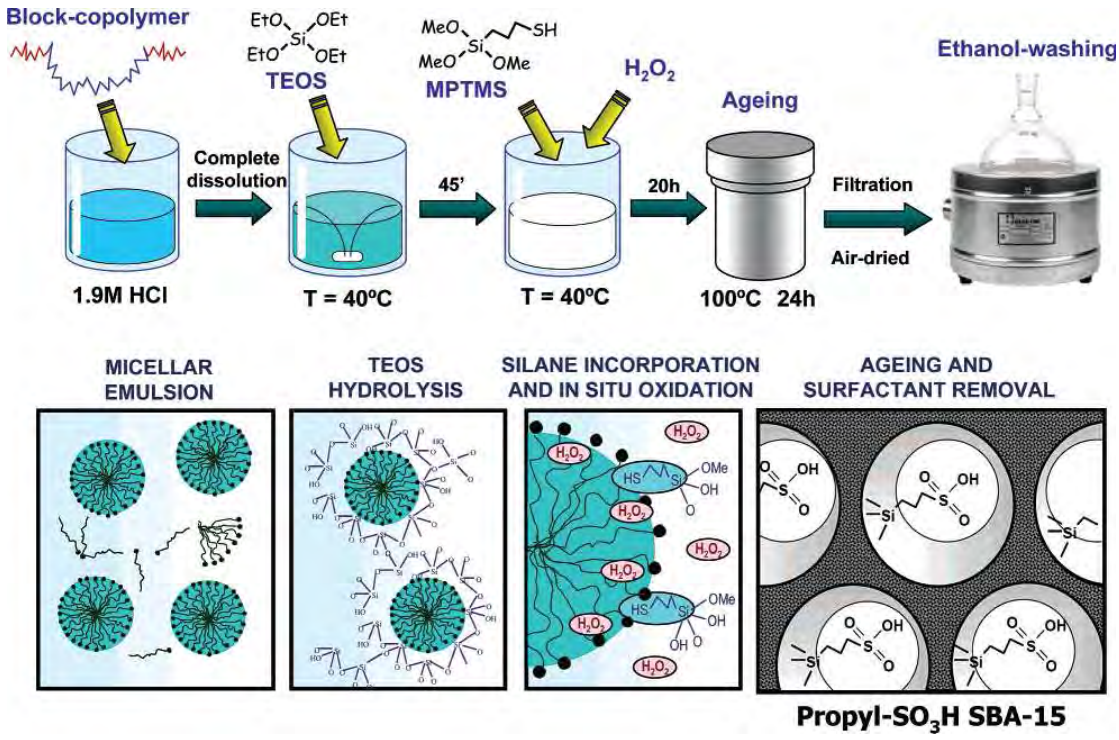

Figure 2.21 In-situ oxidation synthesis strategy for the preparation of sulfonic-acid-modified mesostructured material [40].

2.7.2 Post synthesis (Grafting method)

Grafting procedure based on modification of the silica surface with organic groups through silylation reaction occurring on isolated (≡Si-OH) and germinal (=Si(OH)$_2$) silanol groups using trichloro- or trialkoxyorganosilane and silylamines as organic precursors [40]**.**

Synthesis of sulfonic functionalized SBA-15 by post synthesis is shown in Figure 2.22. In typical procedure, calcined SBA-15 is treated with a silating agent like 3-mercaptopropyltrimethoxysilane (MPTMS) in nonpolar solvent (commonly toluene) to immobilize thiol groups on the surface. These thiol functionalities are then oxidized, normally using hydrogen peroxide. The most apparent advantage of this procedure is good preservation of the mesostructure after post-modification.

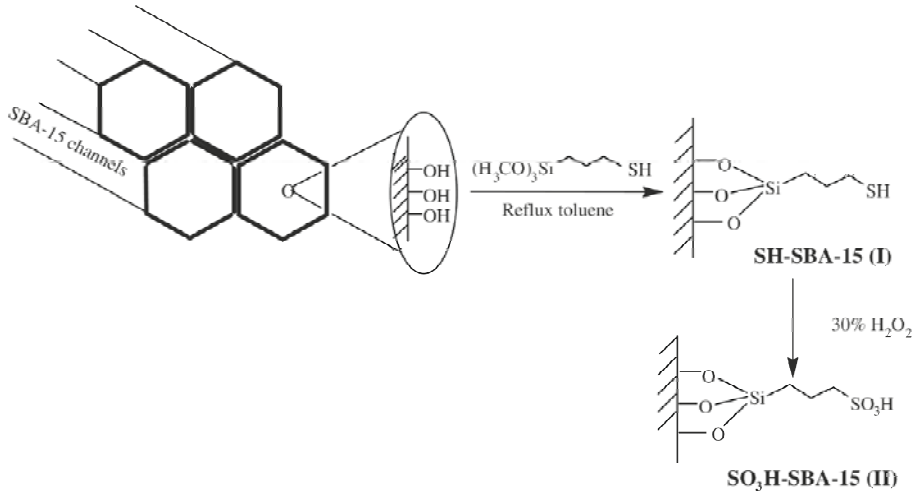

Figure 2.22 Post synthesis procedures for the preparation of sulfonic-acid-modified mesostructured materials [40].

2.8 Microwaves energy

Microwaves are a form of electromaganetic energy. Microwave, like all electromagnetic radiation, have an electric component as well as a magnetic component. The microwave portion of the electromagnetic spectrum is characterized by wavelengths between 1 mm and 1 m, and corresponds to frequencies between 300 MHz and 300 GHz. Typically, household microwave uses it is important to recognize that the energy delivered by microwave is insufficient for breaking colavent chemical bond. This information can help to narrow speculation on the mechanism for enhancement in specific reaction. Fixed frequency of 2,450 MHz (2.45 GHz) [42, 43].

2.8.1 Microwave interaction with matter

One can broadly characterization how bulk materials behave in a microwave field. Materials can absorb the energy (e.g. water, carbon), they can reflect the energy (e.g. metal), or they can simply pass the energy (e.g. glass, PP). It should be noted that few materials are either pure absorbers, pure reflectors, or completely transparent to microwaves. The chemical composition of the material, as well as the physical size and shape, will affect how it behaves in a microwave field.

Microwave interaction with matter is characterized by a penetration depth. That is, microwaves can penetrate only a certain distance into a bulk material. Not only the penetration depth is a function of the material composition, but it is also less than sample size; it is considered as a “surface heating”. On the contrary, a “volumetric heating” will occur in a bulk material when the penetration depth is larger than a sample size.

2.8.2 Two principle mechanisms for interaction with matter

There are two specific mechanisms of interaction between materials and microwaves: (1) dipole interactions and (2) ionic conduction. Both mechanisms require effective coupling between components of the target material and the rapidly oscillating electrical field of the microwaves.

Dipole interactions occur with polar molecules. The polar ends of a molecule tend to align themselves and oscillate in step with the oscillating electrical field of the microwaves. Collisions and friction between the moving molecules result in heating. Broadly, the more polar a molecule, the more effectively it will couple with (and be influenced by) the microwave field.

Ionic conduction is only minimally different from dipole interactions. Obviously, ions in solution do not have a dipole moment. They are charged species that are distributed and can couple with the oscillating electrical field of the microwaves. The effectiveness or rate of microwave heating of an ionic solution is a function of the concentration of ions in solution.

Materials have physical properties that can be measured and used to predict their behavior in a microwave field. One calculated parameter is the dissipation factor, often called the loss tangent. The dissipation factor is a ratio of the dielectric loss (loss factor) to the dielectric constant. Taken one more step, the dielectric loss is a measure of how well a material absorbs the electromagnetic energy to which it is exposed, while the dielectric constant is a measure of the polarizability of a material, essentially how strongly it resist the movement of either polar molecules or ionic species in the material. Both the dielectric loss and the dielectric constant are measurable properties.

2.9 Microwave and conventional heats

2.9.1 Conventional heating methods [42, 43]

In all conventional means for heating reaction mixtures, heating proceeds from a surface, usually the inside surface of the reaction vessel. Whether one uses a heating mantle, oil bath, steam bath, or even an immersion heater, the mixture must be in physical contact with a surface that is at a higher temperature than the rest of the mixture.

In conventional heating, energy is transferred from a surface, to the bulk mixture, and eventually to the reaction species. The energy can either make the reaction thermodynamically allowed or it can increase the reaction kinetics.

In conventional heating, spontaneous mixing of the reaction mixture many occur through convection or mechanical means (stirring) can be employed to homogeneously distribute the reactants and temperature throughout the reaction vessel. Equilibrium temperature conditions can be established and maintained.

Although it is an obvious point, it should be noted here that in all conventional heating of open reaction vessels, the highest temperature that can be achieved is limited by the boiling point of the particular mixture. In order to reach a higher temperature in the open vessel, a higher-boiling solvent must be used.

2.9.2 Microwave heating methods

Microwave heating occurs somewhat differently from conventional heating. First the reaction vessel must be substantially transparent to the passage of microwaves. The selection of vessel materials is limited to fluoropolymers and only a few other engineering plastics such as polypropylene, or glass fiber filled PEEK (poly ether-ether-ketone).Heating of the reaction mixture does not proceed from the surface of the vessel; the vessel wall is almost always at a lower temperature than the reaction mixture. In fact, the vessel wall can be an effective route for heat loss from the reaction mixture. Second, for microwave heating to occur, there must be some component of the reaction mixture that absorbs the penetrating microwaves. Microwaves will penetrate the reaction mixture, and if they are absorbed, the energy will be converted into heat. Just as with conventional heating, mixing of the reaction mixture may occur through convection, or mechanism means (stirring) can be employed to homogeneously distribute the reactants and temperature throughout the reaction vessel.

Table 2.8 Heating mechanism comparison between conventional and microwave process.

Conventional process	Microwave process
• Radiant heat source: gas burners, electric resistance element • Heat transfer mechanism: - From heat source to surface: convection and radiation - From surface to center: conduction • Surface is at higher temperature than center.	• Microwave source: Magnetrons, traveling wave tube, 25 transmission lines • Heat generation occurs internally. • Sample is at higher temperature than surrounding. • Heat loss from surface by conventional and radiation. • Center is at higher temperature than surface.

2.9.3 Microwave effect

To understand how microwave heating can have effects that are difference from conventional heating techniques, one must focus on what in the reaction mixture is actually absorbing the microwave energy. The simple fact is that materials or component of a reaction mixture can differ in their ability to absorb microwaves. Differential absorption of microwaves will lead to differential heating and localized thermal in homogeneities that cannot be duplicated by conventional heating techniques.

To illustrate the consequences, several examples are presented wherein we consider microwave adsorption by a bulk solvent and/or by the minor concentration of reactants in the solvent are considered.

2.10 Characterization of materials

2.10.1 X-ray powder diffraction (XRD)

X-ray powder diffraction (XRD) is an instrumental technique used for identification of minerals, as well as other crystalline materials. XRD is a technique in which a collimated beams of nearly monochromatic. X-rays is directed onto the flat surface of a relatively thin layer of finely ground material. XRD can provide additional information beyond basic identification. If the sample is a mixture, XRD data can be analyzed to determine the proportion of the different minerals present. Other obtained information can include the degree of crystallinity of the minerals present, possible deviations of the minerals from their ideal compositions, the structural state of the minerals and the degree of hydration for minerals that contain water in their structure.

XRD is a reliable technique that can be used to identify mesoporous structure. Typically, the XRD pattern of hexagonal symmetry shows five well-resolved peaks corresponding to lattice planes of Miller indices (100), (110), (200), (210), and (300) [44]. These XRD peaks appear at low angle (2θ angle between 0.5 and 3 degree) because the materials are not crystalline at atomic level, diffraction at higher angles are not observed.

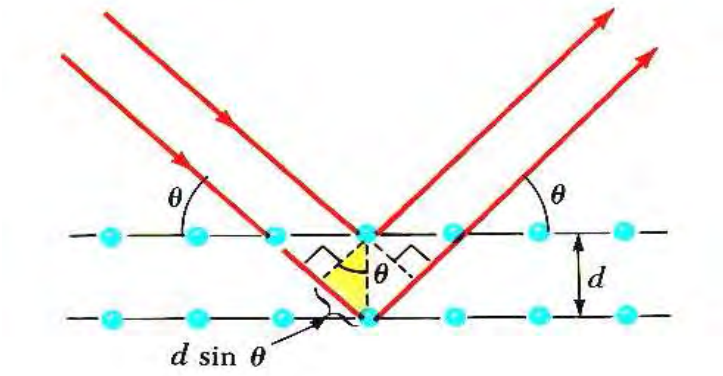

Figure 2.23 Diffraction of X-ray by regular planes of atoms [45].

Figure 2.23 shows a monochromatic beam of X-ray incident on the surface of crystal at an angle θ. The scattered intensity can be measured as a function of scattering angle 2θ. The resulting XRD pattern efficiently determines the different phases present in the sample. Using this method, Braggs' law is able to determine the interplanar spacing of the samples, from diffraction peak according to Bragg's angle.

$$n\lambda = 2\,d\sin\theta$$

Where the integer *n* is the order of the diffracted beam, λ is the wavelength; *d* is the distance between adjacent planes of the crystal (the *d*-spacings) and θ is the angle between the incident beam and these planes.

2.10.2 Nitrogen adsorption-desorption technique

The N_2 adsorption-desorption technique is used to classify the porous materials and its physical properties such as surface area, pore volume, pore diameter and pore-size distribution of solid catalysts. Adsorption of gas by a porous material is described by an adsorption isotherm, the amount of adsorbed gas by the material at a fixed temperature as a function of pressure. Porous materials are frequently characterized in terms of pore sizes derived from gas sorption data [46, 47]. The IUPAC classification of adsorption isotherms is illustrated in Figure 2.24.

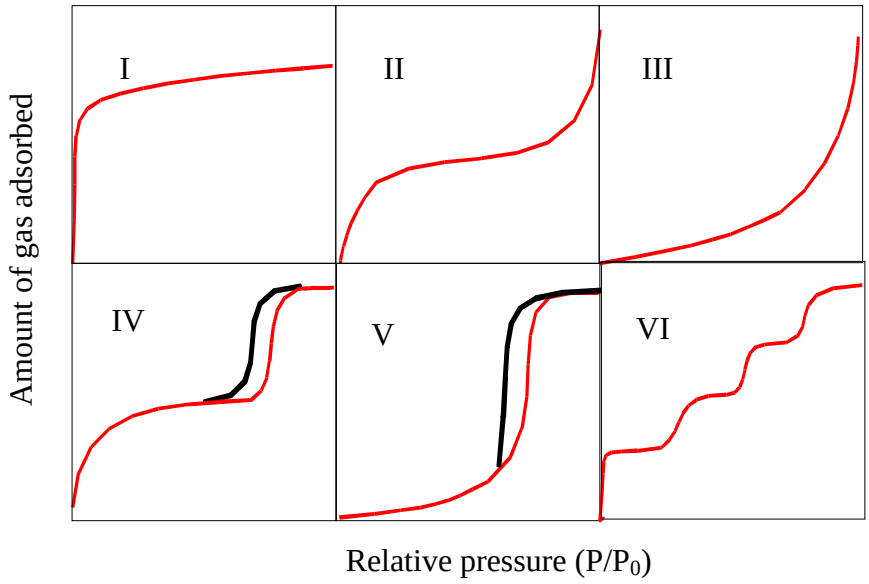

Figure 2.24 The IUPAC classification of adsorption isotherm [46].

As shown in Table 2.9, adsorption isotherms base on the strength of the interaction between the sample surface and adsorptive. Pore size distribution is measured by the use of nitrogen adsorption/desorption isotherm at liquid nitrogen temperature and relative pressures (P/P_o) ranging from 0.05-0.1. The large uptake of nitrogen at low P/P_o indicates filling of the micropores (<20 Å) in the adsorbent. The linear portion of the curve represents multilayer adsorption of nitrogen on the surface of the sample, and the concave upward portion of the curve represents filling of mesoporous and macropores. The multipoint Brunauer, Emmett and Teller (BET) method is commonly used to measure total surface area.

$$\frac{1}{W[(P_o/P)-1]} = \frac{1}{W_mC} + \frac{C-1}{W_mC}(P/P_o)$$

Where W is the weight of nitrogen adsorbed at a given P/P_o, W_m is the weight of gas to give monolayer coverage, and C is a constant that is related to the heat of adsorption. A slope and intercept are used to determine the quantity of nitrogen adsorbed in the monolayer and calculate the surface area. For a single point method, the intercept is taken as zero or a small positive value, and the slope from the BET plot is used to calculate the surface area. The surface area depends upon the method used, as well as the partial pressures at which the data are collected.

Table 2.9 Features of adsorption isotherms.

Type	Interaction between sample surface and gas adsorbate	Porosity	Example of sample-adsorbate
I	relatively strong	Micropores	activated carbon-N_2
II	relatively strong	Nonporous	oxide-N_2
III	weak	Nonporous	carbon-water vapor
IV	relatively strong	Mesopore	silica-N_2
V	weak	Micropores	
		Mesopore	activated carbon-water vapor
VI	relatively strong sample surface has an even distribution of energy	Nonporous	graphite-Kr

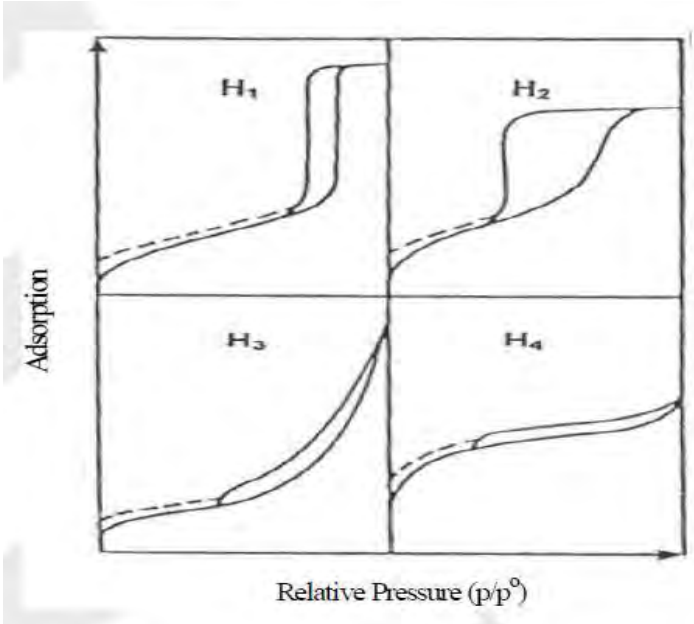

Figure 2.25 IUPAC classification of hysteresis loop.

1. Type H_1: the hysteresis loop associated with pores consisting of agglomerates or compacts of uniform spherical particles with regular array, whose pore size distribution are normally narrow.

2. Type H_2: the hysteresis loop associated with pores with ink-bottle shapes or more complicated net work structures.

3. Type H_3: the hysteresis loop associated with slit-shaped pores formed from aggregrates of plate-like particles.

4. Type H_4: the hysteresis loop associated slit-shaped pores with narrower sizes.

2.10.3 Scanning electron microscope (SEM)

The scanning electron microscope (SEM) has unique capabilities for analyzing surfaces and morphology of materials. It is analogous to the reflected light microscope, although different radiation sources serve to produce the required illumination. Whereas the reflected light microscope forms an image from light reflected from a sample surface, the SEM uses electrons for image formation. The different wavelength of these radiation sources result in different resolution levels: electron have much shorter wavelength than light photons, and shorter wavelength are capable of generating the higher resolution information. Enhanced resolution in turn permits higher magnification without loss of detail. The maximum magnification of the light microscope is about 2,000 times; beyond this level is “empty magnification”, or the point where increased magnification does not provide additional information. This upper magnification limit is a function of the wavelength of visible light, 2000 Å, which equal the theoretical maximum resolution of conventional light microscope. In comparison, the wavelength of electron is less than 0.5 Å, and theoretically the maximum magnification of electron beam instrument is beyond 800,000 times. Because of instrumental parameters, practical magnification and resolution limits are

about 75,000 times and 40 Å in a conventional SEM [33]. The SEM consists basically of four systems:

1. The *illuminating/imaging system* produces the electron beam and directs it onto the sample.
2. The *information system* includes the data released by the sample during electron bombardment and detectors which discriminate among analyze these information signals.
3. The *display system* consists of one or two cathode-ray tubes for observing and photographing the surface of interest.
4. The *vacuum system* removes gases from the microscope column which increase the mean free path of electron, hence the better image quality.

2.10.4 Temperature-programmed desorption of ammonia (NH_3-TPD)

Temperature-programmed desorption of ammonia (NH_3-TPD) is the most widely used method to measure the acidic property of solid in mesoporous materials. On widely various solid-acidic catalysts, it was clarified that desorption was controlled by the equilibrium between the adsorbent and the adsorbed ammonia under usually utilized experimental conditions. There are many variations on the method but it typically involves saturation of the surface with ammonia under some set of adsorption conditions, followed by linear ramping of the temperature of the sample in a flowing inert gas stream. The amount of ammonia desorbing above some 33 characteristic temperature is taken as the acid-site concentration, and the peaks desorption temperature (T*M*) have been used to calculate heats of adsorption. It is well- known that desorption temperature of the ammonia molecule can be related to the strength of acidity of the materials tested. The bond formed between the acid site and the ammonia is broken by an energy supply. Thus, the maximum temperature in

the NH_3 desorption process is a qualitative indication of the strength of the acidic sites [48].

2.10.5 X-ray Fluorescence (XRF)

An electron can be ejected from its atomic orbital by the absorption of a light wave (photon) of sufficient energy. The energy of the photon (hv) must be greater than the energy with which the electron is bound to the nucleus of the atom. When an inner orbital electron is ejected from an atom, an electron from a higher energy level orbital will be transferred to the lower energy level orbital. During this transition a photon maybe emitted from the atom. This fluorescent light is called the characteristic X-ray of the element. The energy of the emitted photon will be equal to the difference in energies between the two orbitals occupied by the electron making the transition. Because the energy difference between two specific orbital shells, in a given element, is always the same (i.e. characteristic of a particular element), the photon emitted when an electron moves between these two levels, will always have the same energy. Therefore, by determining the energy (wavelength) of the X-ray light (photon) emitted by a particular element, it is possible to determine the identity of that element.

For a particular energy (wavelength) of fluorescent light emitted by an element, the number of photons per unit time (generally referred to as peak intensity or count rate) is related to the amount of that analyte in the sample. The counting rates for all detectable elements within a sample are usually calculated by counting, for a set amount of time, the number of photons that are detected for the various analytes' characteristic X-ray energy lines. It is important to note that these fluorescent lines are actually observed as peaks with a semi-Gaussian distribution because of the imperfect resolution of modern detector technology. Therefore, by determining the energy of the X-ray peaks in a sample's spectrum, and by calculating the count rate of the various elemental peaks, it is possible to qualitatively establish the elemental composition of the samples and to quantitatively measure the concentration of these elements [49].

2.11 Biodiesel

Biodiesel can be obtained from vegetable oil and animal fats using esterification and transesterification. Biodiesel is a non-fossil fuel alternative to petrodiesel. It can also be mixed with petrodiesel in any amount in modern engines, though when frist using it, the solvent properties of the fuel tend to dissolve accumulated deposits and can clog fuel filters. Biodiesel has a higher gel point than petrodiesel, but is comparable to diesel. This can be overcome by using a biodiesel/petrodiesel blend or by installing a fuel heater, but this is only necessary during the colder months. A diesel-biodiesel mix result in lower emissions than either can achieve alone except for NO_x emissions. A small percentage of biodiesel can be used as an additive in low-sulfur formulations of diesel to increase the lubricity lost when the sulfur is removed. In the event of fuel spills, biodiesel is easily washed away with ordinary water and is nontoxic compared to other fuels.

Biodiesel can be produced using kits. Certain kits allow for processing of used vegetable oil that can be run though any conventional diesel motor with modifications. The modification needed is the replacement of fuel lines from the intake and motor and all affected rubber fittings in injection and feeding pump. This is because biodiesel is an effective solvent and will replace softeners within unsuitable rubber with itself over time. Synthetic gaskets for fittings and hoses prevent this. Chemically, most biodiesel consist of alkyl (usually methyl) esters instead of the alkanes and aromatic hydrocarbons of petroleum derived diesel. However, biodiesel has combustion properties very similar to petrodiesel, including combustion energy and cetane ratings. Paraffin biodiesel also exists. Due to the purity of the source, it has a higher quality than petrodiesel [50].

2.12 The production of biodiesel

2.12.1 Direct use and blending

All research focusing on the use of vegetable oils to feed diesel engine showed coking and trumpet formation on the injectors to such an extent that fuel atomization does not occur properly or is even prevented. There have been many problems associated with using vegetable oils directly in diesel engines, such as: decrease in power output and thermal efficiency of the engine; thickening or gelling of the lubricating oil as result of contamination by vegetable oils. Other disadvantage to the use of vegetable oils and especially animal fats are the high viscosity (about 11-17 times higher than diesel fuel) and lower volatility that result in carbon deposits in engines due to incomplete combustion.

In 1980, Bartholomew addressed the concept of using food for fuel. It was not practical to substitute 100% vegetable oil for diesel fuel. But a blend of 20% vegetable oil and 80% diesel fuel was successful. Mixture of degummed soybean oil and No.2 diesel fuel in the ratio of 2:1 and 1:1 were tested for engine performance, problems associated with the use of vegetable oil as fuels were oil deterioration and incomplete combustion [51].

2.12.2 Thermal cracking (pyrolysis)

To solve the problem of high viscosity of vegetable oils, the pyrolysis was chosen to produce the biodiesel. The pyrolysis of fats has been investigated for more than 100 years, especially in areas without deposits of petroleum. Copra oil and palm oil stearin were checked over SiO_2/Al_2O_3 at 450°C to produce biodiesel fuels. The chemical compositions of diesel fraction were similar to fossil fuel. Pyrolyzed soybean oil has 79.0% of carbon and 11.9% of hydrogen. Its cetane number (43) is higher than (37.9) and its viscosity (10.2 cSt at 38°C) is lower than the vegetable oil viscosity (32.6 cSt at 38°C). Nevertheless, this value is higher than that required for biodiesel (7.5 cSt). Pyrolysed oils have acceptable levels of sulfur, water and

particulate matter. Otherwise, they have unacceptable levels of ashes and carbon deposits and high pour point [52].

2.12.3 Transesterification (alcoholysis)

Transesterification is widely used to reduce vegetable oil viscosity. Most industrial processes employ alkaline catalysis and methanol. In almost all countries methanol is more available than ethanol. Transesterication or alcoholysis is the displacement of alcohol is used instead of water. A catalyst is usually used to improve the reaction rate and yield. Because the reaction is reversible, excess alcohol is used in shifting the equilibrium to the product side. The reaction can be catalyzed by alkali, acid or enzyme such as NaOH, KOH, H_2SO_4 and lipase, respectively. Pure biodiesel fuel (00% esters of fatty acids) is called B100. When blended with diesel fuel the designation indicates the amount of B100 in the blend, *e.g.* B20 is 20% biodiesel and 80% diesel, and B5 used in Europe is contains 5% B100 in diesel [52]. The transesterification reaction diagram of triglyceride is presented in the Figure 2.26.

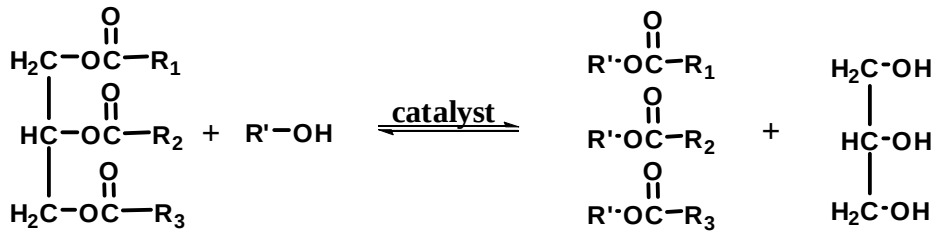

Figure 2.26 Typical transesterification diagram of triglyceride.

Transesterification of triglyceride (TGs) with alcohol proceeds via three consecutive and reversible reactions where the FFA ligands combine with alcohol to produce a fatty acid alkyl ester, diglyceride and monoglyceride intermediates, and finally glycerol by-product. The stoichiometric reaction requires 1 mole of TG and 3 mole of methanol to produce 3 mole of linear ester and 1 mole of glycerol. In presence of excess alcohol, the forward reaction is pseudo-frist order and the reverse reaction is found to be second-order. It was observed that transesterificaton is faster when catalyzed by alkali. The mechanism of acid and

alkali-catalyzed transesterification is described in Figure 2.27 and 2.28, respectively [53].

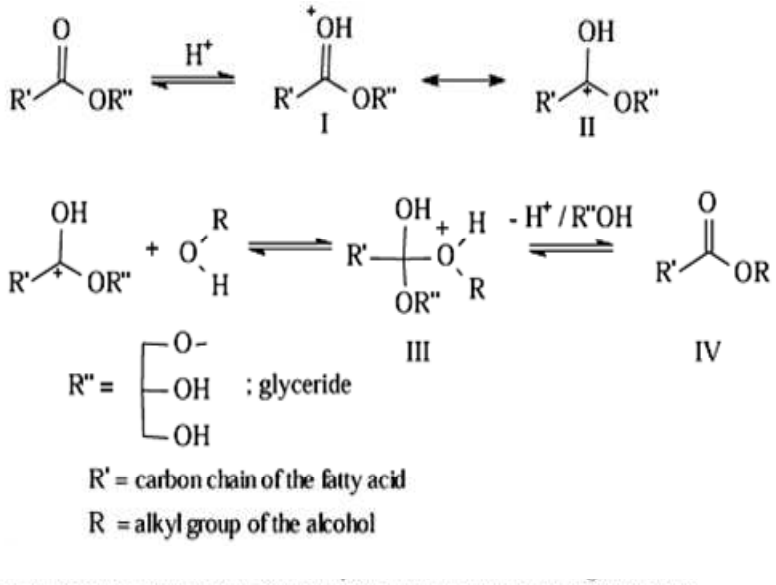

Figure 2.27 Mechanism of acid catalyzed transesterification reaction

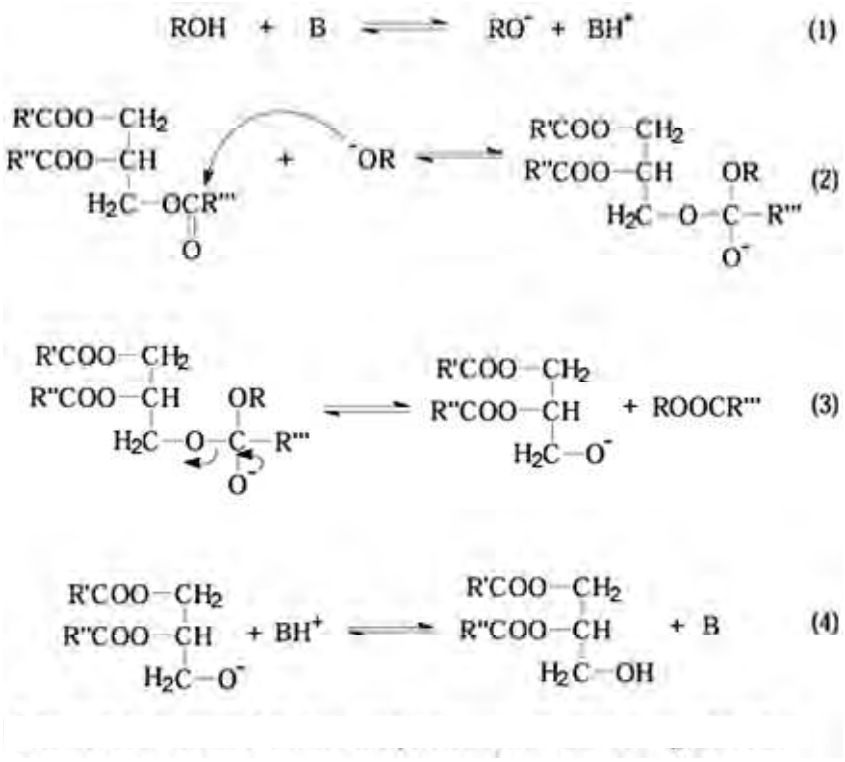

Figure 2.28 Mechanism of base catalyzed transesterification reaction

2.12.4 Esterificaton

Esterificaton is the chemical process for making ester, which are compounds for the chemical structure R-COOR', where R and R' are either alkyl or aryl groups. The most common method for preparing esters is to heat a carboxylic acid or free fatty acid with an alcohol, while removing the water that is formed. Esterification is among the simplest and most often performed organic transformation. The esterification reaction diagram of free fatty acid is shown in the Figure 2.29. The mechanism of acid and alkali catalyzed esterifications are presented in Figure 2.30 and 2.31, recpectively.

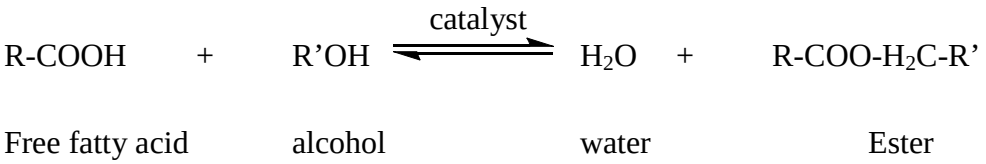

Figure 2.29 Typical esterification diagram of free fatty acid.

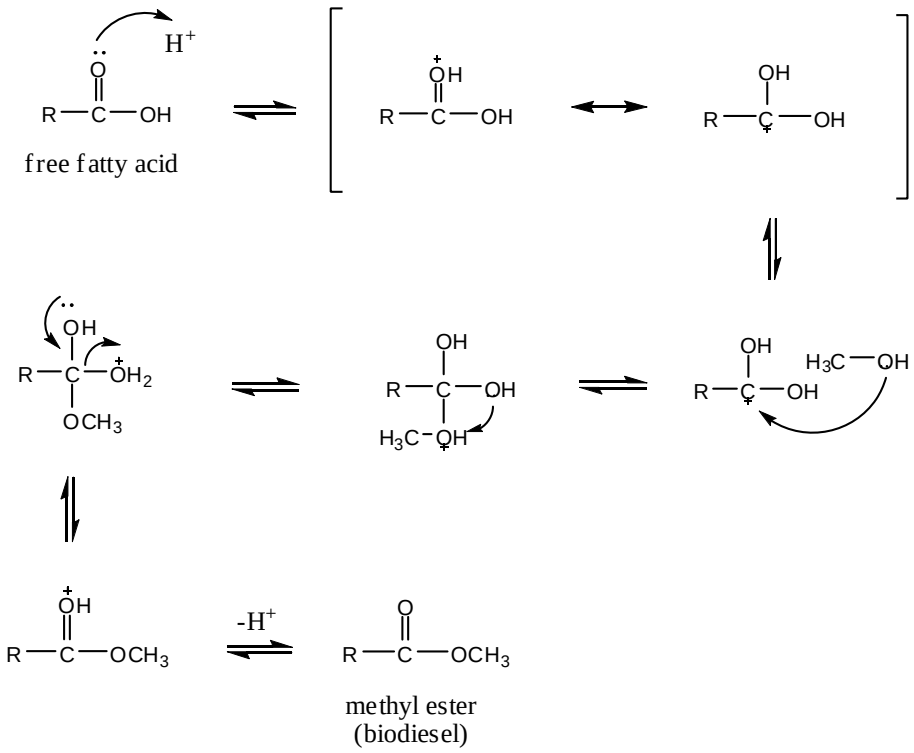

Figure 2.30 Mechanism of acid catalyzed esterification of free fatty acid.

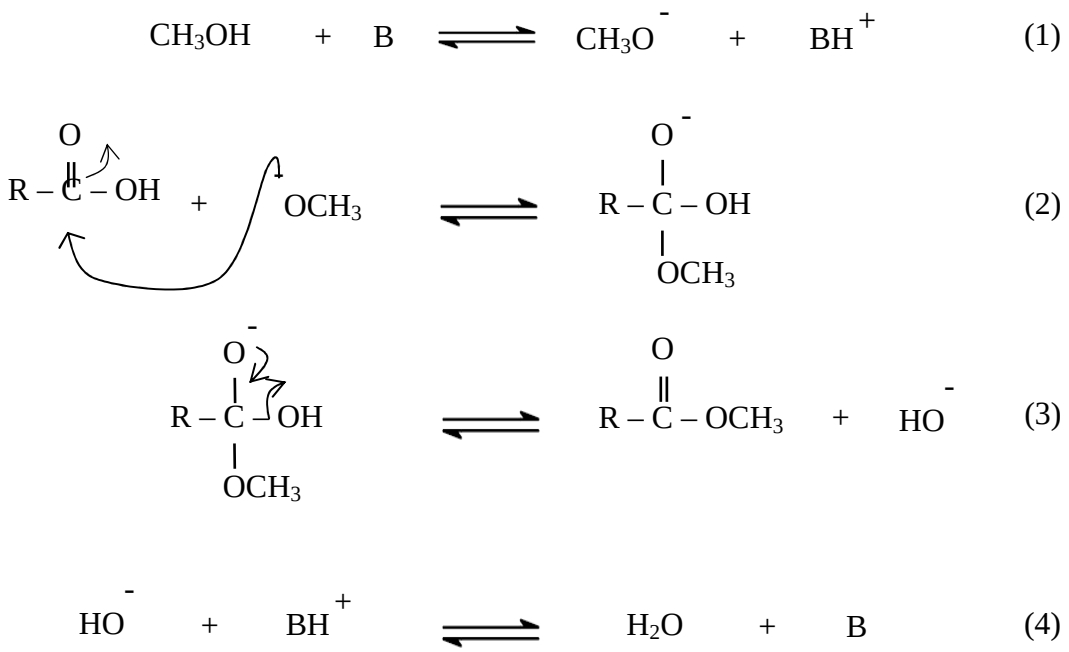

Figure 2.31 Mechniam of base catalyzed esterification of free fatty acid.

2.12.4.1 Esterification parameters

The most relevant parameters that influence the esterification reactions are the following

(a) Moisture and free fatty acid

All materials should be substantially anhydrous. If the acid value was greater than 1, NaOH was required to neutralize the free fatty acids. Water also caused soap formation, which consumed the catalyst and reduced catalyst efficiently.

(b) Molar ratio of alcohol to free fatty acid

One of most important variables affecting the yield of ester is the molar ratio of alcohol to FFA. The molar ratio is associated with the type of catalyst used. Higher molar ratios result in greater ester conversion in a shorter time.

(c) Catalyst type and concentration

Catalysts in esterification reaction are classified as alkali, acid, or enzyme. Acid-catalyzed reaction is more efficient and less side reaction than alkali-catalyzed. It is suitable if the glycerides contain high free fatty acid content and more water. Acid catalysts include sulfuric acid (H_2SO_4), hydrochloric acid (HCl), and phosphoric acid (H_3PO_4).

Lipase is enzyme that can be used as catalyst for transesterification and esterification reactions. It has many advantages such as possibility to regeneration and reuse and high thermal stability, but it also has some disadvantages include lose some activity, support enzymes is not uniform and more expensive.

(d) Reaction time

The conversion rate and fatty acid methyl ester yield increasing with increased reaction time.

(e) Reaction temperature

Esterification can occur at differences temperature, depending on the oil used and catalyst types. Temperature clearly influenced the reaction rate and yield of esters.

CHAPTER III

EXPERIMENTS

3.1 Instruments and apparatus

3.1.1 Oven and furnace

Crystallization of X zeolite, Y zeolite and SBA-15 during the synthesis was carried out at a temperature of 90 and 100^{o}C, respectively in static condition using UM-500 oven as heater. The samples were calcined in air at 550±10^{o}C for 5 hrs to remove the organic template in the Carbonite RHF 1600 muffle furnace with programmable heating rate of 1°C/min.

3.1.2 X-ray powder diffractometer (XRD)

The XRD patterns of synthesized mesoporous materials were identified using a Rigaku D/MAX-2200 Ultima^{+} X-ray diffractometer equipped with Cu target X-ray tube (40 kV, 30mA) at 2-theta angle between 0.5 to 3.00 degree with a scan speed of 1.00 degree/min and sampling width of 0.02 degree. The microporous materials were determined at 2-theta angle between 5.00 to 50.00 degree with a scan speed of 5.00 degree/min and sampling width of 0.02 degree. The scattering slit, divergent slit and receiving slit were fixed at 0.5 degree, 0.5 degree, and 0.15 mm, respectively. The measured diffractograms were analyzed using MDI software (Jade 6.5).

3.1.3 Surface area analyzer

N_2 adsorption-desorption isotherms, BET specific surface area, and pore size distribution of the catalysts were carried out using a BEL Japan, BELSORP-mini instrument. The pure materials weights were nearly 40 mg and weighted exactly after pretreatment at 400^{o}C for 3 hrs. The functionalized materials were pretreatment at 150^{o}C for 3 hrs before each measurement.

3.1.4 X-ray fluorescence spectroscopy (XRF)

The element analyses of the catalysts were analyzed using the Oxford ED - 2000 X-ray Fluorescence Spectrometer at the Scientific and Technological Research Equipment Centre of Chulalongkorn University.

3.1.5 Scanning electron microscope (SEM)

The morphology and particle sizes of the catalysts were observed using a JEOL JSM-6480 LV scanning electron microscope. All samples were coated with spluttering gold under vacuum.

3.1.6 Transmission electron microscope (TEM)

The particle size and wall thickness of synthesized materials were investigated by JEOL; JEM-2100 transmission electron microscopy.

3.1.7 Sulfur analyzer

The sulfur content of the catalysts was measured with a sulfur analyzer, model SC-132 from LECO Corporation, by combustion in oxygen at 1350^{o}C and determination of SO_2 by the intensity of infrared adsorption bands.

3.1.8 Ammonia temperature-program desorption (NH_3-TPD)

Acid strength of catalyst was determined using the BEL-CAT Japan instrument. The sample weight was near 0.08 g and pretreatment at 400^{o}C for 20 min before each measurement.

3.1.9 Parr reactor

The esterification reaction of free fatty acids (oleic acid, palmitic acid) over Y zeolite and X zeolite was performed in PARR reactor, model 4565 mini bench top reactor.

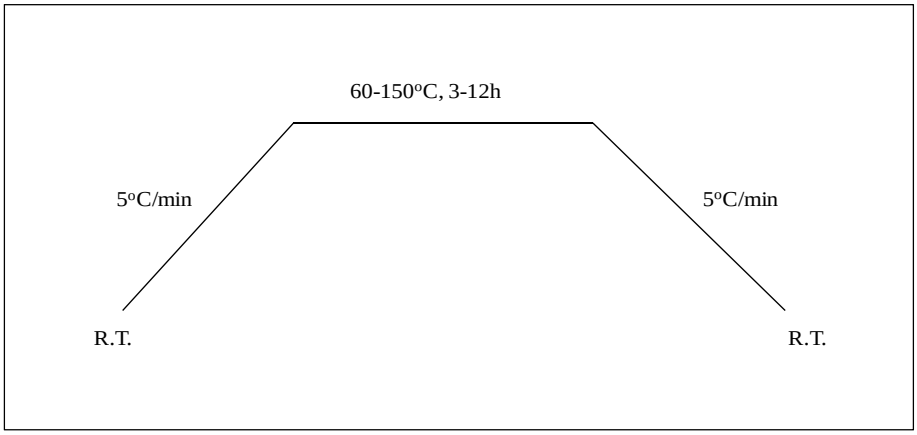

Figure 3.1 The temperature program for esterification reaction

3.1.10 Gas chromatograph (GC)

Reaction mixtures from methyl ester synthesis were analyzed using a Varian CP 3800 gas chromatograph equipped with a 30 m length × 0.25 mm inner diameter CP-Sil 8 capillary column (equivalent to DB-5 and HP-5 column). The detector was a flame ionization detector (FID). The sample volumes were 1 μL. The column oven heating program was illustrated in Figure 3.2.

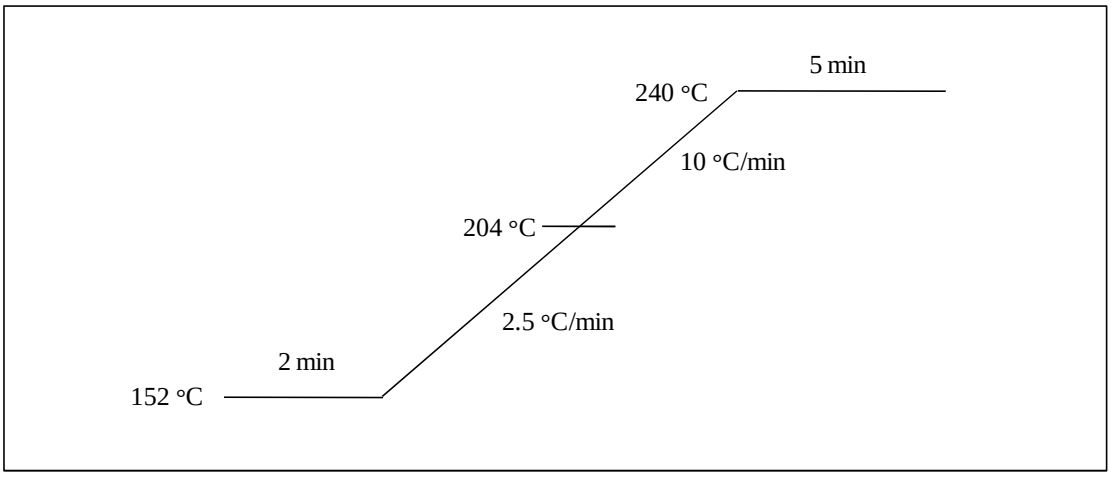

Figure 3.2 The GC heating condition for methyl ester analysis.

3.2 Chemicals

1. Sodium hydroxide, NaOH (Merck, ≥99%)
2. Sodiumaluminate, NaAlO (Riedel-deHaen)
3. water glass (C.Thai Chemical Company Limited)
4. Triblock copolymer pluronic P123 (PEO_{20}-PPO_{70}-PEO_{20}, average molecular weight = 5800) (Aldrich)
5. Tetraethyl orthosilicate, TEOS (Fluka, ≥98 %)
6. Hydrochloric acid, HCl (Fluka, 37 %)
7. (3-Mercaptopropyl)trimethoxysilane, MPTMS (Aldrich, 95 %)
8. Hydrogen peroxide (Merck, 30 %)
9. Toluene (CARLO ERBA, 99.5%)
10. Sulfuric acid, H_2SO_4 (Merck, 95-97%)
11. Nitric acid, HNO_3 (Merck, 65%)
12. Hydrofluoric acid, HF (Merck, 48%)
13. Potassium chloride, KCl (AnalaR)
14. Ammonium chloride, NH_4Cl (Riedel-deHaen)
15. Oleic acid, $C_{18}H_{34}O_2$ (Aldrich, 90%)
16. Plamitic acid, $C_{16}H_{32}O_2$ (Fluka, ≥97%)
17. Methanol, CH_3OH (Merck, ≥ 99.9%)
18. Methyl oleate, $C_{19}H_{36}O_2$ (Aldrich, 99%)
19. Methyl palmitate, $C_{17}H_{34}O_2$ (Fluka, 97%)
20. Tetrahydrofuran, THF (Merck, reagent grade)
21. N-methyl-N-trimethylsilyltrifluoroacetamide, MSTFA (Fluka, derivertization grade)
22. Eicosane, $C_{20}H_{42}$ (Aldrich, 99%)
23. Acetone, C_3H_6O (commercial grade)
24. Sodium chloride, NaCl (CARLO ERBA)

3.3 Synthesis of mesoporous (SBA-15) and microporous (X zeolite and Y zeolite)

This chapter described the preparation mesoporous (SBA-15) and microporous (X zeolite and Y zeolite) via hydrothermal and microwave methods.

3.3.1 Synthesis of SBA-15 by hydrothermal and microwave methods

SBA-15 was synthesized using the gel mole composition of 1.0TEOS: 0.0165 P123: 6.95 HCl: 140 H_2O reported by Stucky *et al*. [13]. In a typical procedure, triblock copolymer Pluronic P123 as template was dissolved in 1.9 M HCl solution at room temperature under stirring. Subsequently, TEOS was added dropwise and stirred for 30 min. Then, aged at 40^{o}C for 24 hrs with stirring. The resulting gel was transferred to a Teflon-lined autoclave for hydrothermal crystallization at 100^{o}C for 48 hrs denoted as SBA-15-HT. As-synthesized SBA-15 was separated by filtration, washed with deionized water for several times, and dried overnight. The template was removed by calcined at 550^{o}C for 5 hrs. The procedure for synthesizing the SBA-15 was illustrated in Scheme 3.1. For microwave method, except for crystallizations at 300 Watt for 0.5, 1, 1.5, 2, 2.5, 3 and 4 hours under stirring and without stirring were various (Scheme 3.2). The sample is denoted as SBA-15-MW*x* where *x* denoted as aging time in hour for microwave method.

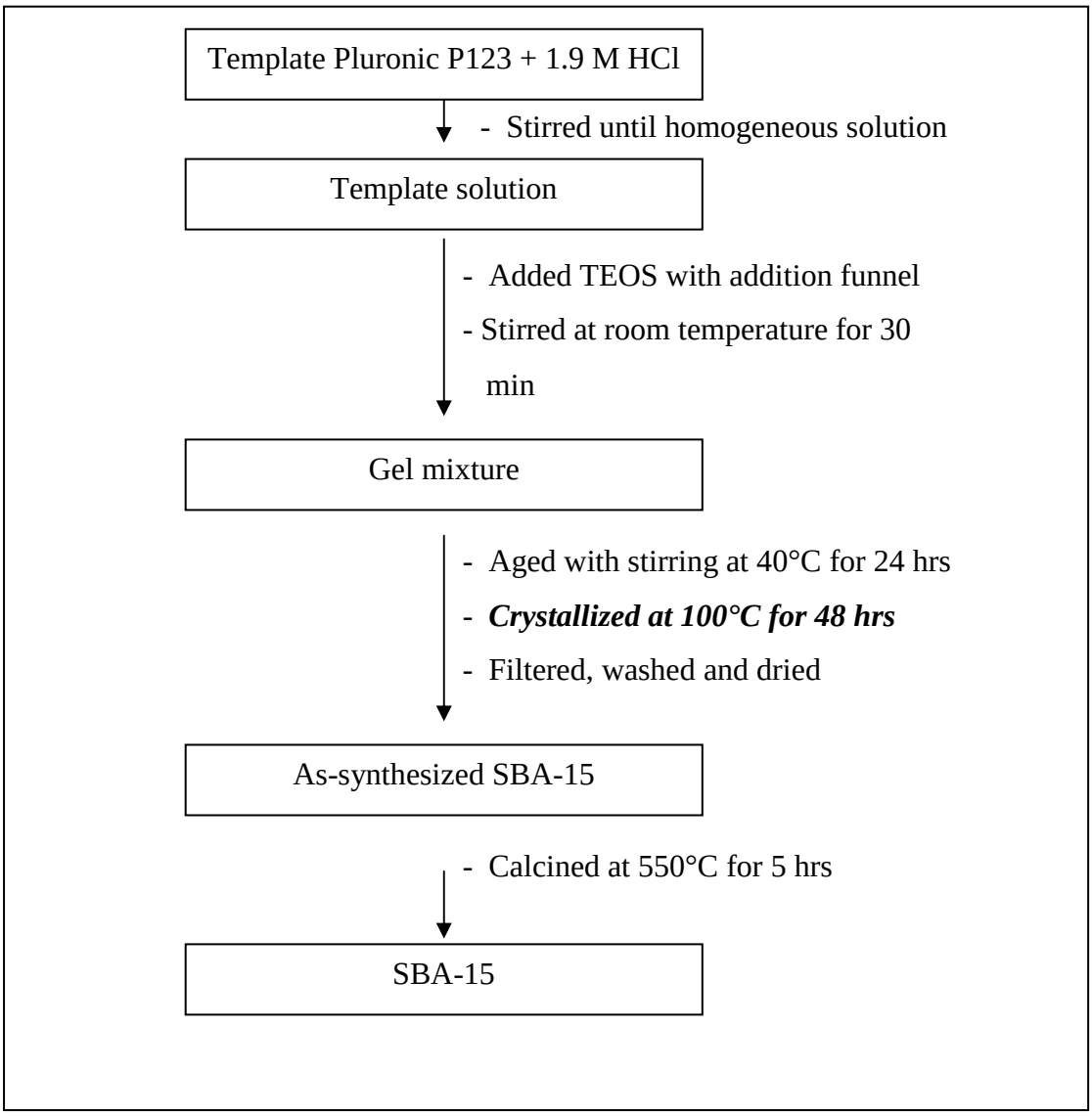

Scheme 3.1 Preparation diagram for SBA-15 by hydrothermal method.

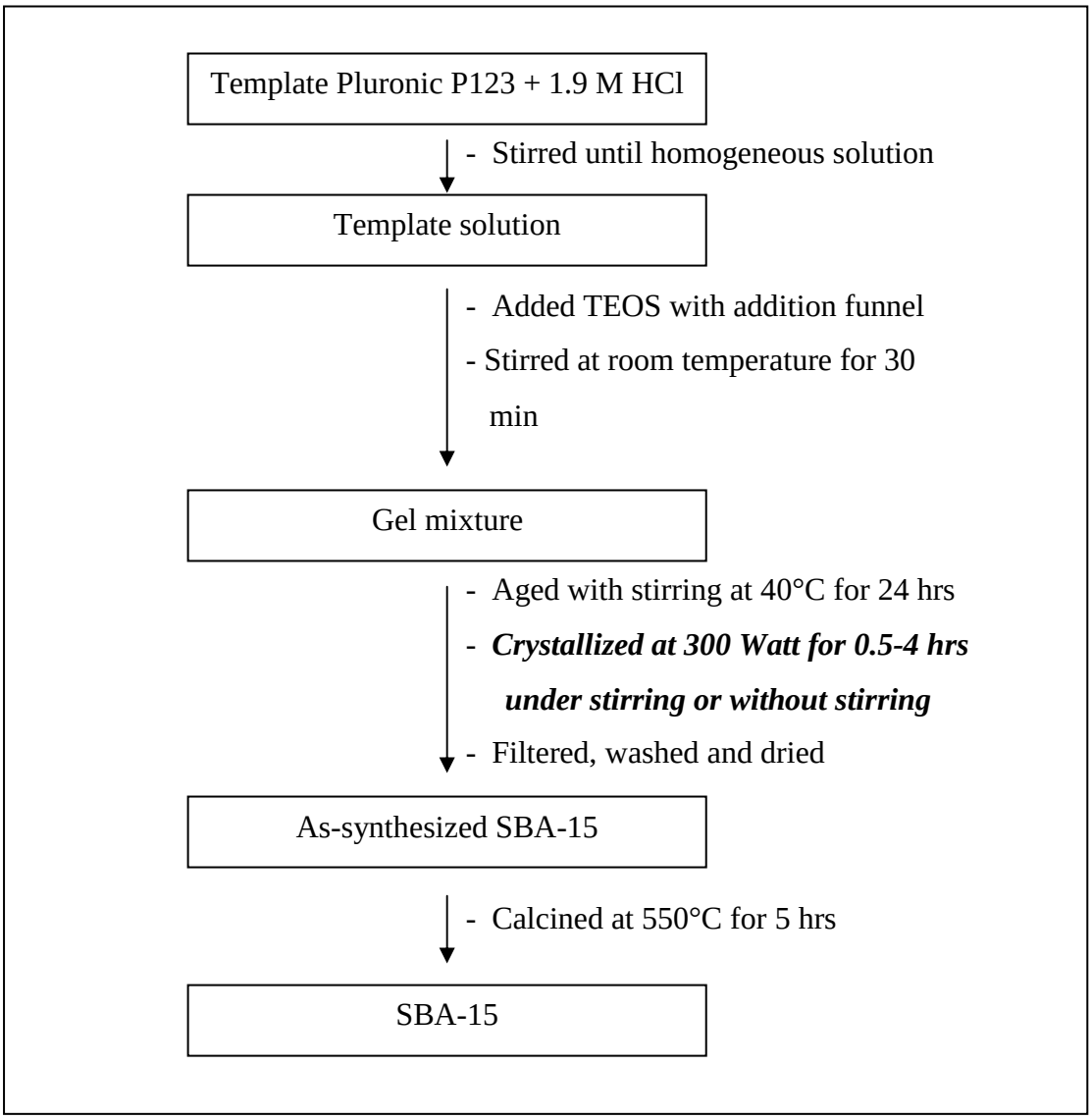

Scheme 3.2 Preparation diagram for SBA-15 by microwave method.

3.3.2 Synthesis of Y Zeolite by hydrothermal and microwave methods

3.3.2.1 Preparation of the nucleation centers

Nucleation center was synthesized by using the gel molar composition ratio of 19.26 SiO_2: 13.84 Na_2O: Al_2O_3: 249.11 H_2O reported by Ginter *et al*. [54]. In a typical procedure, 4.07 g of sodium hydroxide and 1.40 g of sodium aluminate were dissolved in deionized water at room temperature under stirring until clear solution. Then, 22.72 g of water glass was added dropwise and homogeneous solution at room temperature at least 10 min. After that, the solution was aged for 120 hrs at room temperature for hydrothermal method, whereas microwave method was aged at the system operated by household microwave at a frequency of 2.45 GHz and up to 100% at full power 300 Watt for 0.5, 1, 2, 3 and 4 hrs in microwave oven. The flowchart at the process is shown in Scheme 3.3.

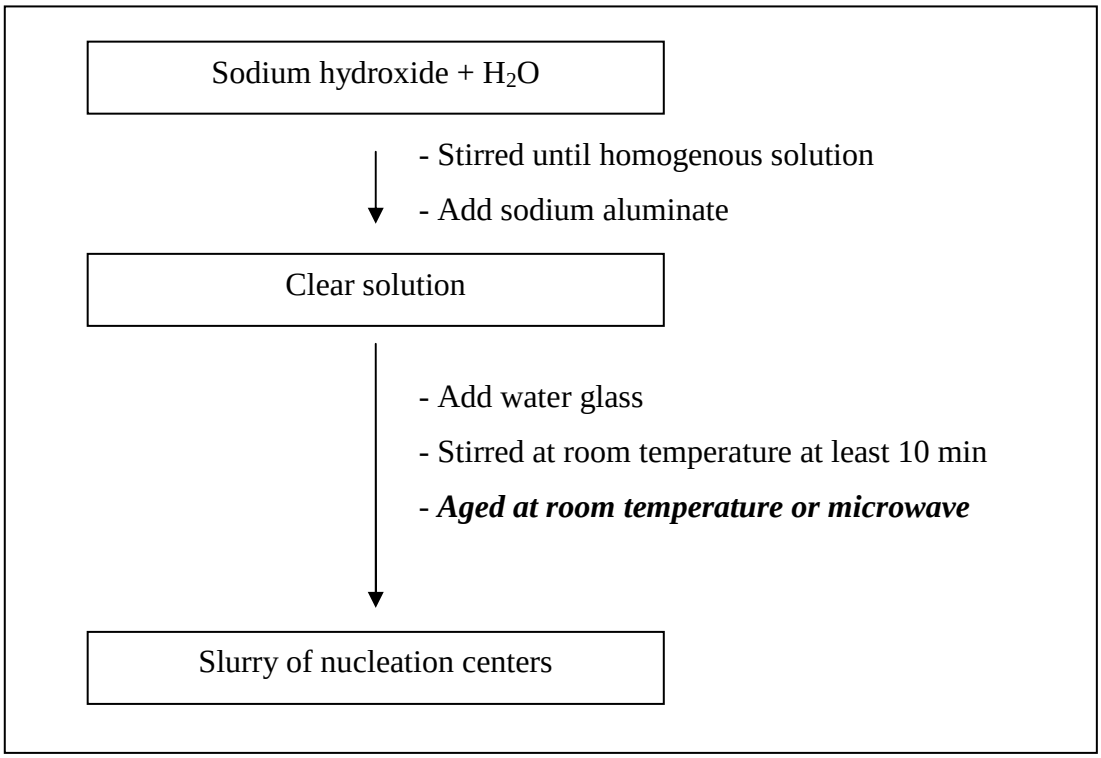

Scheme 3.3 Preparation diagram for nucleation centers.

3.3.2.2 Preparation of Y Zeolite crystals

Cryatals of Y Zeolite was synthesized from the gel mol composition ratio of 13.09 SiO_2: 5 Na_2O: Al_2O_3: 166.76 H_2O. In a typical procedure, 0.14 g of Sodium hydroxide and 13.09 g of sodium aluminate was dissolved in deionized water at room temperature under stirring. Then, 142.43 g of water glass was added dropwise and stirred until the gel appeared smooth. Moreover, nucleation centers were slowly added to feedstock gel, stirred at room temperature for 10 min. Then the molar ratio of the overall gel was 13.41 SiO_2: 5.41 Na_2O: Al_2O_3: 171 H_2O and transferred to Teflon-lined autoclave for hydrothermal crystallization at 90^oC for 24 hrs as shown in scheme 3.4. After the reaction was quenched, white solid sample was separated by filtration, washed with deionized water and dried in oven for overnight at 110°C. The sample is denoted as NaY-ART*x* where *x* is aging time in hour at room temperature and denoted as NaY-AMWx for microwave method.

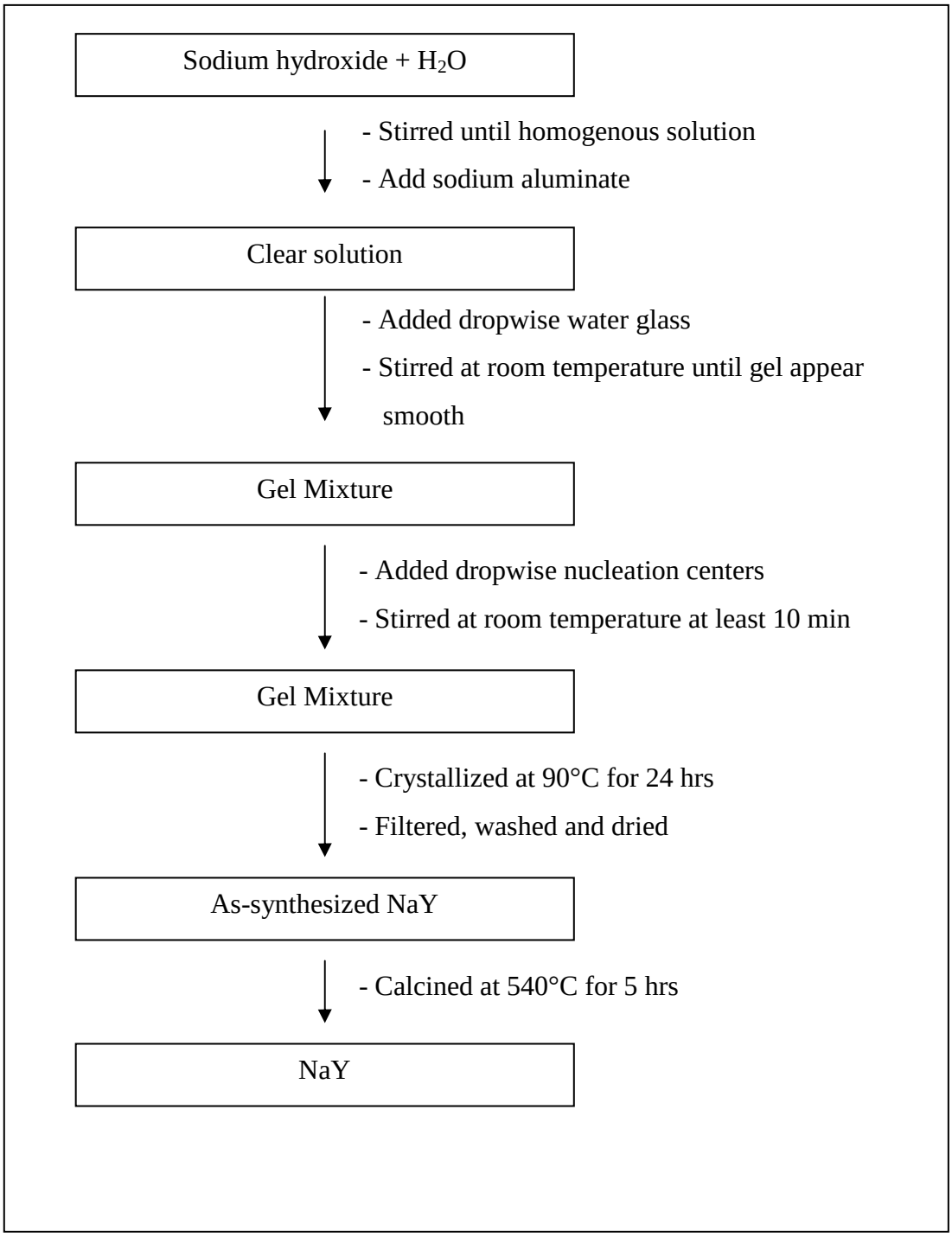

Scheme 3.4 Preparation diagram for Y-Zeolite by hydrothermal method.

3.3.3 Synthesis of X zeolite by hydrothermal and microwave methods

X zeolite synthesis was followed by the report by Ginter *et al*. [54]. A typical synthesis was same as Y zeolite synthesis except for changing ratio of Si/Al from 1.0 to 2.5.

3.4 Propyl sulfonic functionalized microporous and mesoporous materials

3 g of microporous or mesoporous material was suspended with (3-mercaptoproply)tri-methoxysilane and toluene, refluxed at 60^{o}C for 6 hrs. Then thiol groups were oxidized to sulfonic groups by 30%H_2O_2. The wet material was suspended in 0.2 M H_2SO_4 for 2 hrs [55]. Finally, the obtained product was filtered and dried in oven for overnight at 80^{o}C. For microporous materials (Y zeolite and X zeolites) were followed by above method except for changing H_2SO_4 concentration to 0.05-0.10 M stirring at room temperature for 0.5 hr.

3.4.1 Acid-base titration

The acid capacities of sulfonic acid groups in the functionalized mesoporous materials were quantified using 2M NaCl solution as the ion-exchange agent (Scheme 3.5). Approximately 0.05xx g of the catalysts was exchanged with 15 ml of solution for 30 min under constant agitation at room temperature and titration with 0.01 M NaOH by using phenolphthalein as indicator [56].

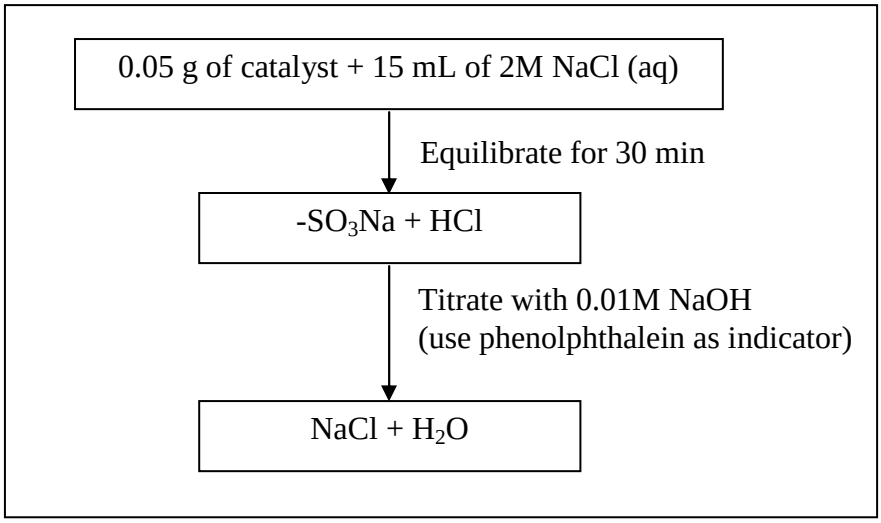

Scheme 3.5 Diagram for acid-base titration.

3.5 Procedure in biodiesel preparation

The synthesis of methyl ester was carried out in a round-bottomed flask fitted with a reflux condenser. In each experiment, 5 g of oleic acid and methanol using the prepared catalyst were added to a round-bottom flask or PARR reactor (Scheme 3.6). The reaction considers were 60 to 150^{o}C, 0.25 to 12 hrs, the catalyst loading 1 to 15% of reactant and the 3:1 to 15:1 molar ratio of methanol to oleic acid. The catalysts were separated from the reaction mixture by centrifuge and washed with acetone. The catalysts were dried at 60^{o}C for overnight and then used again.

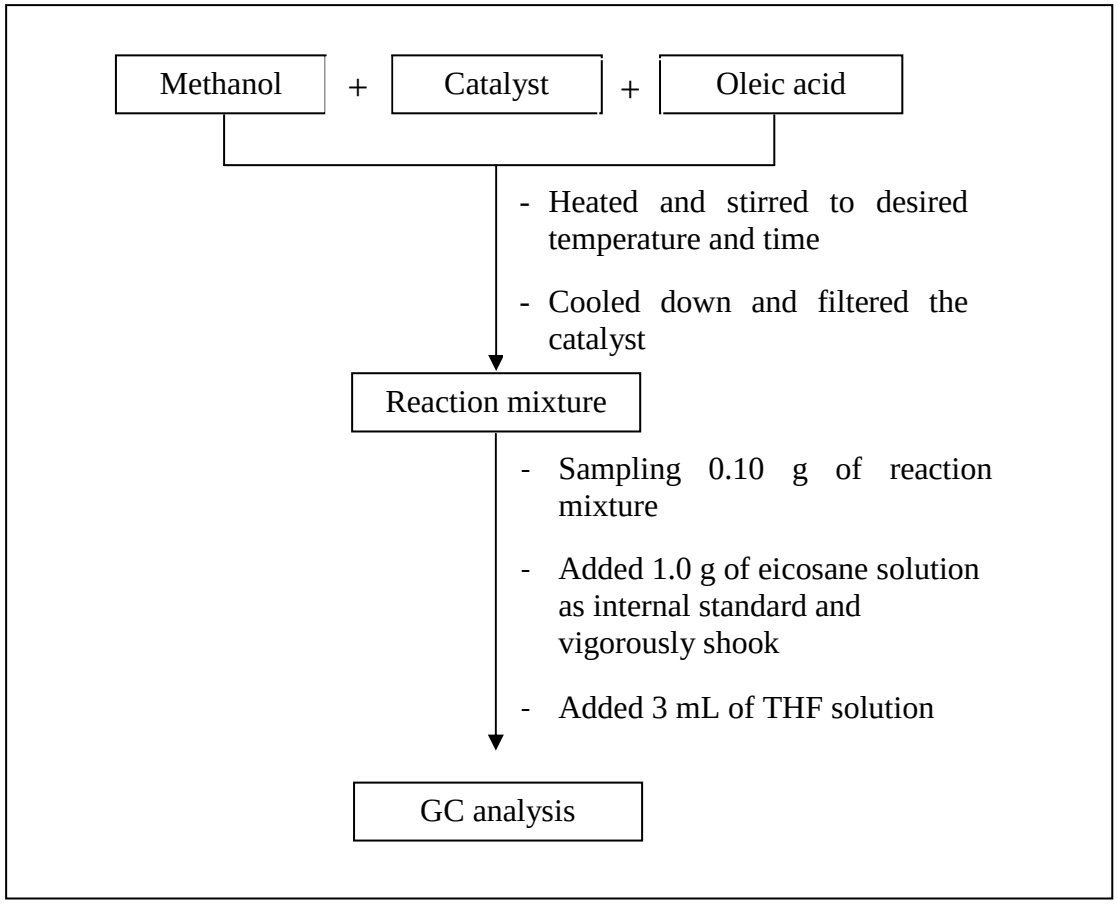

3.6 Recycle of catalysts

After the first reaction, the used catalyst was filtered and washed several times with acetone. The catalyst was dried at 80°C overnight, and then this catalyst was denoted as reused catalyst. The regenerated catalyst was grafting the used catalyst with MPMTS in toluene, H_2O_2 and H_2SO_4, respectively (Scheme 3.7). Then, catalyst was characterized by XRD, surface area analysis and SEM before testing in subsequent experiment. The reaction was performed in the similar way to described in Section 3.4.

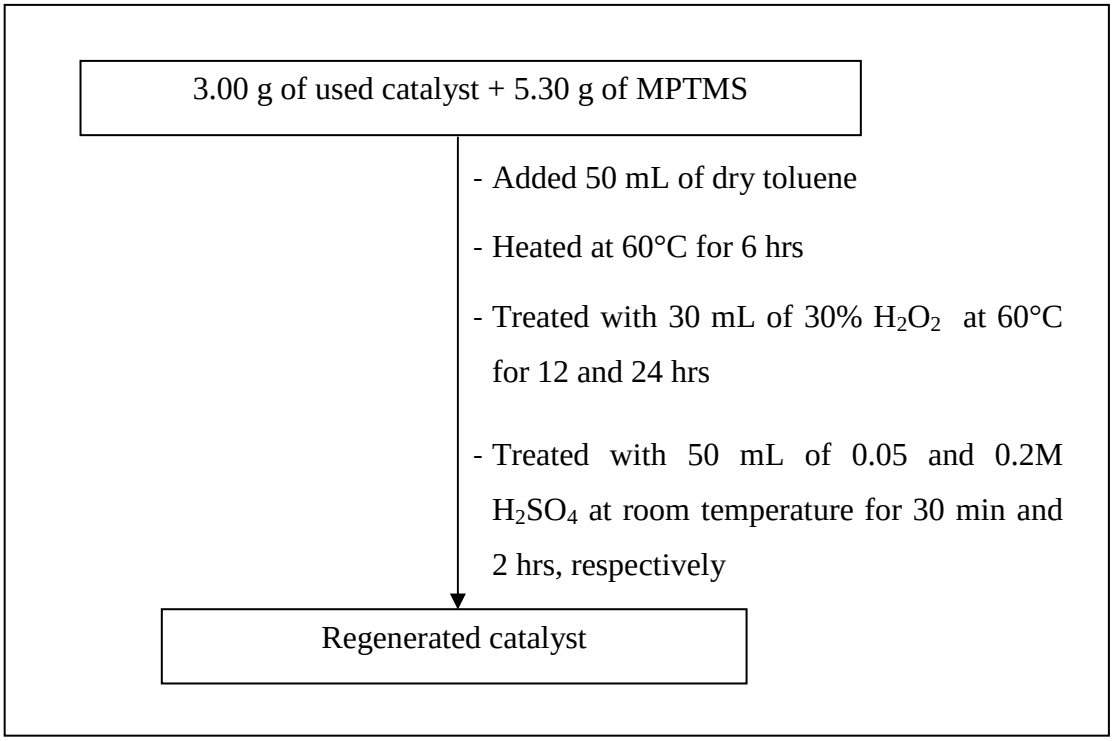

Scheme 3.7 Preparation diagram for regenerated catalyst.

CHAPTER IV

RESULTS AND DISCUSSION

4.1 Synthesis of SBA-15 catalysts

4.1.1 The physical properties of SBA-15

4.1.1.1 XRD results

The X-ray powder diffraction patterns of all SBA-15 materials synthesized by hydrothermal and microwave methods were showed in Figure 4.1 and Figure 4.2. All samples exhibited the typical pattern of hexagonal structure [13], SBA-15 exhibited the peak positions which had one very intense peak and two weak peaks indexed to (100), (110) and (200) diffractions, respectively. In the comparison with SBA-15-HT, diffractogram of the SBA-15 which was synthesized by microwave method shifted to higher value of 2-Theta meaning to lower d-spacing in pores structure. The SBA-15-MW2 under stirring showed the best condition in microwave synthetic method due to expressing highest intensity of 100 peak. For non stirring samples were exhibited lower intensity and surface area than stirring samples at the same crystallization time.

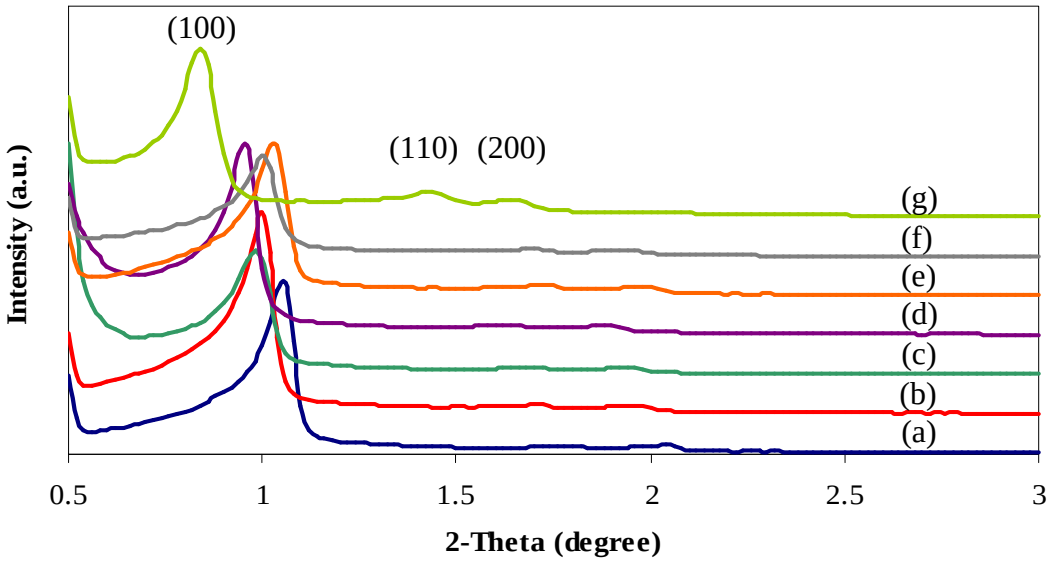

Figure 4.1 X-ray powder diffraction patterns of synthesized SBA-15 with microwave irradiation under stirring for 0.5 (a), 1.0 (b), 1.5 (c), 2.0 (d), 2.5 (e), 3.0 (f) in hour, respectively, prepared with hydrothermal method (g).

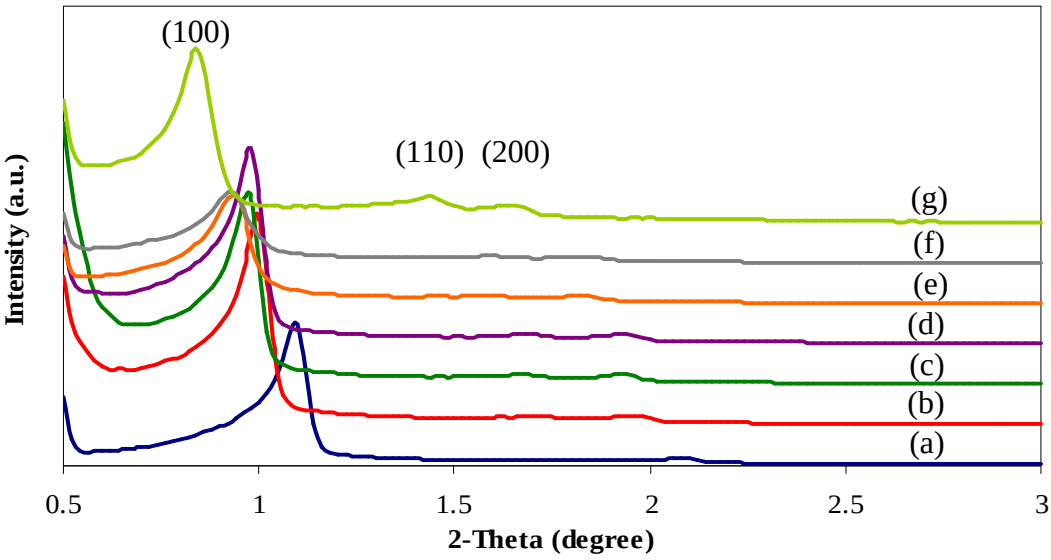

Figure 4.2 X-ray powder diffraction patterns of synthesized SBA-15 with microwave irradiation under without stirring for 0.5 (a), 1.0 (b), 1.5 (c), 2.0 (d), 2.5 (e), 3.0 (f) in hour, respectively, prepared with hydrothermal method (g).

4.1.1.2 Nitrogen adsorption-desorption

The N_2 adsorption-desorption isotherm and pore size distribution of synthesized SBA-15 by hydrothermal method (SBA-15-HT) were shown in Figure A-1 (in appendices). It performed a type IV adsorption isotherm of IUPAC classification which was a characteristic pattern of mesoporous materials and exhibited a hysteresis loop H1-type which the pores consisting of agglomerates or compacts of uniform spherical particles with regular arrays, whose pore size distribution was normally narrow [13]. The synthesized SBA-15 by hydrothermal method has pore diameter of 9.23 nm using Barrett-Joiner-Halenda (BJH) method. The total surface area was calculated using Brunauer, Emmett and Teller (BET) equation, which was found as 791 m^2/g. Synthesized samples by microwave methods revealed that SBA-15-MW2-stir exhibited high surface area as 810 m^2/g with wall thickness *ca.* 5.69 nm which higher than previous report by Park *et al*. which has surface area as 565 m^2/g and wall thickness as 4.55 nm [16], indicating the thermal stability should be higher than SBA-15-HT. Moreover, total surface area was decreased when stirring time was increased. However, these materials contained lower pore volume and narrower pore diameter than SBA-15-HT corresponding to XRD result. For synthesis samples under non-stirring condition, the energy might not spread throughout the mixture then gave random result in this condition.

From the *d*-spacing of the (100) reflection plane and the pore size distribution determined by N_2 adsorption, the estimated mean thickness of the pore walls of the mesoporous silicas could be calculated based on the equation as follows [57]:

Wall thickness = a_0-pore size

Where; $a_0 = 2 \times d_{(100)} / \sqrt{3}$

$d_{(100)}$ = *d*-spacing of the (100) reflection plane from XRD method

Table 4.1 Textural properties of synthesized SBA-15 with hydrothermal method, prepared with microwave method for 0.5, 1.0, 1.5, 2.0, 2.5 and 3.0 hrs under stirring and without stirring.

Catalyst	Total specific surface area[a] ($m^2 \cdot g^{-1}$)	Pore size distribution[b] (nm)	Mesopore volume ($cm^3 \cdot g^{-1}$)	Wall thickness[c] (nm)
SBA-15-HT	791	9.23	1.07	2.92
SBA-15-MW0.5-stir	606	5.41	0.50	4.27
SBA-15-MW1.0-stir	691	6.18	0.57	4.06
SBA-15-MW1.5-stir	775	6.18	0.62	4.29
SBA-15-MW2.0-stir	810	6.18	0.65	5.69
SBA-15-MW2.5-stir	734	6.18	0.68	3.81
SBA-15-MW3.0-stir	735	6.18	0.69	4.03
SBA-15-MW0.5-nostir	523	5.41	0.42	3.91
SBA-15-MW1.0-nostir	676	6.18	0.56	4.07
SBA-15-MW1.5-nostir	744	6.18	0.62	4.30
SBA-15-MW2.0-nostir	762	6.18	0.64	4.27
SBA-15-MW2.5-nostir	670	6.18	0.61	4.70
SBA-15-MW3.0-nostir	730	7.05	0.65	4.02

[a]Calculated using the BET plot method,
[b]Calculated using the BJH method,
[c]Calculated as: a_0-pore size ($a_0 = 2 \times d_{(100)} / \sqrt{3}$)

4.1.1.3 SEM images

The SEM images of pure synthesized SBA-15 by hydrothermal method (SBA-15-HT) at different magnifications were illustrated in Figure 4.3. Morphology of SBA-15-HT was uniform rope-like particle shape aggregated particles. Furthermore, the average size of particle was 0.59 × 0.79 μm which small in comparison previous report by Stuck *et al*. that was 1 μm.

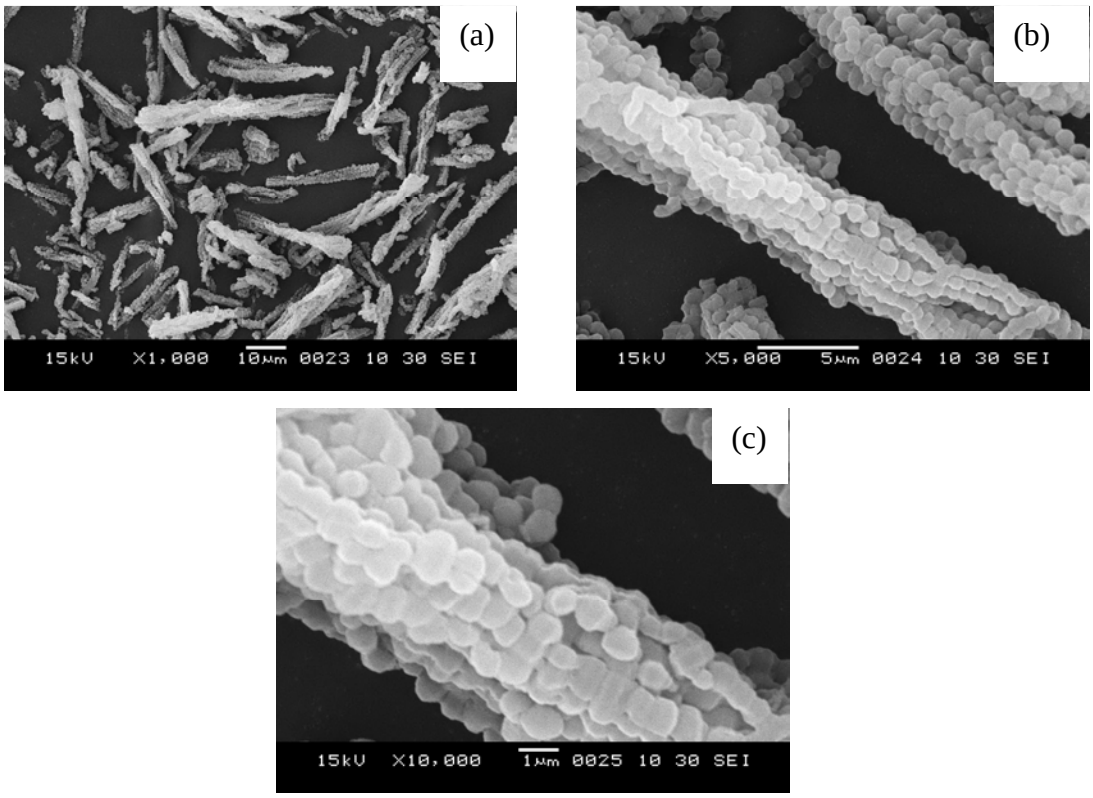

Figure 4.3 SEM images of synthesized SBA-15 with hydrothermal method at different magnifications: ×1000 (a), ×5,000 (b), and ×10,000 (c).

SEM images of prepared mesoporous SBA-15 by microwave methods (MW0.5-MW2) has similar morphology to synthesized SBA-15 via hydrothermal method were showed in Figure 4.4. The images showed uniform aggregated rope-like particles when compared to Park *et al.* exhibited cubic morphology which mesostructure morphology is depending on the microwave-irradiation times [58]. Moreover, crystallization with stirring longer than 2 hrs, the particle shape was changed to strand shape. Hence, the optimum crystallization time for synthesis by

microwave method is 2 hrs. Synthesized SBA-15 by microwave was faster than hydrothermal method as 24 times because it can increase dissolve solubility and also particle formation.

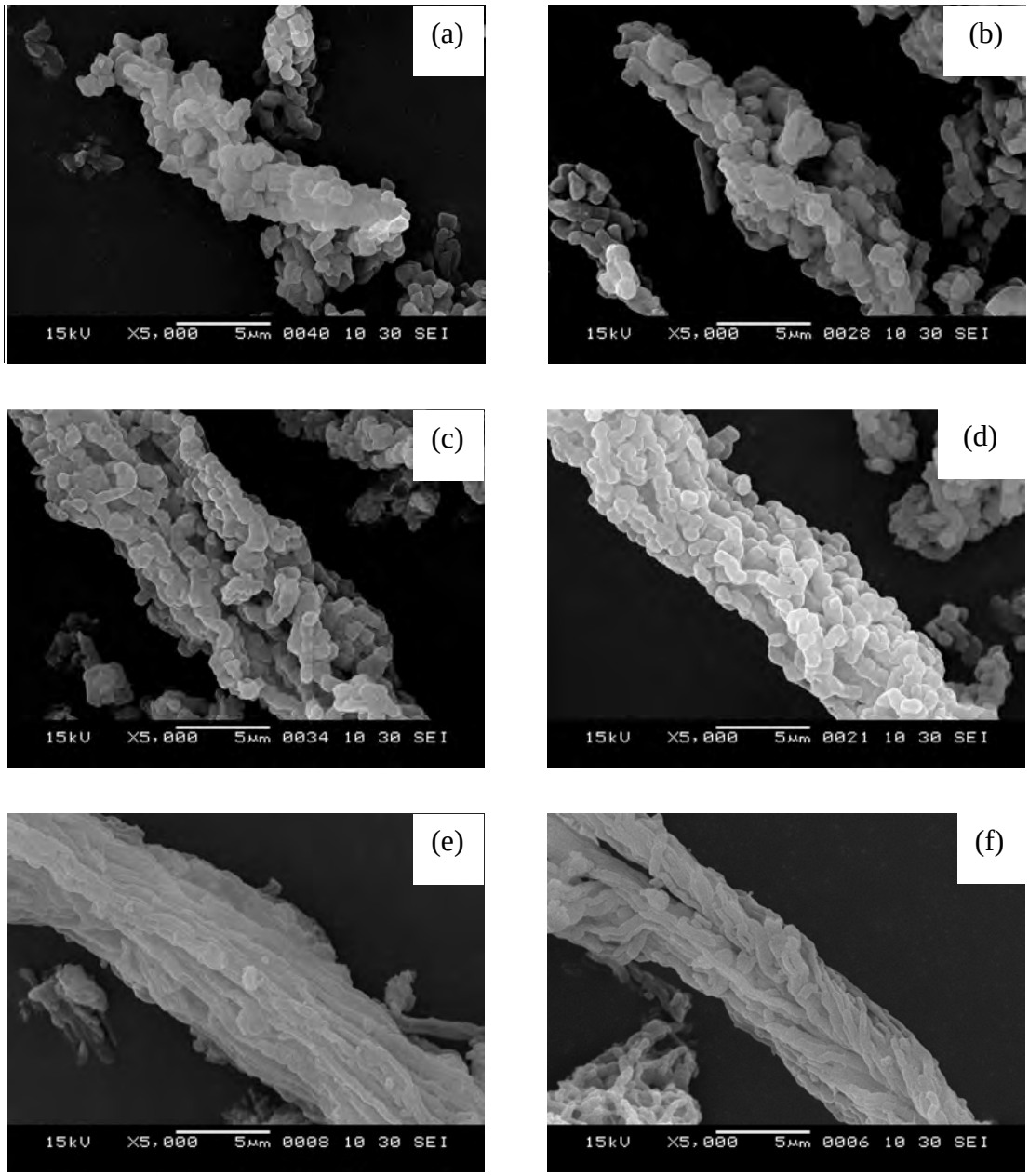

Figure 4.4 SEM images of synthesized SBA-15 with microwave at different crystallization time under stirring for 0.5 (a), 1.0 (b), 1.5 (c), 2.0 (d), 2.5 (e), 3.0 (f) in hour, respectively.

4.1.2 Thermal stability of SBA-15

4.1.2.1 XRD results

The hydrothermal stability test of synthesized SBA-15 by hydrothermal method (SBA-15-HT) and microwave method (SBA-15-MW2-stir) was examined by heating sample in boiling water for 24 hrs under reflux [59]. After hydrothermal stability test, both samples remained hexagonal structure. The crystallinity of SBA-15-MW2-stir sample decreased less than SBA-15-HT after treatment (Figure 4.5). After hydrothermal stability test, peaks of materials were shifted to higher 2-Theta value due to decreasing in wall thickness as shown in Table 4.2.

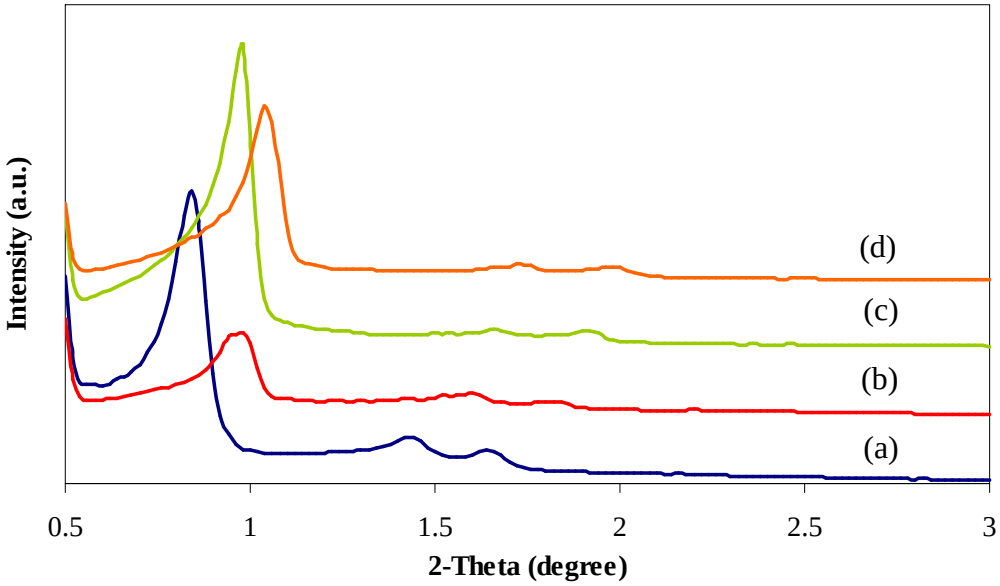

Figure 4.5 X-ray powder diffraction patterns of synthesized SBA-15 with hydrothermal method before (a), after (b) hydrothermal stability test and synthesized SBA-15 with microwave method before (c), after (d) hydrothermal stability test.

4.1.2.2 Nitrogen adsorption-desorption

N_2 adsorption-desorption isotherms and pore size distributions of SBA-15-HT and SBA-15-MW2-stir after hydrothermal stability test were presented in Figure A-2 and Figure A-3 (in appendices), respectively. The N_2 adsorption isotherms of both samples remained type IV. The pore diameter and pore volume were increased while wall thickness was decreased after hydrothermal stability test (Table 4.2). A relatively obviously decreasing on the wall thickness and surface area because of the collapse of mesostructures and reconstruction of frameworks can be observed by the SEM [59-60].

Table 4.2 Textural properties of synthesized SBA-15 with hydrothermal and microwave method before and after thermal stability test.

Catalyst	Total specific surface area[a] ($m^2 \cdot g^{-1}$)	Pore size distribution[b] (nm)	Mesopore volume ($cm^3 \cdot g^{-1}$)	Wall thickness[c] (nm)
SBA-15-HT (before)	791	9.23	1.07	2.92
SBA-15-HT (after)	554	10.57	1.09	1.22
SBA-15-MW2-stir (before)	810	6.18	0.65	5.69
SBA-15-MW2-stir (after)	547	7.05	0.68	3.63

[a]Calculated using the BET plot method,
[b]Calculated using the BJH method,
[c]Calculated as: a_0-pore size ($a_0 = 2 \times d_{(100)} / \sqrt{3}$)

4.1.2.3 SEM images

Additionally, SEM images (Figure 4.6) exhibited the same morphology SBA-15-MW2-stir as before hydrothermal stability test whereas SBA-15-HT, the rope-like morphology, was reduced to small particles. All these results demonstrated that the SBA-15-MW2-stir sample exhibited higher hydrothermal stability under reflux with water for 24 hrs. than the hydrothermal synthesized sample.

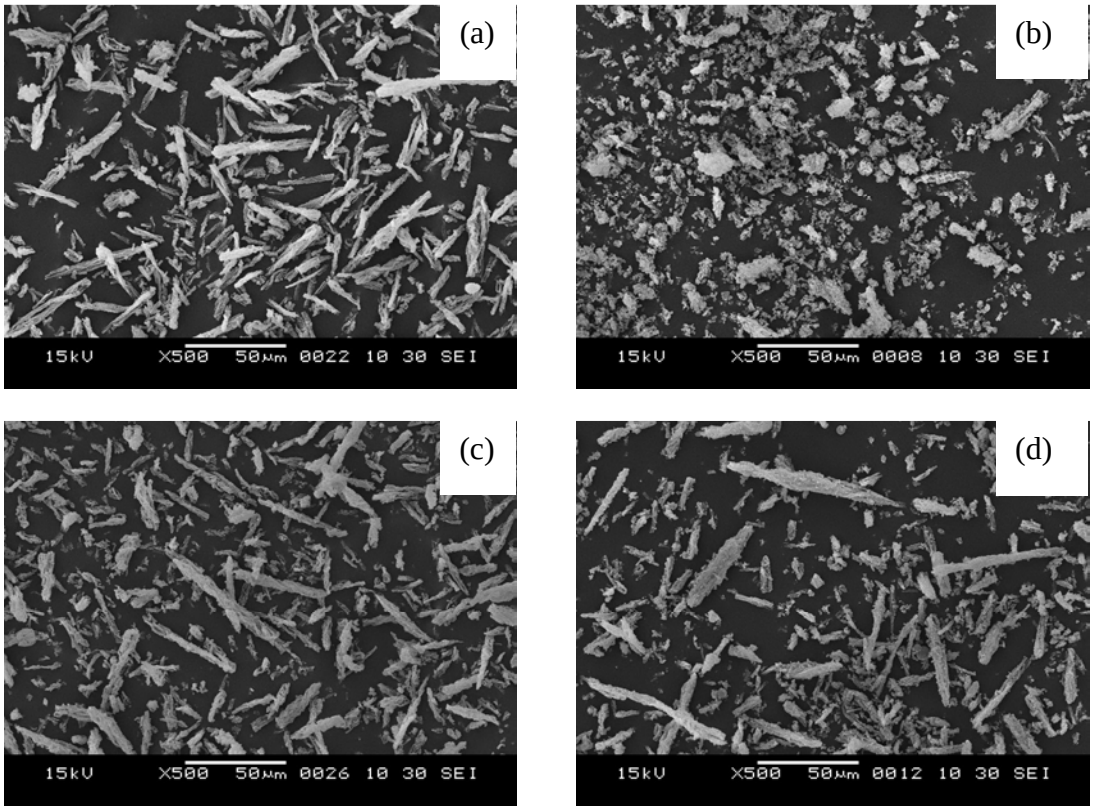

Figure 4.6 SEM images of synthesized SBA-15 with hydrothermal method before (a), after (b) hydrothermal stability test and synthesized SBA-15 with microwave method before (c), after (d) hydrothermal stability test.

4.1.3 The physico-chemical properties of sulfonic functionalized SBA-15

4.1.3.1 XRD results

The XRD pattern of sulfonic acid functionalized SBA-15 catalysts synthesized by hydrothermal and microwave methods were showed in Figure 4.7. The sulfonic functionalized SBA-15 exhibited lower crystallinity compared to pure SBA-15 due to incorporation of organo sulfonic group in mesoporous material. In comparison with SBA-15, the diffraction peaks of sulfonic functionalized SBA-15 materials were slightly shifted to higher 2 theta values, indicating the presence of bulky functional group on the surface of SBA-15 would decrease void volume and wall thickness.

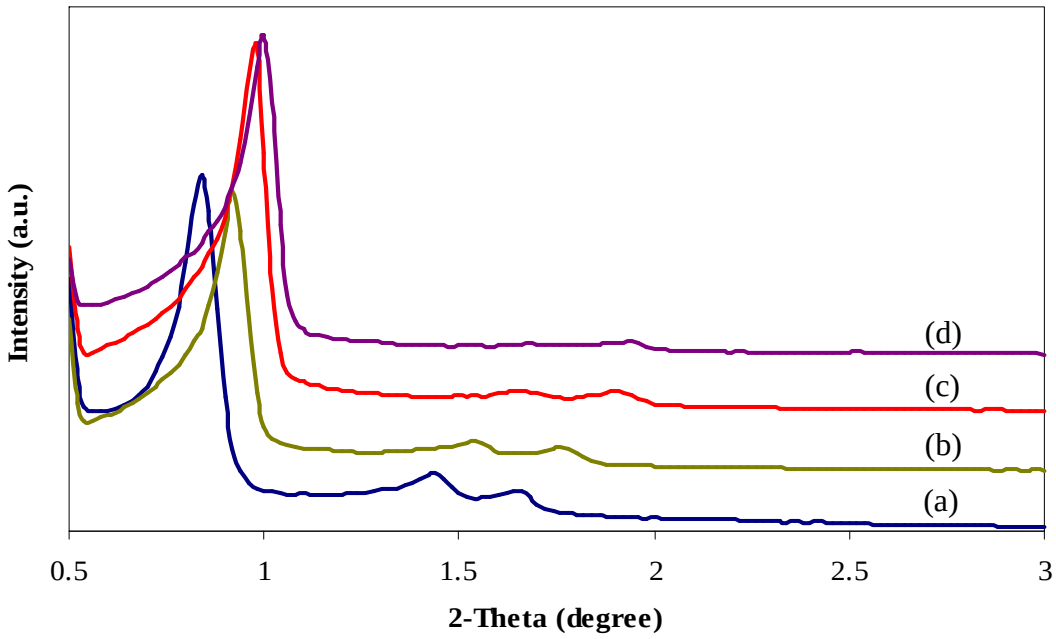

Figure 4.7 X-ray powder diffraction patterns of synthesized SBA-15 with hydrothermal method before (a), after (b) sulfonic functionalization and synthesized SBA-15 with microwave method before (c), after (d) sulfonic functionalization.

4.1.3.2 Nitrogen adsorption-desorption

The N_2 adsorption-desorption isotherm of functionalized SBA-15 catalysts indicated the presence of type IV isotherm with H1 hysteresis loops [16]. Some physical properties derived from the adsorption isotherm of SBA-15 and sulfonic functionalized samples were complied in Table 4.3. SBA-15-HT-SO_3H and SBA-15-MW2-stir-SO_3H samples exhibited lower surface area and mesopore volume when compared with the pure SBA-15 because the organo sulfonic functional transfer into pore structure that was corresponding with their intensity of XRD pattern results. Moreover, it also induced decreasing of surface area and pore volume.

Table 4.3 Textural properties of SBA-15 and sulfonic functionalized SBA-15.

Catalyst	Total specific surface area[a] ($m^2 \cdot g^{-1}$)	Pore size distribution[b] (nm)	Mesopore volume ($cm^3 \cdot g^{-1}$)	Wall thickness[c] (nm)	Particle size (μm) width x length
SBA-15-HT	791	9.23	1.07	2.92	0.59 x 0.79
SBA-15-HT-SO_3H	370	9.23	0.79	1.87	0.47 x 1.07
SBA-15-MW2-stir	810	6.18	0.65	5.69	0.67 x 0.86
SBA-15-MW2-stir-SO_3H	462	6.18	0.54	4.23	0.66 x 0.98

[a]Calculated using the BET plot method,
[b]Calculated using the BJH method,
[c]Calculated as: a_0-pore size ($a_0 = 2 \times d_{(100)} / \sqrt{3}$)

4.1.3.3 SEM images

The SEM images of functionalized SBA-15 at different magnifications were showed in Figure 4.8. The SBA-15-HT-SO_3H and SBA-15-MW2-stir-SO_3H samples display a similar morphology as pure SBA-15.

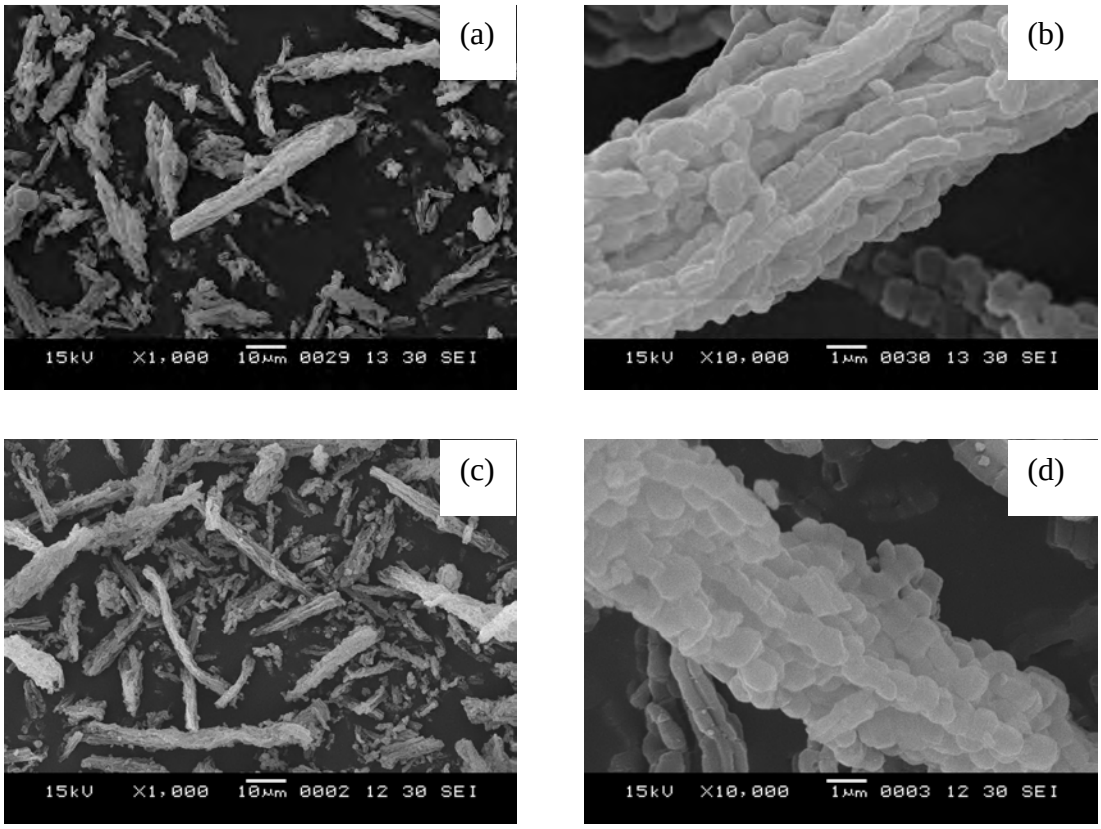

Figure 4.8 SEM images of SBA-15-HT-SO_3H at different magnifications: x 1000 (a), x 10,000 (b), and SBA-15-MW2-stir-SO_3H x 1000 (c), x 10,000 (d).

4.1.3.4 Elemental analysis and acid-base titration

The number of sulfonic acid groups in the mesoporous silica was measured quantitatively by acid-base titration using NaCl as ion-exchange agent. The sulfur content of the modified mesoporous silica were determined by sulfur analysis complied in Table 4.4. In this work, the acid value and sulfur content of SBA-15-HT-SO_3H was higher than SBA-15-MW2-stir-SO_3H due to the large pore diameter of prepared SBA-15 by hydrothermal method thus, the organosulfonic group could be easy incorporate into the pore.

Table 4.4 Sulfur analysis and acid value of sulfonic functionalized SBA-15.

Catalyst	Pore size distribution (nm)	Sulfur analysis[a] (wt%)	H^+ content[b] (mmol/g)
SBA-15-HT-SO_3H	9.23	2.77	2.13
SBA-15-MW2-stir-SO_3H	6.18	1.31	1.93

[a]Sulfur analysis, measured from Sulfur analyzer,
[b]Acid capacity defined as millimole of acid centers per gram of catalyst, obtained directly by titration (mmol H^+/g)

4.1.3.5 Acidity of catalysts

The acid site distribution and acid amount of SBA-15-HT-SO_3H and SBA-15-MW2-stir-SO_3H samples were determined by NH_3-TPD measurements. The NH_3-TPD profiles of both samples were shown in Figure A-4 (in appendices). The desorption temperature of NH_3 depends on the strength of acid site [55]. Because the NH_3 desorption peak associated with difference acid sites cannot be isolated from each other. The results indicated that the number of acid site in SBA-15-HT-SO_3H is higher than SBA-15-MW2-stir-SO_3H due to the large pore diameter of prepared SBA-15 by hydrothermal method as shown in Table 4.5.

Table 4.5 The quantity of acidic sites of SBA-15-HT-SO_3H and SBA-15-MW2-stir-SO_3H.

Catalyst	The number of acid site (arbitrary unit/g)
SBA-15-HT-SO_3H	1.84
SBA-15-MW2-stir-SO_3H	1.45

4.2 Synthesis of Y zeolite catalysts

4.2.1 The physical properties of Y zeolite

4.2.1.1 XRD results

XRD patterns of sample denoted as MW, which were synthesized with microwave irradiation for various periods in aging time were presented in Figure 4.9 in comparison with the one prepared by hydrothermal method without microwave irradiation and standard Y zeolite (Aldrich). All XRD patterns of samples showed the typical characterization pattern of faujasite (FAU) structure when compared to joint committee of powder diffraction standard (JCPDS 38-2039) and no other crystalline phases were observed [61].

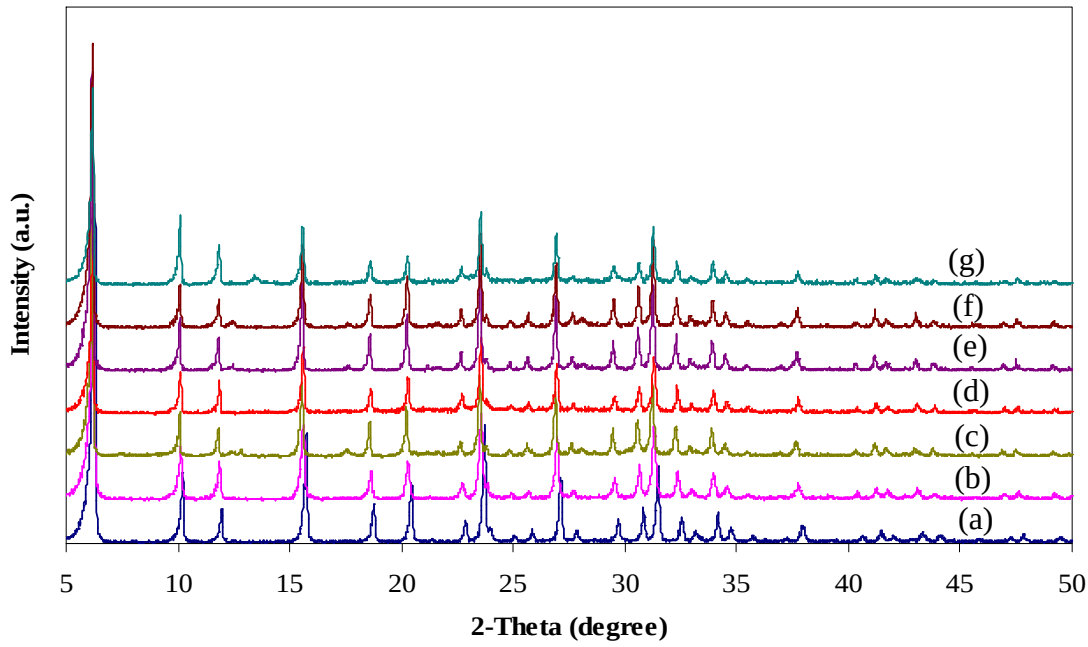

Figure 4.9 X-ray powder diffraction patterns of standard Y zeolite (a), prepared with hydrothermal method (b), synthesized with microwave irradiation prior to hydrothermal method for 0.5 (c), 1.0 (d), 2.0 (e), 3.0 (f), 4.0 (g), in hour, respectively.

The synthetic Y zeolite by hydrothermal method from this work has 85.70% crystallinity when compared to standard Y zeolite (Aldrich). Moreover, the synthesized Y zeolite by microwave method exhibited the highest % crystallinity at 2 hrs when increasing crystallization time the %crystallinity was decreased due to the partially dissolving of Y zeolite particles crystals as shown in Table 4.6. Moreover, the microwave method can be reducing the synthesis time because it can increase solubility and also rate of seed formation. The method for determining the percent crystallinity was calculated by:

$$\%\text{Crystallinity} = (\sum I_u / \sum I_s) \times 100$$

Here $\sum I_u$ and $\sum I_s$ represented the sum of characteristic peak intensity of unknown (synthetic Y zeolite) and standard (Y zeolite from Aldrich) at Bagg's angle 2θ of 6.3, 10.2, 11.9, 15.7, 18.8, 20.4, 23.7, 27.1, 30.8 and 31.4 in XRD data. The NaY-AMW2 was selected to be the test condition for further studies due to its highest % crystallinity. From the result exhibited microwave energy could be reduced period time about 60 times in aging step compared to hydrothermal synthesis method.

Table 4.6 Percent crystallinity of standard and synthetic Y zeolites various aging time for 0.5 to 4 hours.

Sample	**% Crystallinity**
Standard Y Zeolite (Aldrich)	100%
NaY-ART120 (hydrothermal method)	85.70%
NaY-AMW0.5 (microwave method)	68.48%
NaY-AMW1	51.90%
NaY-AMW2	79.59%
NaY-AMW3	76.74%
NaY-AMW4	57.61%

4.2.1.2 Nitrogen adsorption-desorption

The N_2 adsorption-desorption isotherm and pore size distribution of synthesized Y zeolite catalysts by hydrothermal method were showed in Figure A-5 (in appendices). All samples were fitted as type I isotherm, characteristic of microporous materials [62]. The textural properties of all samples were listed in Table 4.7. Synthetic Y zeolite via microwave method showed bigger particle size than hydrothermal sample. The BET total specific surface area (all surface area included external and internal surface area) and external surface area of microwave prepared sample were slightly lower than hydrothermal prepared one. All synthetic materials showed pore size of 0.6 nm.

Table 4.7 Textural properties of Y zeolite samples; prepared with hydrothermal method and synthesized with microwave irradiation for 0.5, 1.0, 2.0, 3.0 and 4.0 hrs in aging time, respectively.

Catalyst	Total specific surface area[a] ($m^2 \cdot g^{-1}$)	External surface area[b] ($m^2 \cdot g^{-1}$)	Micropore volume[b] ($cm^3 \cdot g^{-1}$)	Pore size distribution[c] (nm)
NaY-ART120	832	27	0.30	0.6
NaY-AMW0.5	706	7	0.27	0.6
NaY-AMW1	544	3	0.20	0.6
NaY-AMW2	824	8	0.31	0.6
NaY-AMW3	830	9	0.31	0.6
NaY-AMW4	651	11	0.24	0.6

[a]Calculated using the BET plot method,
[b]Calculated using the t-plot method,
[c]Calculated using the MP-plot method,

4.2.1.3 SEM images

The SEM images of all samples were showed in Figure 4.10. The particles of all samples showed a cubic-like morphology. The particle shape and surface appearance of these samples exhibited very similar except for particle size of synthetic sample as 1.93 μm via microwave was larger than synthesized Y zeolite as 0.47 μm by hydrothermal method.

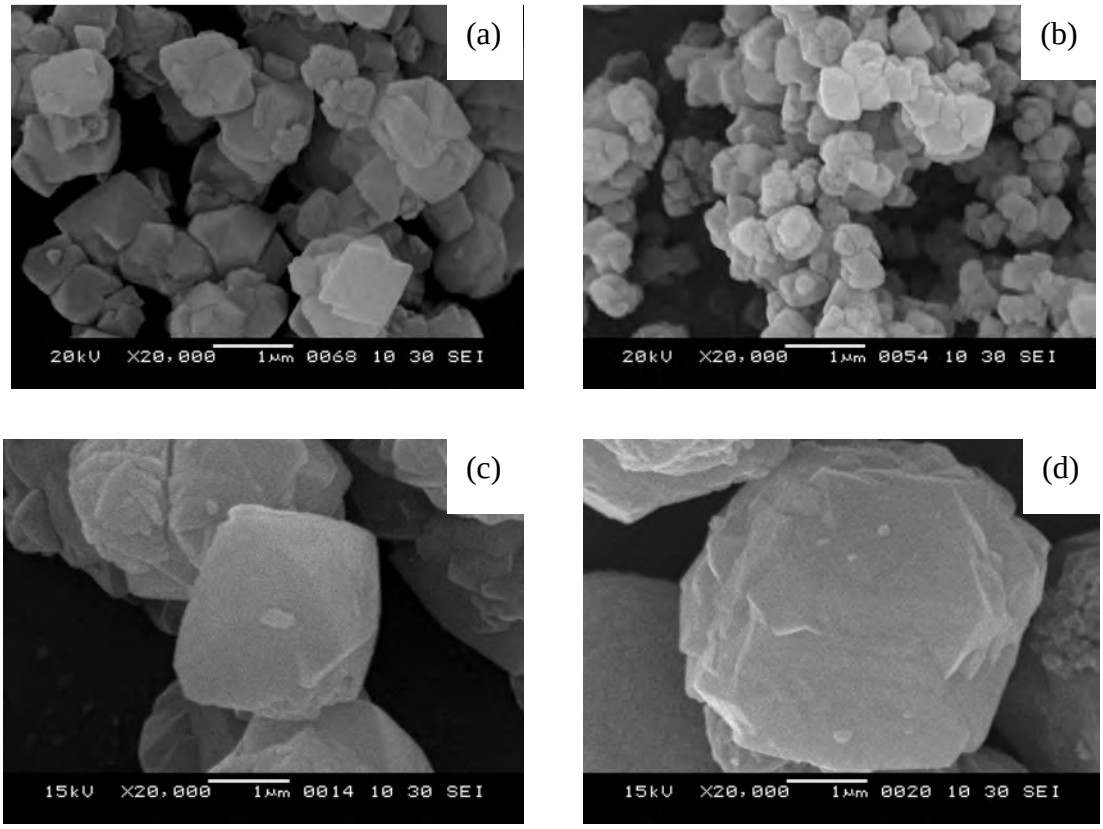

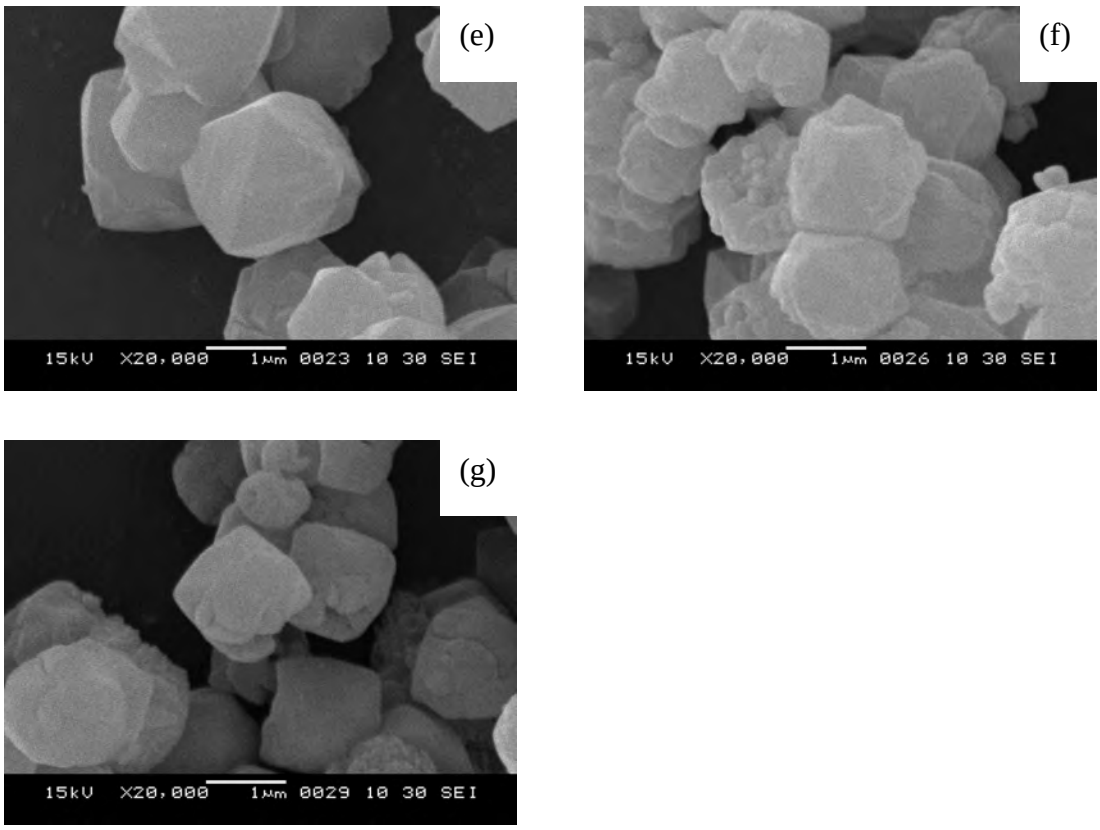

Figure 4.10 SEM images of Y zeolite samples: standard Y zeolite (Aldrich) (a), prepared with hydrothermal method (b), synthesized with microwave irradiation for 0.5 (c), 1.0 (d), 2.0 (e), 3.0 (f) and 4.0 (g) hrs in aging time, respectively.

4.2.2 The physico-chemical properties of sulfonic functionalized Y zeolite

4.2.2.1 XRD results

The XRD patterns of sulfonic acid functionalized Y zeolite catalysts synthesized by hydrothermal method were showed in Figure 4.11. The sulfonic functionalized Y zeolite could not prepare by the same method as SBA-15 because zeolite structure was destroyed (Figure 4.11(a)) due to long oxidization time and high acid concentration. Therefore, the oxidization time and concentration of H_2SO_4 were reduced from 24 to 12 hrs and 0.20 to 0.05-0.10 M, respectively. As a result, the synthesized materials still obtained the Y zeolite structure which 0.05 M of H_2SO_4 and 12 hrs of oxidization time was the optimum condition for Y zeolite sulfonic acid functionalization.

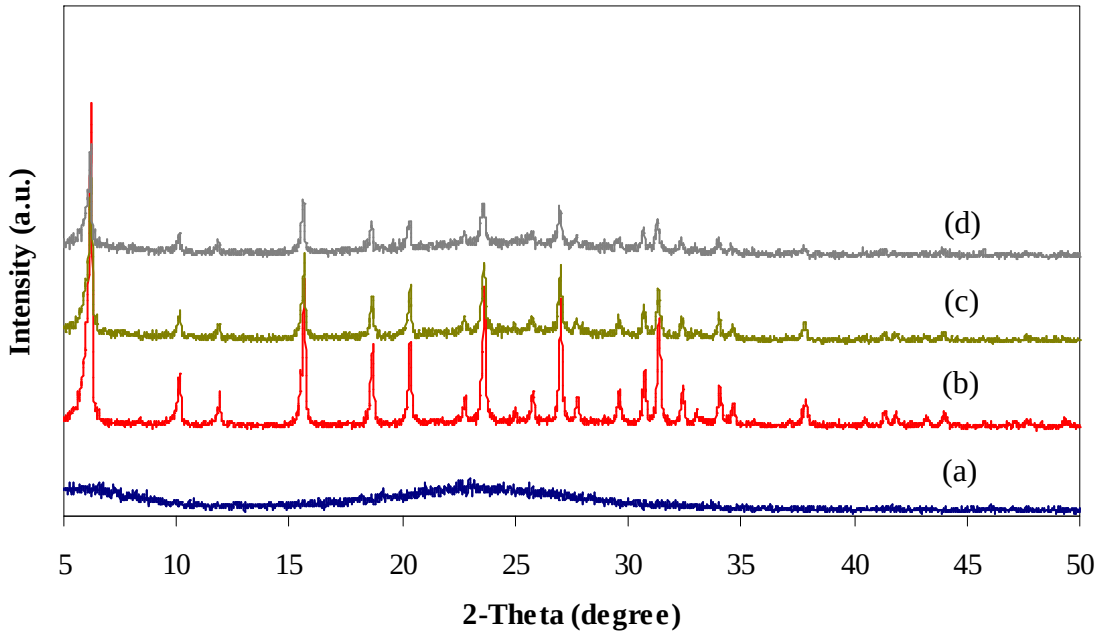

Figure 4.11 XRD patterns of sulfonic functionalized of Y zeolite by hydrothermal method; the same method of SBA-15 (a), oxidation step for 12 hrs and acidify with 0.05 M H_2SO_4 (b), oxidation step for 12 hrs and acidify with 0.075 M H_2SO_4 (c), oxidation step for 12 hrs and acidify with 0.1 M H_2SO_4 (d).

The suitable condition for sulfonic functionalization was applied to other Y zeolite samples. The XRD patterns of sulfonic acid functionalized Y zeolite catalysts synthesized by hydrothermal and microwave methods were showed in Figure 4.12. The results showed similar pattern as pure Y zeolite which slightly decreased in its crystallinity.

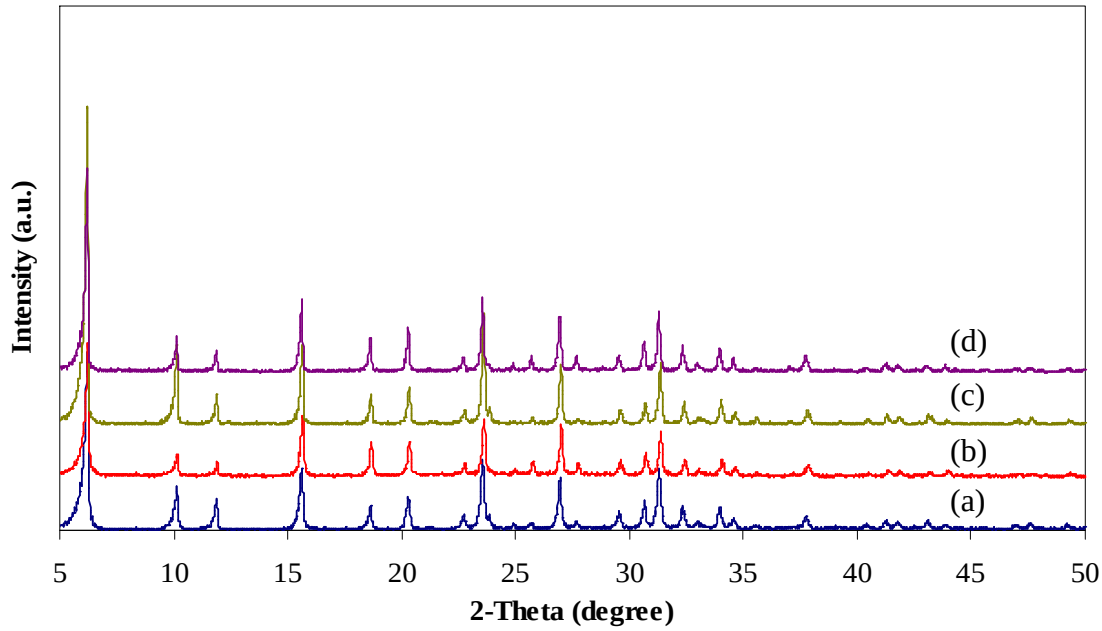

Figure 4.12 X-ray powder diffraction patterns of sulfonic functionalized of Y zeolite by oxidation step for 12 hrs and acidify with 0.05 M H_2SO_4; NaY-ART120 (a), NaY-ART120-SO_3H (b), NaY-AMW2 (c), NaY-AMW2-SO_3H (d).

4.2.2.2 Nitrogen adsorption-desorption

The N_2 adsorption-desorption isotherm of functionalized Y zeolite catalysts indicated the presence of type I isotherm. Some physical properties derived from the adsorption isotherm of Y zeolite and sulfonic functionalized samples were complied in Table 4.8. NaY-ART120-SO_3H and NaY-AMW2-SO_3H samples exhibited lower surface area compared with the pure Y zeolite because the sulfonic functional group were transferred into pore structure that corresponding with their intensity of XRD pattern results. Moreover, it also induced decreasing of pore volume. The external surface area of NaY-AMW2-SO_3H was increase due to the smaller particle size.

Table 4.8 Textural properties of Y zeolite and sulfonic functionalized Y zeolite**.**

Catalyst	Total specific surface area[a] ($m^2 \cdot g^{-1}$)	External surface area[b] ($m^2 \cdot g^{-1}$)	Micropore volume[b] ($cm^3 \cdot g^{-1}$)	Pore size distribution[c] (nm)	Particle size (μm)
NaY-ART120	832	27	0.30	0.6	0.47
NaY-ART120-SO_3H	195	13	0.07	0.6	0.47
NaY-AMW2	824	8	0.31	0.6	1.93
NaY-AMW2-SO_3H	257	10	0.11	0.6	1.78

[a]Calculated using the BET plot method,
[b]Calculated using the t-plot method,
[c]Calculated using the MP-plot method,

4.2.2.3 SEM images

The SEM images of functionalized Y zeolites at different magnifications were showed in Figure 4.13. The NaY-ART120-SO_3H and NaY-AMW2-SO_3H samples displayed a similar morphology as pure of theirs Y zeolites which particle size was 0.47 μm and 1.78 μm, respectively.

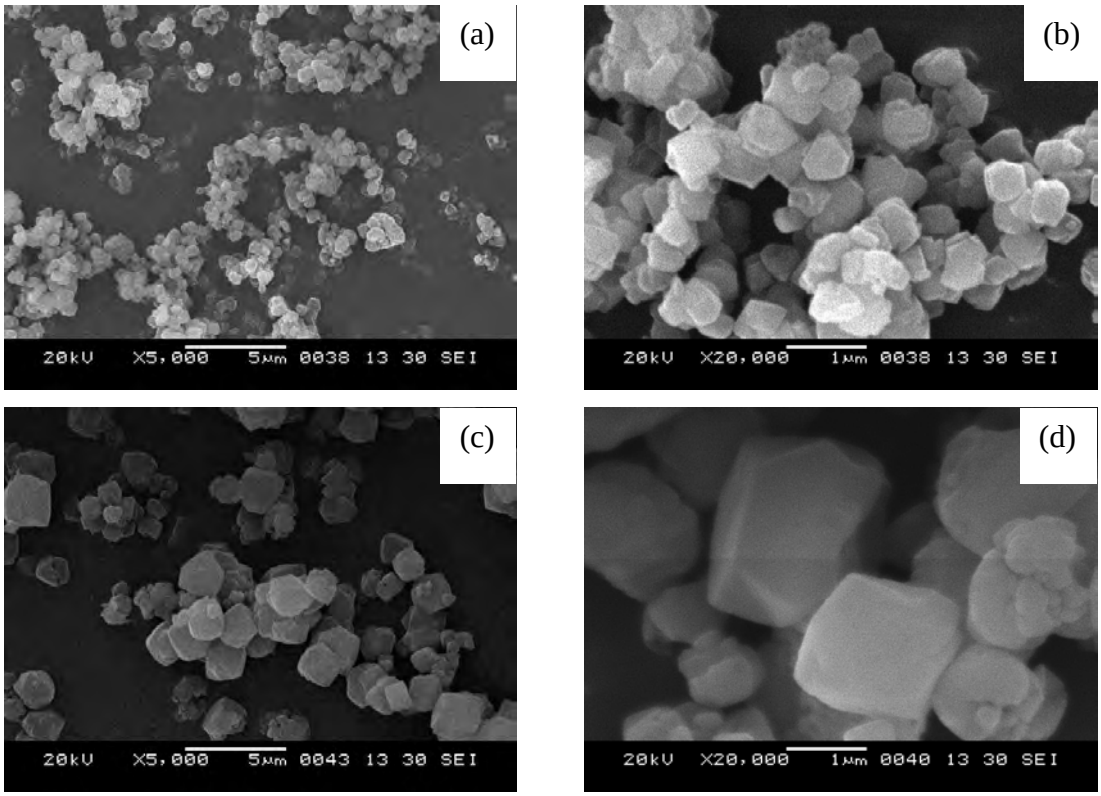

Figure 4.13 SEM images of functionalized of Y zeolite by hydrothermal method at different magnifications; x 5,000 (a), x 20,000 (b) and functionalized of Y zeolite by microwave method; x 5,000 (c), x 20,000 (d).

4.2.2.4 Elemental analysis and acid-base titration

The number of sulfonic acid groups in the Y zeolite was measured quantitatively by acid-base titration using sodium chloride as ion-exchange agent. The sulfur content of the modified zeolite was determined by sulfur analysis were complied in Table 4.9. In this work, the acid value and sulfur content of NaY-AMW2-SO_3H was higher than NaY-ART120-SO_3H because the microwave synthetic had higher pore volume.

Table 4.9 Sulfur analysis and acid value of sulfonic functionalized Y zeolite.

Catalyst	Sulfur analysis[a] (wt%)	H^+ content[b] (mmol/g)
NaY-ART120-SO_3H	0.17	1.69
NaY-AMW2-SO_3H	0.25	1.84

[a]Sulfur analysis, measured from Sulfur analyzer,
[b]Acid capacity defined as millimole of acid centers per gram of catalyst, obtained directly by titration (mmol H^+/g)

4.2.2.5 Acidity of catalysts

From NH_3-TPD experiment, total amount of ammonia desorbed was related to the number of acid site whereas the maximum temperature of desorption provided an indication of acid strength. The NH_3-TPD profiles of both samples were showed in Figure A-6 (in appendices). There were two peaks of Y zeolite, one was low temperature corresponding to desorption of the adsorbed NH_3 on weaker acid sites and the other found at high temperature corresponding to desorption of the adsorbed NH_3 on stronger acid sites. A number of acid sites from NH_3-TPD analysis were showed in Table 4.10. The results indicated that the number of acid site in NaY-AMW2-SO_3H was higher than NaY-ART120-SO_3H.

Table 4.10 The quantity of acidic sites of NaY-ART120-SO_3H and NaY-AMW2-SO_3H.

Catalyst	The number of acidic site (arbitrary unit/g)
NaY-ART120-SO_3H	2.11
NaY-AMW2-SO_3H	2.40

4.3 Synthesis of X zeolite catalysts

4.3.1 The physical properties of X zeolite

4.3.1.1 Effect of Si/Al ratio on X zeolite formation

The effect of Si/Al ratio was investigated by varying the ratio as 1.5, 2.0, 2.3 and 2.5 for the preparation of X zeolite by hydrothermal method with aging gel for 1 day and crystallization time for 24 hrs at 90^{o}C. XRD patterns of sample were showed in Figure 4.14. All samples showed the characteristic peaks of X zeolite except for the Si/Al ratio 1.5 it exhibited characteristic peaks of A zeolite instead because Si/Al ratio 1.5 was too low and close to Si/Al ratio of A zeolite . The XRD pattern of X zeolite at Si/Al ratio 2.3 showed highest crystallinity thus, it was chosen for the further study.

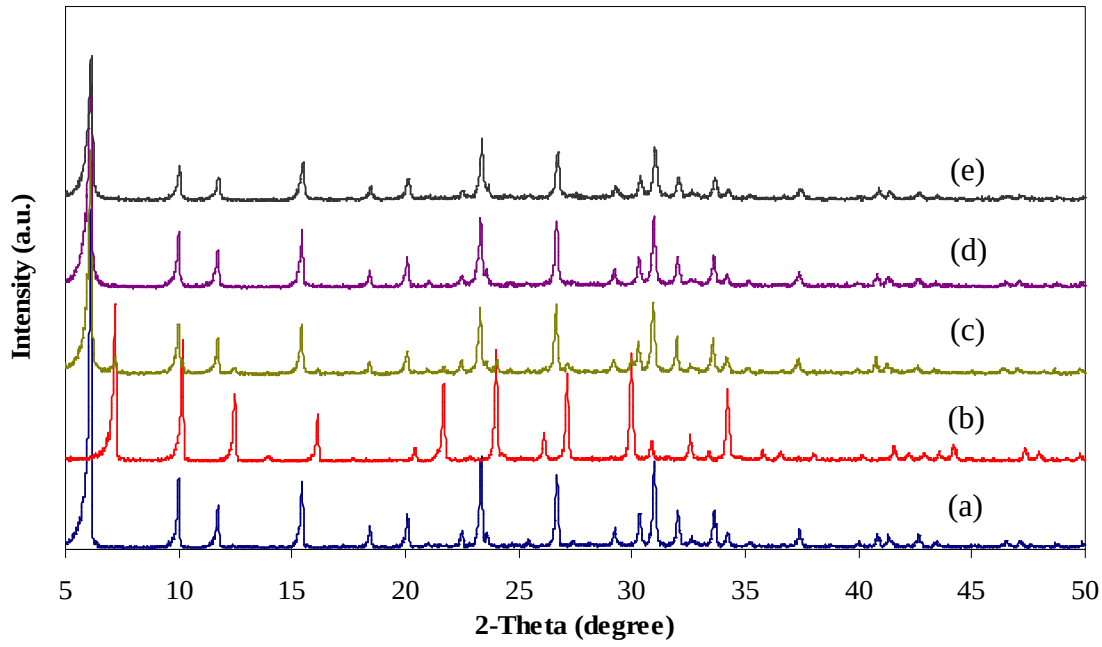

Figure 4.14 XRD patterns of X zeolite; standard X zeolite (Lion Corporation (Thailand) Limited) (a), and X zeolite prepared from various mole ratio of Si/Al; 1.5 (b), 2.0 (c), 2.3 (d), 2.5 (e).

From XRF result, the mole ratio of Si/Al in gel composition of synthesized X by hydrothermal method (NaX-ART24) was showed in Table 4.11. The result suggested that of all samples had Si/Al ratio in range of X zeolite. However, the X zeolite at Si/Al in gel ratio 2.3 has highest crystallinity corresponding to XRD result thus, it was chosen for the further study.

Table 4.11 Si/Al molar ratio in catalyst and %cryatallinity of synthesized X zeolite with hydrothermal method.

Sample	% crystallinity	Si/Al molar ratio in catalyst
NaX-ART24 (Si/Al ratio 2.0)	84.19	1.6
NaX-ART24 (Si/Al ratio 2.3)	90.28	1.6
NaX-ART24 (Si/Al ratio 2.5)	83.34	1.5

4.3.1.2 XRD results

The effect of aging time from 0.5 to 4.0 hrs on crystal gel formation of X zeolite (Si/Al = 2.3) was studied with microwave irradiation. All XRD patterns of the synthesized products were showed in Figure 4.15, the characteristic peaks of X zeolite were compared to NaX-ART120. The synthesized materials with aging time by microwave for 1 hr and above exhibited contaminant phase at 2-Theta of 13°.

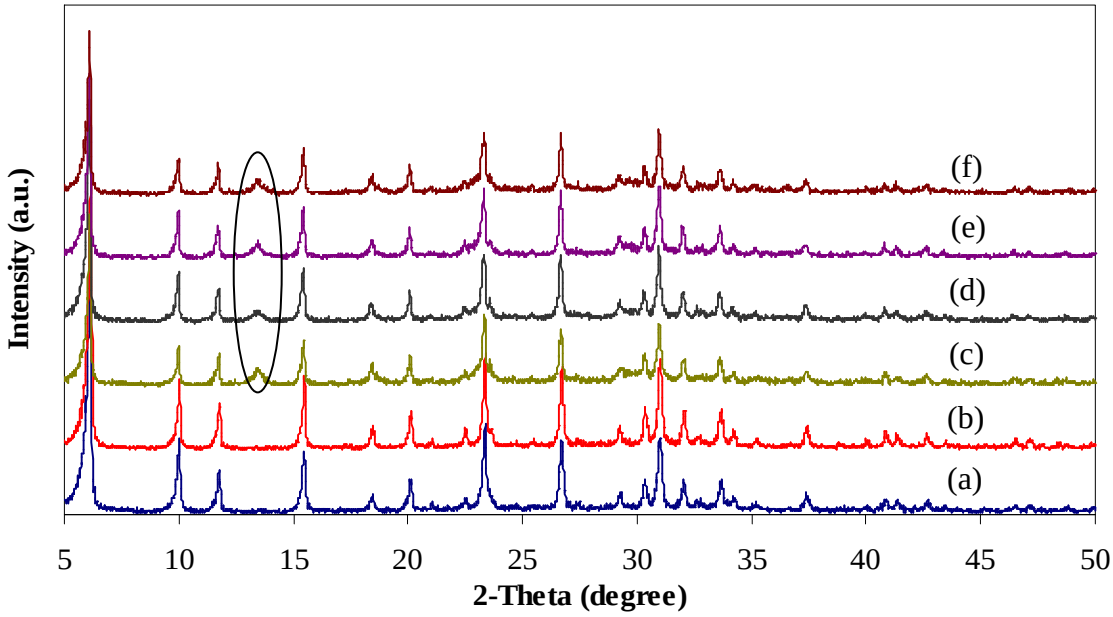

Figure 4.15 X-ray powder diffraction patterns of X zeolite samples; X zeolite prepared with hydrothermal method (a), and synthesized with microwave irradiation for 0.5 (b), 1.0 (c), 2.0 (d), 3.0 (e), 4.0 (f) hrs in aging time, respectively.

The synthetic X zeolite by hydrothermal method from this work had 78.14% crystallinity when compared to standard X zeolite (Lion Corporation (Thailand) Limited). Moreover, the microwave synthesized X zeolite exhibited the highest % crystallinity at crystallization time 0.5 hrs as shown in Table 4.12. The result exhibited lower period time from 120 hrs. in aging step.

Table 4.12 Percent crystallinity of standard and synthetic X zeolite various aging time for 0.5 to 4.0 hrs.

Sample	% Crystallinity
Standard X zeolite (Lion Corporation (Thailand) Limited)	100%
NaX-ART120	78.44%
NaX-AMW0.5	71.96%
NaX-AMW1	48.67%
NaX-AMW2	59.62%
NaX-AMW3	52.53%
NaX-AMW4	49.54%

4.3.1.3 Nitrogen adsorption-desorption

The N_2 adsorption-desorption isotherm and pore size distribution of synthesized X zeolite catalysts by hydrothermal method indicated the presence of type I isotherm were showed in Figure A-7 (in appendices). The textural properties of all samples were listed in Table 4.13. The textural properties of NaX-ART120 sample showed higher surface area, external surface area and pore volume than NaX-AMW0.5. All synthetic materials showed pore size of 0.6 nm.

Table 4.13 Textural properties of X zeolite samples; prepared with hydrothermal method and microwave irradiation for 0.5 hr.

Catalyst	Total specific surface area[a] ($m^2 \cdot g^{-1}$)	External surface area[b] ($m^2 \cdot g^{-1}$)	Micropore volume[b] ($cm^3 \cdot g^{-1}$)	Pore size distribution[c] (nm)
NaX-ART120	532	47	0.19	0.6
NaX-AMW0.5	467	32	0.17	0.6

[a]Calculated using the BET plot method,
[b]Calculated using the t-plot method,
[c]Calculated using the MP-plot method,

4.3.1.4 SEM images

The SEM images of NaX-ART120 and NaX-AMW0.5 showed average particle size around 2.02 μm and 1.75 μm, respectively, as shown in Figure 4.16. The particles of all samples have a cauliflower-like morphology. The particle shape, particle size and surface appearance of all samples were very similar.

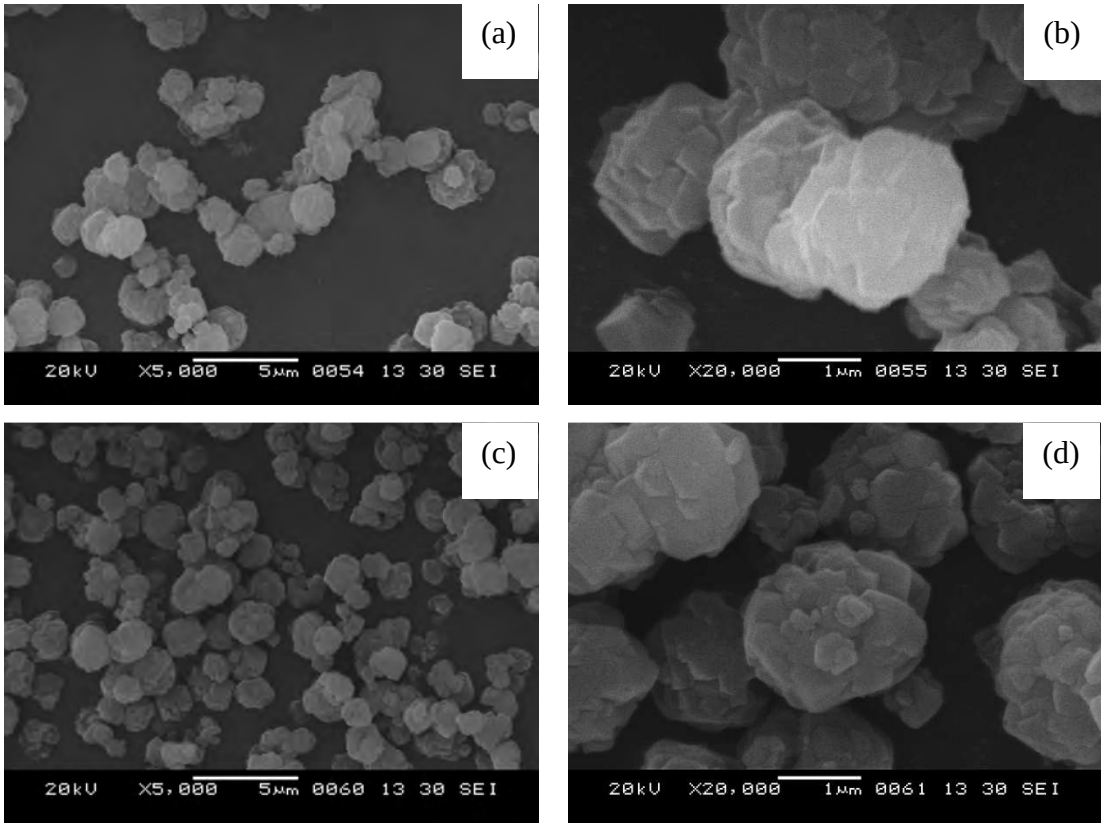

Figure 4.16 SEM images of X zeolite samples; prepared with hydrothermal method at different magnifications; x 5,000 (a), x 20,000 (b) and synthesized with microwave irradiation for 0.5 hr in aging time x 5,000 (c), x 20,000 (d).

4.3.2 The physico-chemical properties of functionalized X zeolite

4.3.2.1 XRD results

The XRD patterns of sulfonic acid functionalized X zeolite catalysts synthesized by hydrothermal and microwave method were showed in Figure 4.17. The results showed similar pattern as pure X zeolite which was slightly decreased in its crystallinity in both two samples.

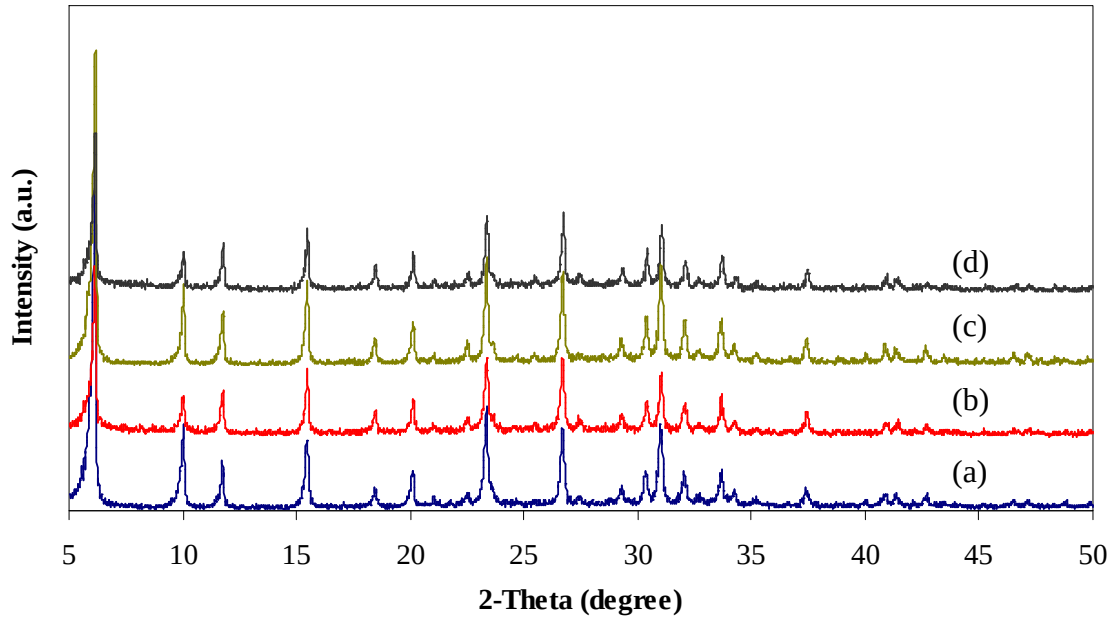

Figure 4.17 X-ray powder diffraction patterns of sulfonic functionalized of X zeolite by oxidation step for 12 hrs and acidify with 0.05 M H_2SO_4; NaX-ART120 (a), NaX-ART120-SO_3H (b), NaX-AMW0.5 (c), NaX-AMW0.5-SO_3H (d).

4.3.2.2 Nitrogen adsorption-desorption

The N_2 adsorption-desorption isotherm and pore size distribution of X zeolite catalysts indicated the presence of type I isotherm were showed in Figure A-7 (in appendices). The textural properties derived from the adsorption isotherm of X zeolite and sulfonic functionalized samples were complied in Table 4.14. The NaX-ART120-SO_3H and NaX-AMW0.5-SO_3H samples exhibited lower surface area and pore volume compared with the pure X zeolite because the sulfonic group transferred into pore structure that corresponding with their intensity of XRD pattern results. However, the external surface area and pore size distribution value were higher than pure X zeolite might be due to the some parts of zeolite structure were destroyed.

Table 4.14 Textural properties of X zeolite and sulfonic functionalized X zeolite**.**

Catalyst	Total specific surface area[a] ($m^2 \cdot g^{-1}$)	External surface area[b] ($m^2 \cdot g^{-1}$)	Micropore volume[b] ($cm^3 \cdot g^{-1}$)	Pore size distribution[c] (nm)	Particle size (μm)
NaX-ART120	532	47	0.19	0.6	2.02
NaX-ART120-SO_3H	95	76	0.02	1.4	1.63
NaX-AMW0.5	467	32	0.17	0.6	1.75
NaX-AMW0.5-SO_3H	116	72	0.04	1.6	1.62

[a]Calculated using the BET plot method,
[b]Calculated using the t-plot method,
[c]Calculated using the MP-plot method

4.3.2.3 SEM images

The SEM images of functionalized X zeolites at different magnifications were showed in Figure 4.18. The NaX-ART120-SO_3H and NaX-AMW0.5-SO_3H samples displayed a similar morphology as pure X zeolite. Moreover, both of samples showed average particle size around 1.63 and 1.62 μm, respectively.

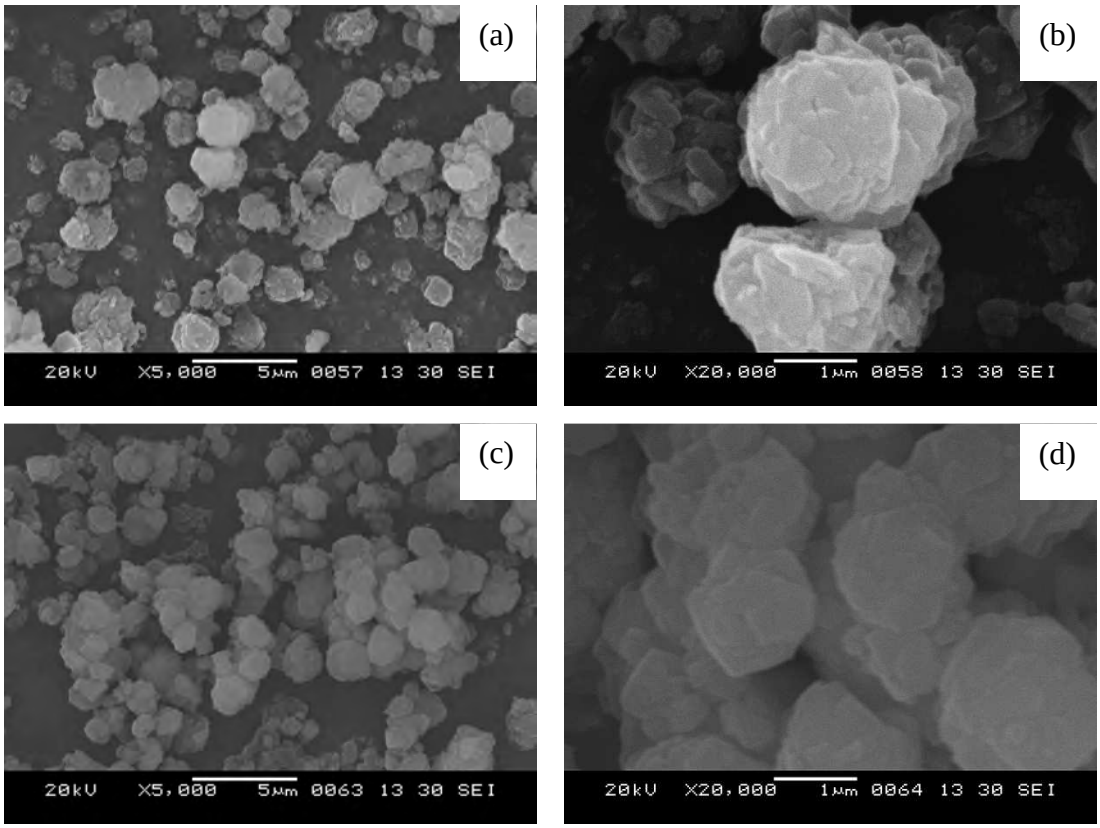

Figure 4.18 SEM images of functionalized of X zeolite by hydrothermal method at difference magnifications; x 5,000 (a), x 20,000 (b) and functionalized of X zeolite by microwave method; x 5,000 (c), x 20,000 (d).

4.3.2.4 Elemental analysis and acid-base titration

The number of sulfonic acid groups in the X zeolite was measured quantitatively by acid-base titration using sodium chloride as ion-exchange agent. The sulfur content of the modified zeolite was determined by sulfur analysis were complied in Table 4.15. In this work, the acid value and sulfur content of NaX-AMW0.5-SO_3H was higher than NaX-ART120-SO_3H.

Table 4.15 Sulfur analysis and acid value of sulfonic functionalized NaX zeolite.

Catalyst	Sulfur analysis[a] (wt%)	H^+ content[b] (mmol/g)
NaX-ART120-SO_3H	0.08	0.48
NaX-AMW0.5-SO_3H	0.19	1.59

4.3.2.5 Acidity of catalysts

The NH_3-TPD profiles of NaX-ART120-SO_3H and NaX-AMW0.5-SO_3H were showed in Figure A-8 (in appendices), both samples exhibited two peaks corresponding to different acid site of samples. The high temperature peak was due to the stronger acid sites and the occurrence of the low temperature peak was related to the interaction of ammonia with weaker acid sites. The data from NH_3-TPD analysis were showed in Table 4.16. The results indicated that the number of acid site in the NaX-AMW0.5-SO_3H was higher than the NaX-ART120-SO_3H. Hence, the NaX-AMW0.5-SO_3H was higher acidity than the NaX-ART120-SO_3H.

Table 4.16 The quantity of acidic sites of NaX-ART120-SO_3H and NaX-AMW0.5-SO_3H

Catalyst	The number of acid site (arbitrary unit/g)
NaX-ART120-SO_3H	0.07
NaX-AMW0.5-SO_3H	0.12

4.4 Reaction mixture analysis

A gas chromatogram of reaction mixture was showed in Figure A-9 and Figure A-10. Peak identification was achieved by comparison with authentic samples. In esterification reaction between free fatty acids (oleic acid and palmitic acid) and methanol, desired product was methyl ester and water was by-product. In this research, methyl ester was synthesized over acidic porous materials. Structures of obtained products from methyl ester synthesis were illustrated in Figure 4.19.

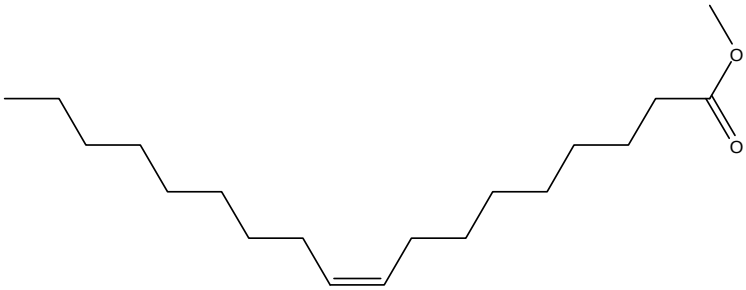

Methyl oleate

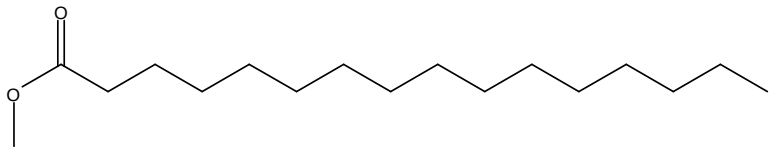

Methyl palmitate

Figure 4.19 Structures of obtained products from methyl ester synthesis.

For the quantitative analysis, calibration curves of methyl oleate and methyl palmitate were carried out as shown in Figure A-11 and Figure A-12 (in appendices). Free fatty acid methyl ester contents were evaluated in terms of (%) methyl ester yield. Free fatty acid methyl ester was silylated with MSTFA then, shaken vigorously and stored at room temperature. Inclusion of MSTFA appeared to help reduce boiling point of the free fatty acid methyl ester (biodiesel). After that, internal standard stock solution (1.2×10^{-1} M eicosane in THF) and THF were added before gas chromatography analysis. Each GC run contained 1 μl of solution. The silylation procedure was illustrated in scheme 4.1.

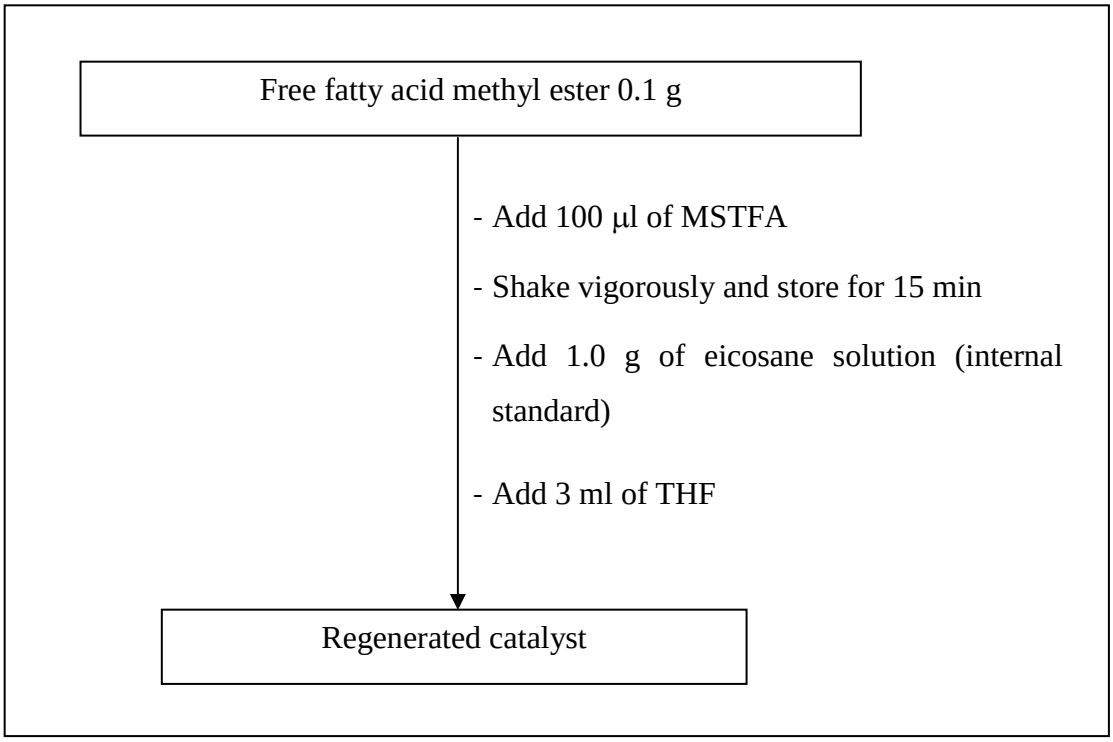

Scheme 4.1 Diagram of silylation of free fatty acid.

4.5 Catalytic activities of sulfonic functionalized SBA-15 in esterification of oleic acid

In this research, the catalytic performances of synthetic SBA-15 derivatives were evaluated in biodiesel preparation.

4.5.1 Effect of catalyst amount

The catalyst amount was varied in the range of 1.0 to 15% based on the starting material weight, while the remaining variables kept constant. The effect of the catalyst amount over the methyl oleate yield was presented in Table 4.17. It was obvious that, with increased catalyst amount, the acid sites of catalyst for reaction were also increased. However, increasing amount of catalyst more than 3%, slurry phase was formed which might cause the reduction of methyl ester product [63]. According to the methyl oleate yield, 3 wt% of the catalyst amount to reactant mixture was chosen for the further study.

Table 4.17 Catalytic activities in esterification of oleic acid over SBA-15-MW2-SO_3H at various ratios of catalyst amount.

Catalyst amount (wt %)	% Yield of methyl oleate
1	62.30
3	87.91
5	77.64
10	76.13
15	73.92

Reaction condition: methanol/oleic acid molar ratio 9:1, reaction temperature 60°C and reaction time 1 h.

4.5.2 Effect of methanol to oleic acid molar ratio

The esterification reaction was carried out at constant temperature 60^{o}C for 1 h and 3 wt% of SBA-15-MW2-stir-SO_3H. In this work, ratios of methanol to oleic acid were varied from 3 to 15. Table 4.18 showed the effect of methanol to oleic acid molar ratio. The stoichiometic ratio for esterification reaction requires one mole of methanol and one mole of oleic acid to produce one mole of methyl oleate and water. The molar ratio of methanol and oleic acid is also one of most important variables affecting the yield of methyl esters. In this reaction, an excess of methanol was used in order to shift the equilibrium to the right hands of the products. By increasing reactant molar ratio from 3 to 12, the methyl oleate yield was increased from 42.31 to 98.14%. As a result, the methanol to oleic acid molar ratio of 12 was optimum condition due to giving the highest yield. Above the molar ratio of 12 mol mol^{-1}, the excessively added methanol had decreasing methyl oleate yield, due to the acidity of the catalysts decreased.

Table 4.18 Catalytic activities in esterification of oleic acid over SBA-15-MW2-SO_3H at various ratios of methanol to oleic acid.

Methanol/Oleic acid (mol mol^{-1})	**% Yield of methyl oleate**
3	42.31
6	60.52
9	87.91
12	98.14
15	81.56

Reaction condition: catalyst amount 3 wt%, reaction temperature 60°C and reaction time 1 h.

4.5.3 Effect of reaction temperature

To determine the effect of reaction temperature, the experiments were conducted at temperature ranging from 50 to 80°C. As shown in Table 4.19, the catalytic activity depended on the reaction temperature. By increasing temperature from 50 to 80°C, the methyl oleate yield was increased significantly. The reaction at 60^{o}C had no thermal acitivity. Thus, it was selected for the further study owing to energy saving and catalytic activity comparison.

Table 4.19 Catalytic activities in esterification of oleic acid over SBA-15-MW2-SO_3H at various ratios of temperature.

Temperature (°C)	**% Yield of methyl oleate (non catalyst)**	**% Yield of methyl oleate (catalyst)**
50	0.00	62.78
60	0.68	72.79
70	3.76	78.29
80	5.96	82.50

Reaction condition: methanol/oleic acid molar ratio 12:1, catalyst amount 3 wt%, and reaction time 15 min.

4.5.4 Effect of reaction time

The effect of reaction time was investigated. The catalytic activities of SBA-15-HT-SO_3H and SBA-15-MW2-stir-SO_3H were presented in Table 4.20. The reaction time was varied in the range of 0.25-2 hrs. As a result, the methyl oleate yield was increased when the reaction time was raised. At the reaction time of 60 min, SBA-15-HT-SO_3H could reach high methyl oleate yield to 100% indicating the reaction was complete within 60 min. Therefore, the optimum reaction time was 60 min. On the other hand, SBA-15-MW2-stir-SO_3H gave high methyl oleate yield as 98.14% at the same reaction time.

Table 4.20 Catalytic activities in esterification of oleic acid over SBA-15-MW2-stir-SO_3H and SBA-15-MW2-stir-SO_3H for different reaction times.

Reaction time (min)	% Yield of methyl oleate over SBA-15-MW2-stir-SO_3H	% Yield of methyl oleate over SBA-15-HT-SO_3H
15	43.19	67.60
30	58.60	73.70
45	72.31	81.32
60	98.14	100
90	100	100
120	100	100

Reaction condition: methanol/oleic acid molar ratio 12:1, catalyst amount 3 wt% and reaction temperature 60°C.

The corresponding plot of methyl oleate yield over SBA-15-HT-SO_3H and SBA-15-MW2-stir-SO_3H *versus* reaction time was showed in Figure 4.23. The initial rate was sharply risen of first one have close to 100%. The kinetic rate of SBA-15-HT-SO_3H was faster than SBA-15-MW2-stir-SO_3H because pore size was larger than another was synthesized by microwave method which active site was easier to be reached. However, for the longer reaction time SBA-15-HT-SO_3H could exhibit the

same activity with SBA-15-MW2-stir-SO_3H in biodiesel production. From all effects in biodiesel production, these concluded that the optimum condition was methanol to oleic acid molar ratio of 12, catalyst amount of 3wt% at 60 °C for 1 h. This optimized condition was applied in further study with palmitic acid.

4.5.5 Reused and regenerated of sulfonic functionalized SBA-15

One of the main advantages of using heterogeneous catalysts is the ease of separation and reusability in the successive catalytic cycles. In this research, SBA-15-MW2-stir-SO_3H was chosen to study in reuse and regeneration. The used catalyst was washed with acetone for several times and dried at 60°C overnight. In addition, the used catalyst was regenerated using the procedure described in Section 3.4. The used and regenerated catalysts were characterized prior testing in the next reactions.

4.5.5.1 Characterization of reused and regenerated catalysts

The XRD patterns of fresh, 1st reused, 2nd reused and regenerated SBA-15-MW2-stir-SO_3H catalysts were showed in Figure 4.24. As a result, all materials still exhibited three characteristic peaks of hexagonal phase similar to the fresh catalyst. The adsorption-desorption isotherms of those catalysts were presented type IV isotherm, mesoporous materials. The used catalyst had the specific surface area of 462 m^3/g that was reduced only 8 % as compared to the fresh one (Table 4.21). Moreover, the pore size of 1st and 2nd used catalysts was larger than the fresh catalyst due to some part of catalyst destroyed, while the wall thickness was decreasing due to leaching out of sulfonic group. However, the pore size of regenerated catalyst was decreased and wall thickness was increased due to the regrafting of sulfonic group.

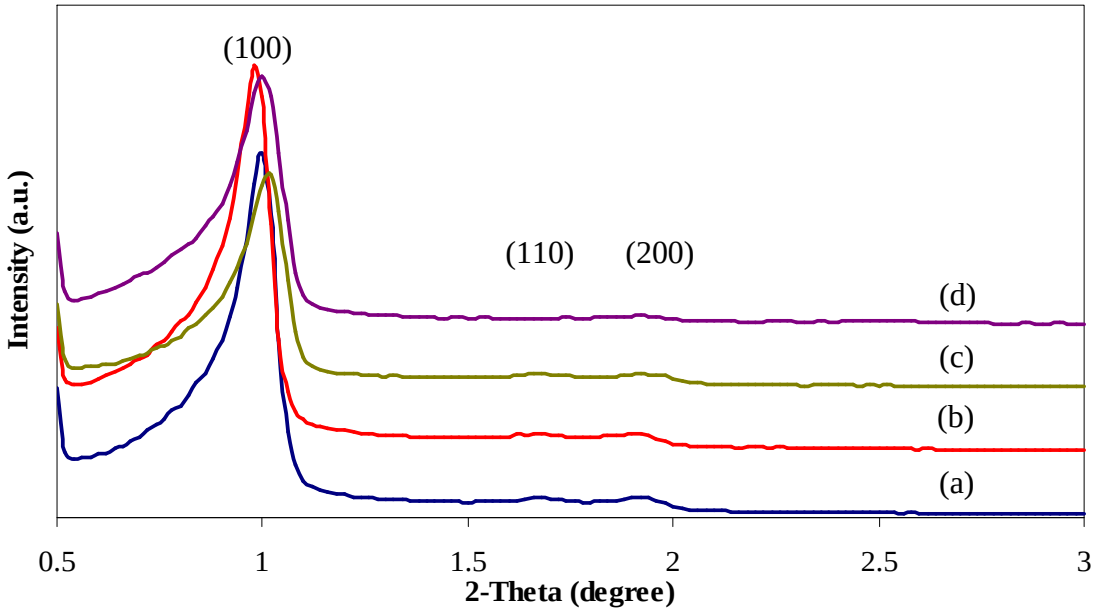

Figure 4.20 XRD patterns of fresh (a), 1st reused (b), 2nd reused (c), regenerated (d) SBA-15-MW2-stir-SO_3H catalysts.

Table 4.21 Textural properties of fresh, reused and regenerated SBA-15-MW2-stir-SO_3H.

Catalyst	Total specific surface area[a] ($m^2 \cdot g^{-1}$)	Pore size distribution[b] (nm)	Mesopore volume ($cm^3 \cdot g^{-1}$)	Wall thickness[c] (nm)
Fresh	462	6.18	0.54	4.23
1st reused	427	7.05	0.48	3.36
2nd reused	413	7.05	0.52	2.98
Regenerated	274	6.18	0.41	4.02

[a]Calculated using the BET plot method,
[b]Calculated using the BJH method,
[c]Calculated as: a_0-pore size ($a_0 = 2 \times d_{(100)} / \sqrt{3}$)

The SEM images exhibited the morphology of reused SBA-15-MW2-stir-SO_3H catalysts which similar to the fresh catalyst in Figure 4.25. On the other hand, the morphology of regenerated catalysts was changed slightly too non aggregated form.

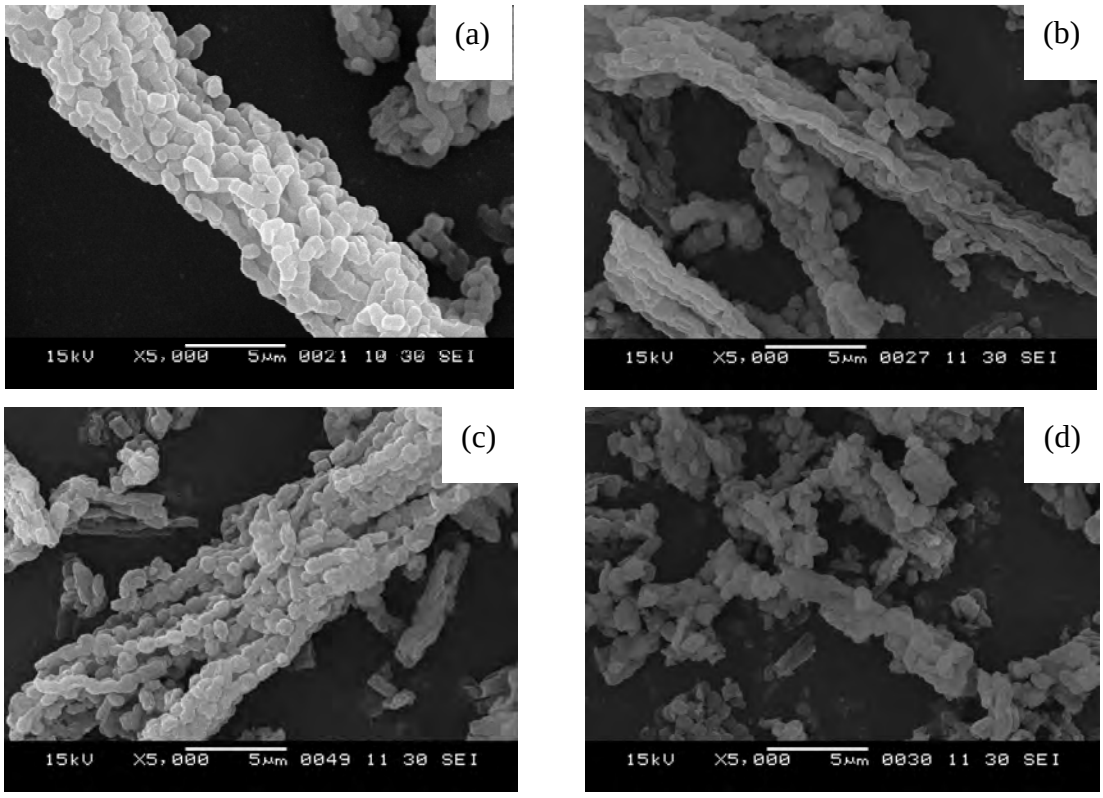

Figure 4.21 SEM images of fresh (a), 1st reused (b), 2nd reused (c) and (d) regenerated SBA-15-MW2-stir-SO_3H.

4.5.5.2 Catalytic activity of reused and regenerated SBA-15-MW2-stir-SO_3H catalysts

The catalytic activities of fresh, 1st reused, 2nd reused and regenerated catalysts in the esterification of oleic acid were showed in Figure 4.26. Reused SBA-15-MW2-stir-SO_3H exhibited a significant drop in activity from 98.14% methyl oleate yield of fresh to 61.96% yield of 1st reused and 25.11% yield of 2nd reused SBA-15-MW2-stir-SO_3H under the same operational condition. The loss in activities of catalyst might be from the deactivation of catalytic active site. However, the used catalyst was developed in order to improve its performance. After 2nd use, catalyst was regrafted with sulfonic group. The methyl oleate yield was improved from 25.11% to 100% for regenerated SBA-15-MW2-stir-SO_3H catalyst, nearly the fresh one. Therefore, the SBA-15-MW2-stir-SO_3H catalyst can be regenerated successfully notice from surface area and pore volume decrease due to regrafting of sulfonic group.

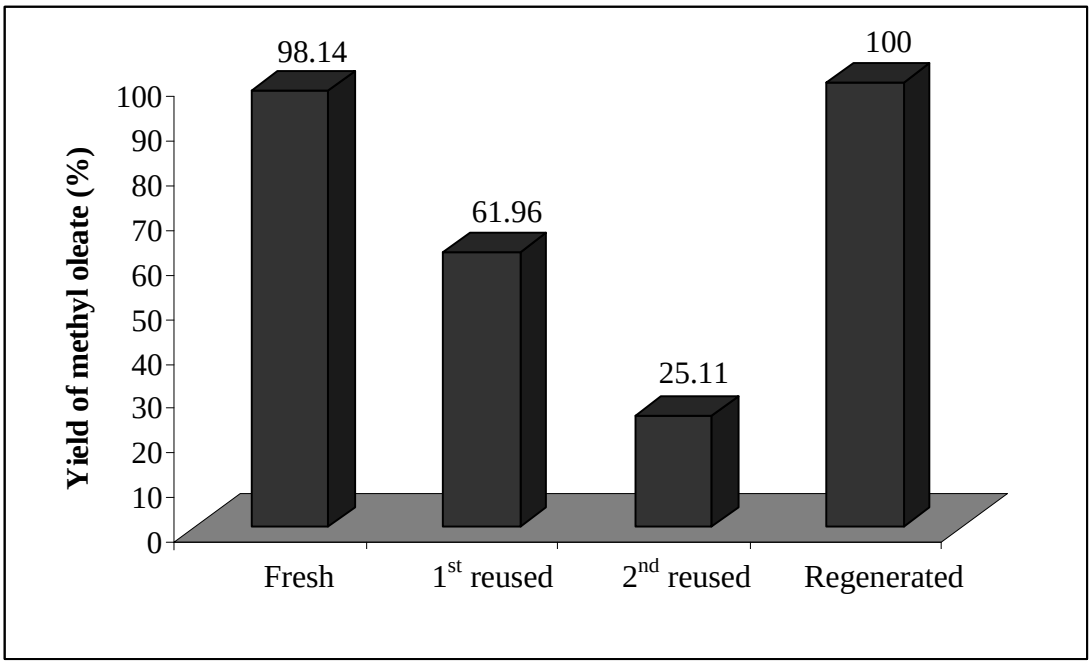

Figure 4.22 Catalytic activities of fresh, 1st, 2nd reused and regenerated SBA-15-MW2-stir-SO_3H in biodiesel preparation (Reaction conditions: methanol/oleic acid molar ratio 12:1, catalyst amount 3 wt%, reaction temperature 60°C and reaction time 1 h).

4.6 Catalytic activities of sulfonic functionalized Y zeolite in esterification of oleic acid

4.6.1 Effect of reaction temperature

To determine the effect of reaction temperature, the experiments were conducted at temperature ranging from 60 to 150°C. As shown in Table 4.22, the catalytic activity depended on the reaction temperature. By increasing temperature from 60 to 120°C, the methyl oleate yield was increased significantly from 4.22 to 68.58%. When increasing the temperature to 150^{o}C, yield of methyl oleate was slightly decreased to 66.71% because the reaction can be reverse to the starting material.

Table 4.22 Catalytic activities in esterification of oleic acid over NaY-AMW2-SO_3H at various ratios of temperature.

Temperature (^{o}C)	**% Yield of methyl oleate**
60	4.22
80	13.35
100	26.95
120	68.58
150	66.71

Reaction condition: methanol/oleic acid molar ratio 9:1, catalyst amount 10 wt% and reaction time 7 hrs.

4.6.2 Effect of catalyst amount

The catalytic performance of sulfonic functionalized Y zeolite at difference loading was studied. The catalytic amount was varied in the range of 1.0 to 15% referred to the starting material weight. As seen in Table 4.23. It can be observed that the yield of methyl oleate was increased by raising the catalyst amount from 1.0 to 5.0 wt%. Moreover, catalyst amount of 5.0 wt% and 3.0 wt% showed close value of methyl oleate yield. This result was expected because catalyst loading increment was proportional to availability of active site. Whereas, the lower yield was surprisingly obtained when the catalyst amount was increased to 10 and 15 wt%. The reason might be the slurry was formed and caused mixing problem [63]. According to methyl oleate yield, 3.0 wt% of catalyst amount was chosen further study.

Table 4.23 Catalytic activities in esterification of oleic acid over NaY-AMW2-SO_3H at various ratios of catalytic amount.

Catalyst amount (wt %)	% Yield of methyl oleate
1	65.42
3	80.00
5	80.71
10	68.58
15	62.70

Reaction condition: methanol/oleic acid molar ratio 9:1, reaction temperature 120°C and reaction time 7 hrs.

4.6.3 Effect of methanol to oleic acid molar ratio

The esterification reaction was carried out at constant temperature 120° C for 7 hrs over 3 wt% of NaY-AMW2-SO_3H. In this work, ratios of methanol to oleic acid were varied from 3 to 15. Table 4.24 showed the effect of methanol to oleic acid molar ratio. The stoichiometer ratio for esterification reaction requires one mole of methanol and one mole of oleic acid to produce one mole of methyl oleate and water. The molar ratio of methanol and oleic acid is also one of most important variables affecting the yield of methyl esters. In this reaction, an excess of methanol was used in order to shift the equilibrium to the products. By increasing reactant ratio from 3 to 9, the methyl oleate yield considerable increased from 50.20 to 80.00%. As a result, the methanol to oleic acid molar ratio of 9 was an optimum condition giving the highest yield. Beyond the molar ratio of 9, the excessively added methanol had decreasing methyl oleate yield, due to the acidity of the catalysts decreased

Table 4.24 Catalytic activities in esterification of oleic acid over NaY-AMW2-SO_3H at various ratios of methanol to oleic acid.

Methanol/Oleic acid (mol mol^{-1})	**% Yield of methyl oleate**
3	50.20
6	64.03
9	80.00
12	59.40
15	59.80

Reaction condition: catalyst amount 3 wt%, reaction temperature 120°C and reaction time 7 hrs.

4.6.4 Effect of reaction time

The effect of reaction time was investigated. The catalytic activities of NaY-AMW2-SO_3H and NaY-ART120-SO_3H were performed in Table 4.25 and the corresponding plot methyl oleate yield shown in Figure 4.30 The reaction time was varied in the range of 1 to 12 hrs. As a result, when reaction time was increased the methyl oleate yield was increased significantly until 7 hrs, resulted as 80% and 79.40% for NaY-AMW2-SO_3H and NaY-ART120-SO_3H, respectively. Moreover, the yield of methyl oleate was constant with increasing time up to 10 and 12 hrs. However, the results of both catalyst the same because the physical properties of synthesized catalyst no significant difference. These concluded that the optimum condition was methanol to oleic acid molar ratio of 9, catalyst amount of 3wt% at 120 °C for 7 hrs. This optimized condition was applied in further study with X zeolite.

Table 4.25 Catalytic activities in esterification of oleic acid over NaY-AMW2-SO_3H and NaY-ART120-SO_3H for different reaction times.

Reaction time (hrs)	% Yield of methyl oleate over NaY-AMW2-SO_3H	% Yield of methyl oleate over NaY-ART120-SO_3H
1	27.61	33.78
3	52.74	52.64
5	66.01	73.44
7	80.00	79.40
10	79.15	80.92
12	78.79	71.41

Reaction condition: methanol/oleic acid molar ratio 9:1, catalyst amount 3 wt% and reaction temperature 120°C.

4.6.5 Reused and regenerated of sulfonic functionalized Y zeolite

In this research, NaY-AMW2-SO_3H was chosen to study in this case. The used catalyst was washed with acetone for several times and dried at 60°C overnight. In addition, the used catalyst was regenerated using the procedure describe in Section 3.4. The used and regenerated catalysts were characterized prior testing in the next reactions.

4.6.5.1 Characterization of reused and regenerated catalysts

The XRD patterns of fresh, used and regenerated NaY-AMW2-SO_3H catalysts were showed in Figure 4.31. As a result, they still exhibited structure of faujasite type like the fresh catalyst. However, the intensity used and regenerated catalysts were decreased when compared to fresh catalyst. The adsorption-desorption isotherms of those catalysts were presented type I isotherm. All catalysts showed the characteristic isotherm of microporous materials. The used catalyst had the specific surface area of 251 m^2/g that was changeless to the fresh one (257 m^2/g) as shown in Table 4.26. However, the pore volume and surface area of regenerated catalyst were decreased due to the regrafting of sulfonic group.

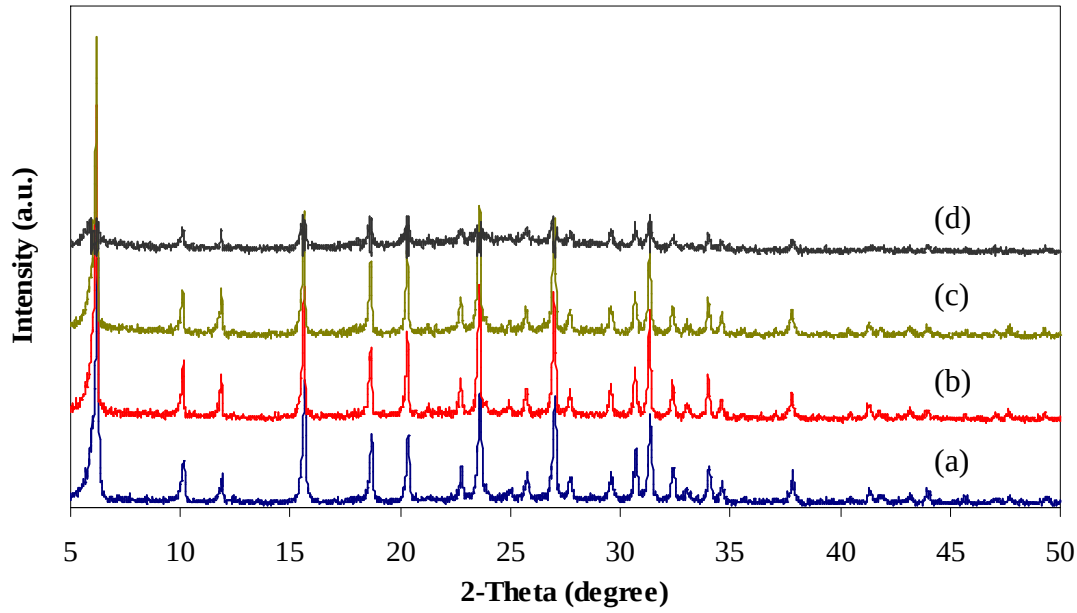

Figure 4.23 XRD patterns of fresh (a), 1st reused (b), 2nd reused (c), regenerated (d) NaY-AMW2-SO_3H catalysts.

Table 4.26 Textural properties of fresh, reused and regenerated NaY-AMW2-SO_3H.

Catalyst	Total specific surface area[a] ($m^2 \cdot g^{-1}$)	External surface area[b] ($m^2 \cdot g^{-1}$)	Micropore volume[b] ($cm^3 \cdot g^{-1}$)	Pore size distribution[c] (nm)
Fresh	257	10	0.11	0.6
1st reused	251	13	0.11	0.6
2nd reused	285	16	0.11	0.6
Regenerated	60	5	0.02	0.6

[a]Calculated using the BET plot method,
[b]Calculated using the t-plot method,
[c]Calculated using the MP-plot method

The SEM images showed the morphology of reused and regenerated NaY-AMW2-SO_3H catalysts similar to fresh catalyst was shown in Figure 4.32.

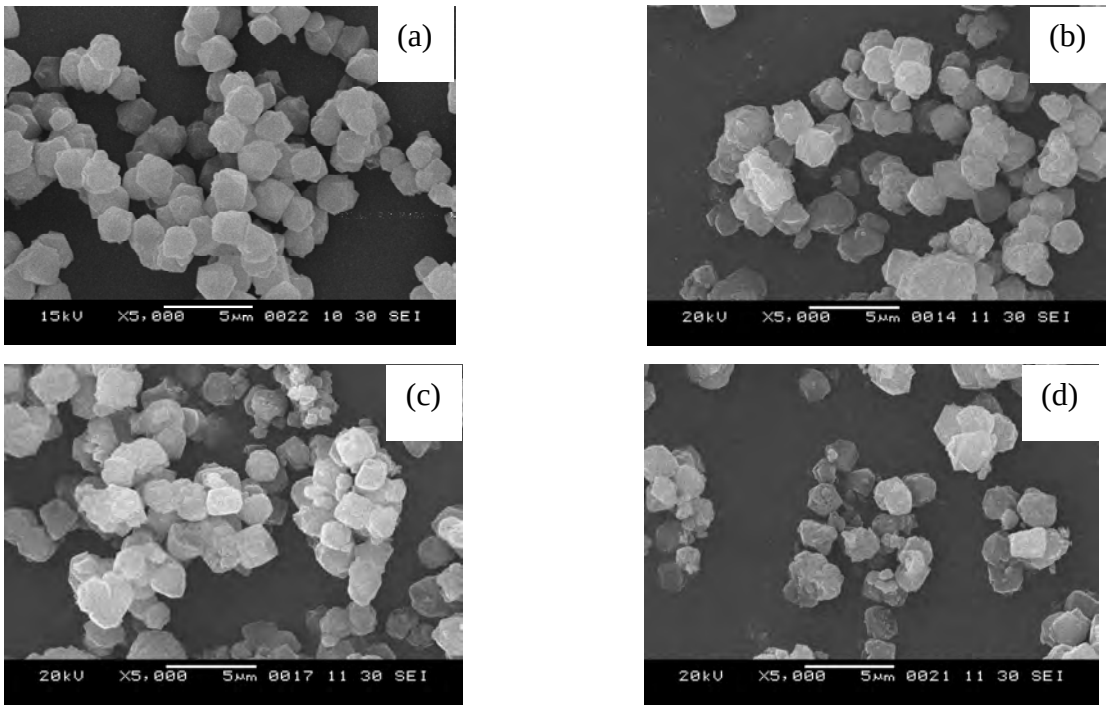

Figure 4.24 SEM images of fresh (a), 1st reused (b), 2nd reused (c) regenerated (d) of NaY-AMW2-SO_3H.

4.6.5.2 Catalytic activity of reused and regenerated NaY-AMW2-SO_3H catalysts

To examine the reusability of NaY-AMW2-SO_3H, it was repeatedly tested in esterification reaction of oleic acid under the optimum condition. As shown in Figure 4.33 when the used NaY-AMW2-SO_3H was utilized, the methyl oleate yield was dramatically decreased from 80 to 59.06% compared with fresh one. The loss in activity of catalyst may be caused by the deactivation of active site. Therefore, the used catalyst was improved properties. After 2nd using, catalyst was grafted with sulfonic group. The methyl oleate yield was improved from 49.27% of 2nd reused catalyst to 84.29% for regenerated NaY-AMW2-SO_3H catalyst, nearly to the fresh one. Therefore, the NaY-AMW2-SO_3H catalyst can be regenerated successfully notice from surface area and pore volume decrease due to regrafting of sulfonic group.

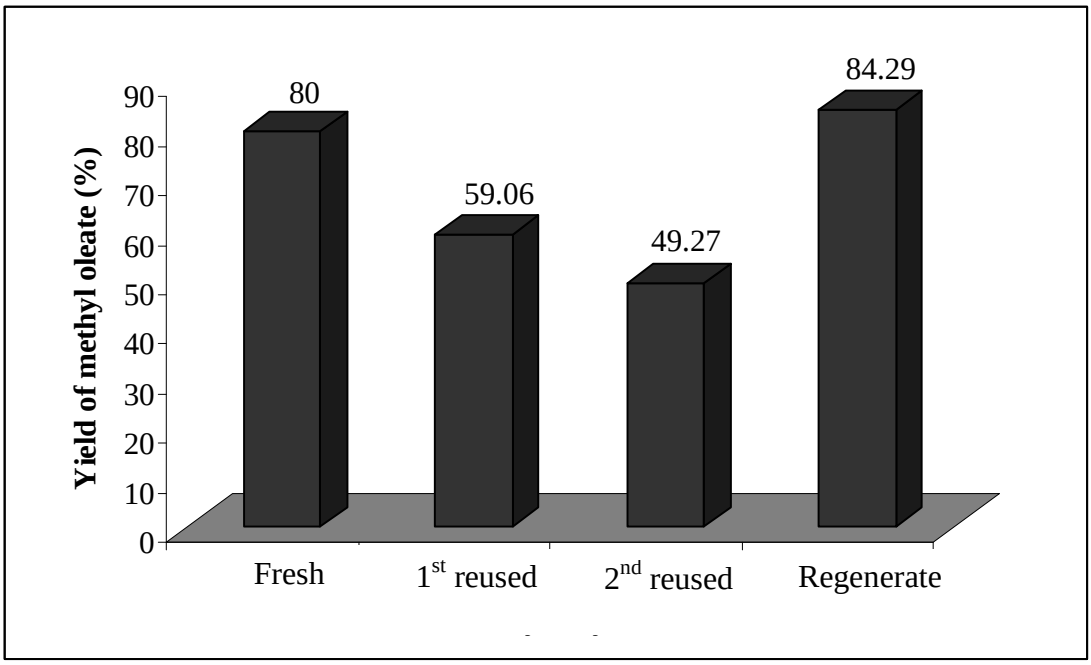

Figure 4.25 Catalytic activities of fresh, 1st, 2nd reused and regenerated NaY-AMW2-SO_3H in biodiesel preparation (Reaction conditions: methanol/oleic acid molar ratio 9:1, catalyst amount 3 wt%, reaction temperature 120°C and reaction time 7 hrs).

4.7 Catalytic activities of sulfonic functionalized X zeolite in esterification of oleic acid

The suitable condition of Y zeolite was applied to test with sulfonic functionalized X zeolite**.** The result NaX-AMW0.5-SO_3H gave higher yield of methyl oleate than NaX-ART120-SO_3H as shown in Table 4.27. As a result, the synthesized X zeolite by microwave method was higher acidity than synthetic by hydrothermal method. Moreover, sulfonic functionalized Y zeolite gave higher yield of methyl oleate than sulfonic functionalized X zeolite owing to Y zeolite contained high acidity as shown in Table 4.9 and 4.15.

Table 4.27 Catalytic activities in esterification of oleic acid over NaX-ART120-SO_3H and NaX-AMW0.5-SO_3H.

Catalysts	% Yield of methyl oleate
NaX-ART120-SO_3H	69.94
NaX-AMW0.5-SO_3H	76.72
NaY-ART120-SO_3H	79.40
NaY-AMW2-SO_3H	80.00

4.8 Catalytic activities of sulfonic functionalized SBA-15 and Y zeolite in esterification of palmitic acid

Palmitic acid is 16-carbon chain carboxylic acid, while oleic acid has 18-carbon chain carboxylic acid consist of one *cis* double bonds. Then the same reaction condition was applied for palmitic acid esterification as shown in Table 4.28. The catalytic activity of SBA-15-MW2-stir-SO_3H and NaY-AMW2-SO_3H exhibited 59.10% and 47.25%, respectively which lower than the esterification of oleic acid due to steric effect and saturated of palmitic acid.

Table 4.28 Catalytic activities in esterification of palmitic acid over SBA-15-MW2-stir-SO_3H and NaY-AMW2-SO_3H.

Catalysts	**Condition methanol:palmitic / wt%catalyst / temp/ time**	**% Yield of methyl palmitate**
SBA-15-MW2-stir-SO_3H	12:1 / 3wt% / 60^oC / 1 hr	59.10
NaY-AMW2-SO_3H	9:1 / 3wt% / 120^oC / 7 hrs	47.25

CHAPTER V

CONCLUSIONS

Mesoporous material, SBA-15, was successfully synthesized via microwave method at 2 hrs under stirring condition which was about 24 times faster than hydrothermal method. The XRD patterns of all samples indicated the hexagonal structure. N_2 adsorption-desorption isotherms exhibited a type IV pattern which showed typical sorption isotherm of mesoporous structure. Morphology of samples was aggregated particles with rope-like structure from SEM images. In addition, Y zeolite and X zeolite were prepared by microwave in aging step for 2 hrs and 0.5 hrs, respectively which was reduced period of time from 120 hrs for hydrothermal method. The synthesized microporous materials exhibited the characteristic peaks of faujasite (FAU). N_2 adsorption-desorption isotherms displayed type I pattern isotherm of microporous structure. Morphology of materials was uniform cubic-like and cauliflower-like particle to SEM images for Y zeolite and X zeolite, respectively. The sulfonic functionalized catalysts were prepared for increasing acid strength which the acidic materials revealed the same physical properties as pure sample, except for decreasing of surface area, pore volume and wall thickness.

All of catalysts were applied in esterification of oleic acid with methanol. SBA-15-HT-SO_3H exhibited 100% of methyl oleate yield whereas SBA-15-MW2-stir-SO_3H gave 98.14%. Furthermore, it could be concluded that the optimum condition was methanol to oleic acid molar ratio of 12, catalyst amount of 3% at 60^oC for 1 hr. In addition, the suitable condition of NaY-AMW2-SO_3 was investigated which was methanol to oleic acid molar ratio of 9, catalyst amount of 3% at 120^oC for 7 hrs. At the optimum condition obtained methyl oleate yields as 80.00% and 79.14% for NaY-AMW2-SO_3H and NaY-ART120-SO_3H, respectively. Moreover, the same condition Y zeolite was applied to NaX-AMW0.5-SO_3H and NaX-ART120-SO_3H which showed the yield of methyl oleate as 69.94% and 76.72%, respectively. In addition, the suitable condition of SBA-15-MW2-stir-SO_3H and NaY-AMW20-SO_3H

was used with palmitic acid which presented the yield of methyl palmitate as 59.10% and 47.25%, respectively. Furthermore, the catalytic activities of reused SBA-15-MW2-stir-SO_3H and NaY-AMW2-SO_3H were decreased in esterification of oleic acid while regeneration of both catalysts exhibited nearly in the product yield when compared to the fresh one.

The suggestion for future work

1. To study effect of microwave irradiation in other synthetic porous materials.
2. To acidic modify porous material with other alkyl sulfonic acid groups to improve the activity of catalyst.

REFERENCES

[1] Energy information administration/the international energy outlook 2010 (IEO2010) [Online]. Available from: http://www.eia.doe.gov/oiaf/ieo/world.html [2011, February 9].

[2] Royon, D., Daz, M., Ellenrieder, G., and Locatelli. Enzymatic production of biodiesel from cotton seed oil using *t*-butanol as a solvent. *Biores. Tech.* 98(2006): 648.

[3] Yadav, G. D., and Lathi, P. S. Lipase catalyzed transesterification of methyl acetoacetate with *n*-butanol. *J. Mol. Cat. B.* 32(2005): 107.

[4] Aracil, J., Vicente, G., and Martinez, M. Integrated biodiesel production: a comparison of different homogeneous catalysts systems. *Biores. Tech.* 92(2004): 297.

[5] Lee, H. J., Kim, Y. M., Kweon, O. S., and Kim, I. J. Crystal growing and reaction kinetic of large NaX zeolite crystals. *J. Eur. Ceram. Soc.* 27(2007): 581-584.

[6] Ferchiche, s., Warzywoda, J., and Sacco, A. Direct synthesis of zeolite Y with large particle size. *Int. J. Inorg. Mater.* 3(2001): 773-780.

[7] Sang, S., Liu, Z., Tian, P., Liu, Z., Qu, L., and Zhang, Y. Synthesis of small crystals zeolite NaY. *Mater. Lett.* 60(2006): 1131-1133.

[8] Youssef, H., Ibrshim, D., and Komarneni, S. Microwave-assisted versus conventional synthesis of zeolite A from matakoalinite. *Micropor. Mesopor Mat.* 115(2008): 527-534.

[9] Zhou, R., Zhong, S., Lin, X, and Xu, N. Synthesis of zeolite T by microwave and conventional heating. *Micropor. Mesopor. Mat.* 124(2009): 117-122.

[10] Brito, A., Borges, M. E., and Otero, N. Zeolite Y as a heterogeneous catalyst in biodiesel fuel production from used vegetable oil. *Energ. Fuel.* 21(2007): 3280-3283.

[11] Xie, W., Huang, X., and Li, H. Soybean oil methyl esters preparation using NaX zeolites loaded with KOH as a heterogeneous catalyst. *Bioresource Technol.* 98(2007): 936-939.

[12] Noiroj, K., Intarapong, P., Luengnaruemitchai, A., and Jai-In, S. A comparative study of KOH/Al_2O_3 and KOH/NaY catalysts for biodiesel production via transesterification from palm oil. *Renew. Energ.* 34(2009): 1145-1150.

[13] Stucky, G.D., et al. Triblock copolymer syntheses of mesoporous silica with periodic 50 to 300 angstorm pores. *Science*. 279(1998): 548-552.

[14] Celer, E. B., and Jaroniec, M. Temperature-Programmed microwave-assisted synthesis of SBA-15 ordered mesoporous silica. (2006).

[15] Yang, L. M., Wang, Y. J., Luo, G. S., and Dal, Y. Y. Functionalization of SBA-15 mesoporous silica with thiol or sulfonic acid groups under the crystallization conditions. *Micropor. Mesopor. Mat.* 84(2005): 275-282.

[16] Saravanamurugan, S., Sujandi., Prasetyanto, E. A., and Park, S. E. Liquid-phase reaction of 2'-hydroxyacetophenone and benzaldehyde over SO_3H-SBA-15 catalysts: Influence of microwave and thermal effects. *Micropor Mesopor. Mat.* 112(2008): 97-107.

[17] Activation energy [Online]. Available from: http://en.wikipedia.org/wiki/Activation_energy [2010, February 14].

[18] Hagen, J. *Industrial Catalysis*. New York: Weinheim Wiley, 1999.

[19] Breck, D.W. *Zeolite Molecular Sieves: Structure, Chemistry, and use*, New York: John Wiley & Sons, (1997): 3-20.

[20] Barrer, R. M. *Zeolite and Clay Minerals as sorbets and Molecular Sieves*. London: Academic Press, (1978).

[21] Szostak, R. *Zeolite Molecular Sieves. Principles of Synthesis and Identification*. New York Van: Nostrand Reinhold, (1989).

[22] Continuation report [Online].Available from: http://mch3w.ch.man.ac.uk/theory/staff/student/mbdtscw/transfer_html/node1.html [2010, February 14].

[23] Dyer, A. *An Introduction to Zeolite Moecular Sieves*, Singapore: John Wiley & Sons, (1988): 12.

[24] Smart, L., and Moore, E. *Solid State Chemistry*, London: Chapman & Hall University, (1992): 184.

[25] Szostak, R. *Molecular Sieves: Principle of synthesis and Identification*, New York: Van Nostrand Reinhold, (1989): 51.

[26] Rollman, L. D. *Zeolites: Science and Technology*, Netherlands: Martinus Nijhoff, (1984): 109.

[27] Breck, D. W. *Crystalline Zeolite Y,* US Patent No. 3,130,007, 21 Apr. (1964).

[28] Whattam, T. V. *Manufacture of Synthetic Zeolite,* US patent No. 4,016,246, 5 Apr. (1977).

[29] Crabtree, R. H. *The Organometallic Chemistry of transition metals,* New York: John Wiley & Sons, (1988): 200.

[30] Kresge, C. T., Leonowicz, M. E., Roth, W. J., Vartuli, J. C., and Beck, J. S. Ordered mesoporous molecular sieves synthesized by a liquid-crystal template mechanism. *Nature* 359(1992): 710.

[31] Beck, J. S., and Vatuli, J. C. Recent advances in the synthesis, characterization and applications of mesoporous molecular sieves. *Curr. Opin. Solid. St. M.* 1(1996): 76.

[32] Inagaki, S.; and Fukushima, Y. Adsorption of water vapor hydrophobicity of ordered mesoporous silica, FSM-16. *Micropor. Mesopor. Mater.* 21 (1998): 667.

[33] Soler-Illia, G. J. A. A., Sanchez, C., Lebeau, B., and Patarin, J. Chemical strategies to design textured materials: from microporous and mesoporous oxides to nanonetworks and hierarchical structures. *Chem. Rev.* 102(2002) 4093.

[34] Ying, J.Y., Mehnert, C.P., and Wong, M.S. Synthesis and application of supramolecular-templated mesoporous materials. *Angew. Chem. Int. Edit.* 38 (1999): 56.

[35] Tanev, P.T. and Pinnavavia, T. J. A neutral templating route to mesoporous molecular sieve. *Science* 267 (1995): 865.

[36] Melosh, N.A., Lipic, P., and Bates, F.A., Stucky G.D. Molecular and mesoscopic structure of transparent block copolymer silica monoliths. *Macromolecules.* 32(1999): 4332.

[37] Beck, J. S., Leonowicz, M. E., Roth, W. J., Vartuli, J. C., and Kresge, C. T. A new family of mesoporous molecular sieves prepared with liquid crystal templates. *J. Am. Chem. Soc.* 114(1992): 10834.

[38] Soler-Illia, G. J. A. A., Crepaldi, E. L., Grosso, D., and Sanchez, C. Block copolymer-templated mesoporous oxides. *Current Opinion in Colloid and Interface Science* 8(2003): 109.

[39] Athens, G. L., Shayib, R. M., and Chmelka, B. F. Functionalization of mesostructured inorganic-organic and porous inorganic materials. *Curr. Opin. Colloid. In.* 14(2009): 281.

[40] Melero, J. A., Grieken, R. V., and Morales, G. Advances in the synthesis and catalytic applications of organosulfonic-functionalized mesostructured materials. *Chem. Rev.* 106(2006): 3790.

[41] Wight, A. P., and Dais, M. E. Design and preparation of organic-inorganic hybrid catalysts. *Chem. Rev.* 102(2002): 3589.

[42] Microwave laboratory System. Synthesis [Online]. Available from: http://www.milestonesci.com/synth-fund.php [2011, February 9].

[43] Arnim, L. H. J. Energy input from microwaves and ultrasound example of new approaches to green chemistry, Geramny (1997).

[44] Moore, D. M., and Reynolds Jr., R. C. *X-Ray Diffraction and the Identifiation and Analysis of Clay Minerals*. New York: Oxford University Press, (1989).

[45] Skoog, D. A. *Principles of Instrumental Analysis*. New York, Harcourt Brace College Publishers, 1997.

[46] BET [Online]. Available from: Basic operating principles of the sorptomatic, http://saf.chem.ox.ac.uk./Instruments/BET/sorpoptprin [2011, February 11].

[47] Analysis software user's manual, Belsorp, Bel Japan, Inc.

[48] Szostak, R. *Zeolite Molecular Sieves. Principles of Synthesis and Identification*. New York, Van: Nostrand Reinhold, (1989).

[49] Theory XRF [online]. Available from: http://www.learnxrf.com/BasicXRFTheory.htm [2011, Mar 1]

[50] Song, C., Hsu, C. S., Mochida, I. Chemistry of Diesel Fuels. New York, Taylor & Francis. 2000.

[51] Ma, F., and Hanna, M.A. Biodiesel production: A review. *Biores. Tech.* 70(1999): 1.

[52] Pintoa, A. C., et al. Biodiesel: An overview. *J. Braz. Chem. Soc.* 16(2005) : 131.

[53] Naik, S. N., Meher, L. C., and Vidya, S. D. Technical aspects of biodiesel production by transesterification: a review. *Renew. Sustain. E. Rev.* 10(2004): 1.

[54] Ginter, D.M., Bell, A.T., Radke, C.J., Linde, T., and Kurtz, C., Synthesis of zeolite Y. [Online]. Available from: http://www.iza-online.org/synthesis/ [2009, October 1].

[55] Reddy, S. S., Raju, B. D., Kumar, V. S., Padmasri, A. H., Narayanan, S., and Rama, R. K. S. *Catal Commun*. 8(2007): 261-266.

[56] Mbaraka, I. K., Radu, D. R., Lin, V. S. Y., and Shanks, B. H. Organosulfonic acid-functionalized mesoporous silicas for the esterification of fatty acid. *J. Catal.* 219(2003): 329.

[57] Sun, Y., Zheng, Y., Su, X., Zhang, X., and Wei, W. Functionalized masoporous SBA-15 silica with propylsulfonic group as catalysts for esterification of salicylic acid with dimethyl carbonate. *Stud. Surf. Sci. Catal*. 156 205-212.

[58] Park, S. E., Kwon, Y. U., Chang, J. S., and Hwang, Y. K. Microwave synthesis of cubic mesoporous silica SBA-16. *Micropor. Mesopor. Mater.* 68(2004): 21-27.

[59] Lou, G. S., Dai, Y. Y., Wang, Y. J., and Yang, L. M. Functionalization of SBA-15 mesoporous silica with thiol or sulfonic acid groups under the crystallization conditions. *Micropor. Mesopor. Mater.* 84(2005): 275-282.

[60] Zhao, D., Ha, C. S., Park, S. S., Tu, B., Wu, Z., and Li, Q. Highly hydrothermal stability of ordered mesoporous aluminosilicates Al-SBA-15 with high Si/Al ratio. *Micropor. Mesopor. Mater*. 135(2010): 95-104.

[61] Hossein, F., and Sedigheh, V. Dehydrogenation of iso-butane over nanoparticles of Pt/Sn Alloy on Pt/Sn/Na-Y catalyst: the effect of Tin precursor on the catalyst behavior. *Iran. J. Chem. Chem. Eng.* 28(2009).

[62] Sato, K., Nishimaru, Y., Matsubayashi, N., Imamura, M., and Shimada, H. Structure changes of Y zeolite during ion exchange treatment: effects of Si/Al of starting NaY. *Micropor. Mesopor. Mater.* 99(2003): 133-146.

[63] Lee, K. Y., et al. Tranesterification of vegetable oil to biodiesel using heterogeneous base catalyst. *Catal. Today* 93(2004): 315.

APPENDICES

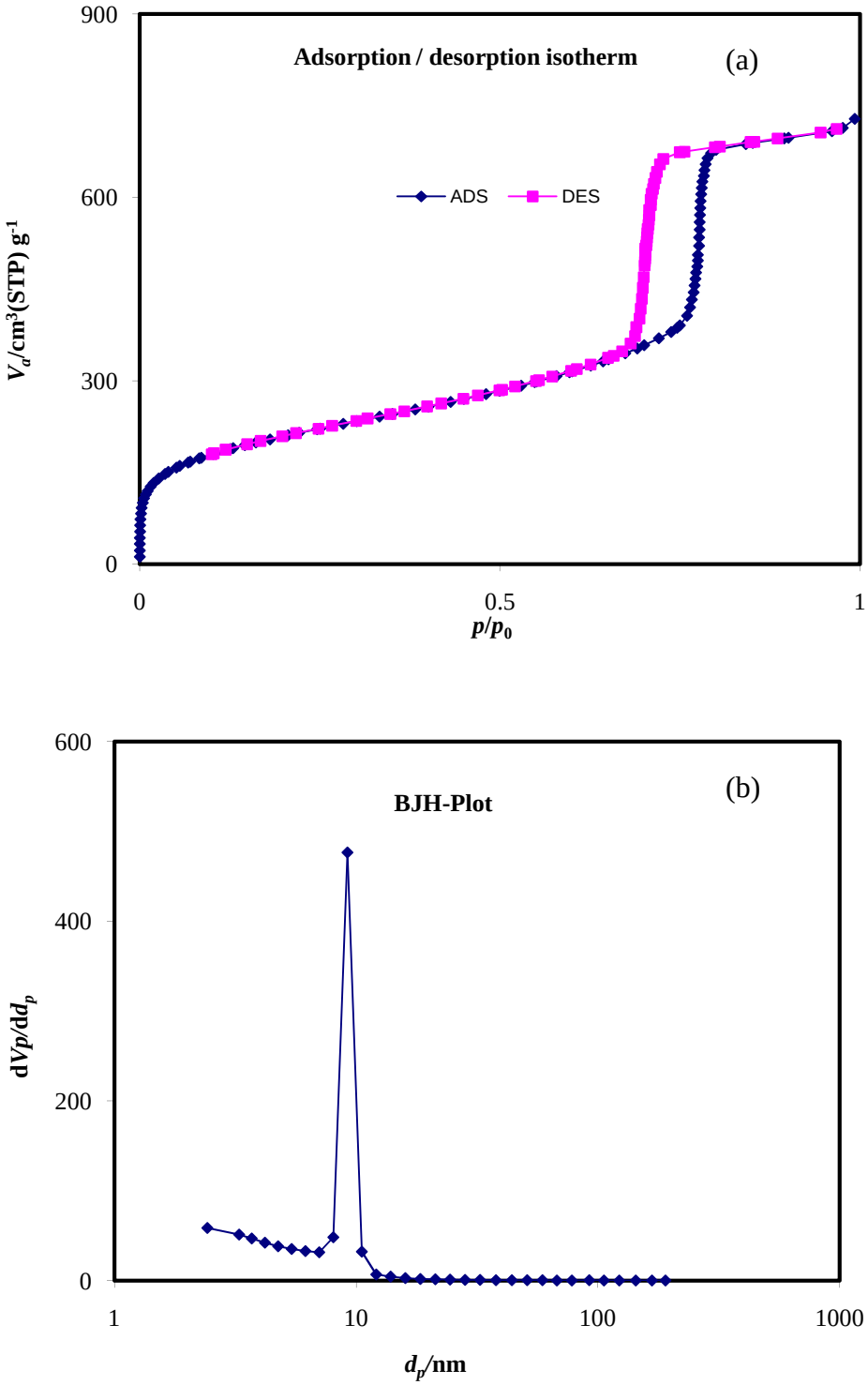

Figure A-1 N_2 adsorption-desorption isotherm (a) and pore size distribution (b) of synthesized SBA-15 with hydrothermal method.

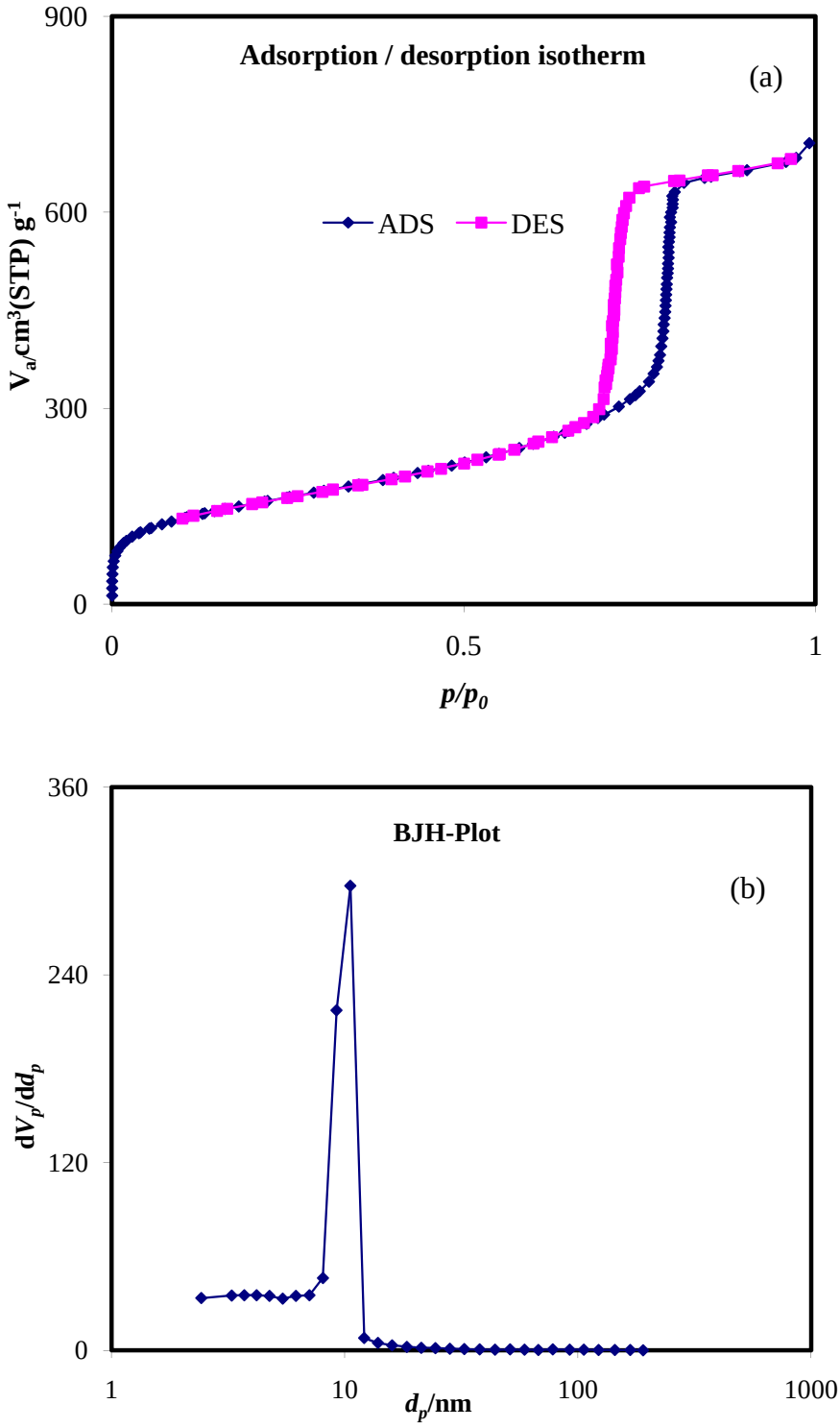

Figure A-2 N_2 adsorption-desorption isotherm (a) and pore size distribution (b) of synthesized SBA-15 with hydrothermal method after hydrothermal stability test.

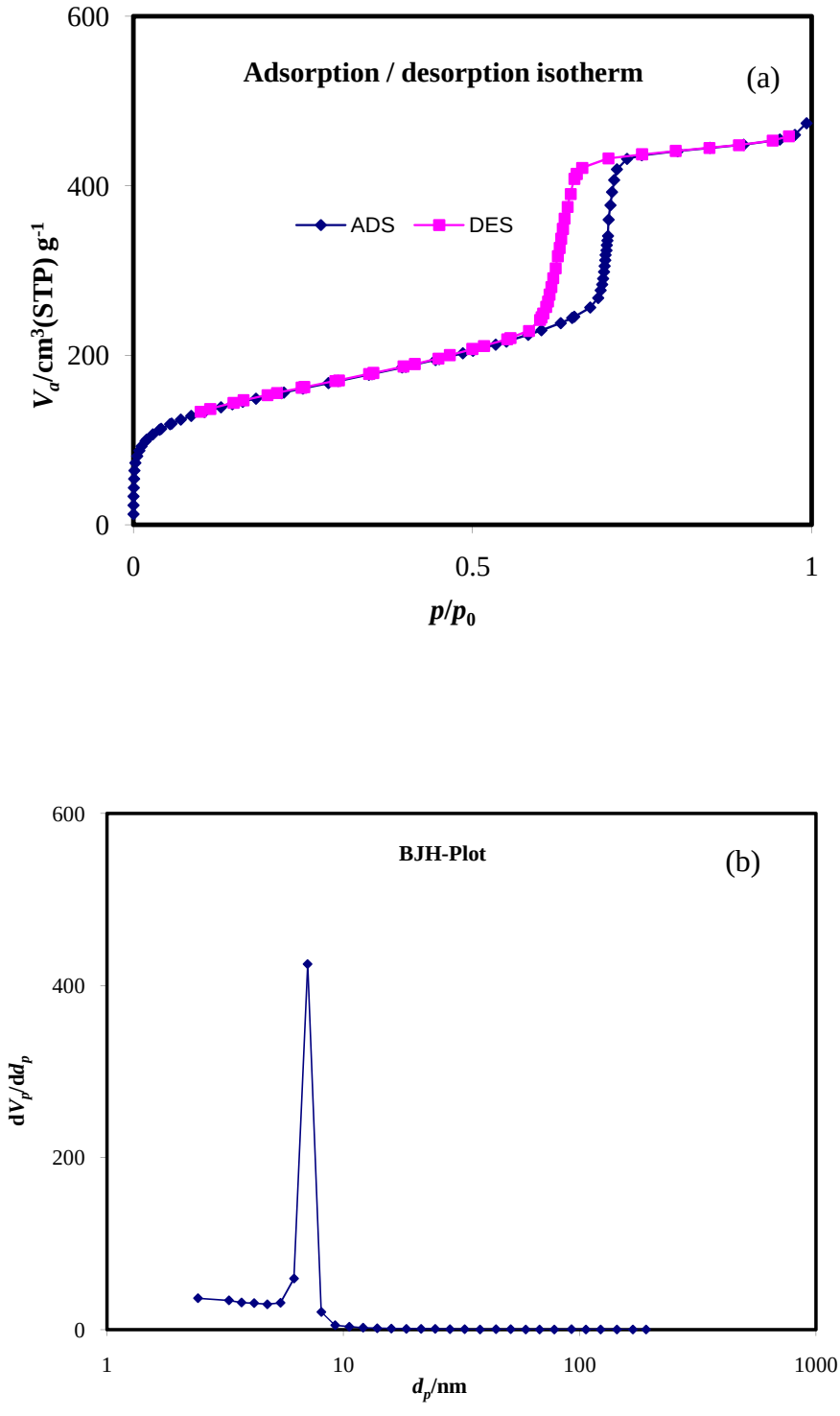

Figure A-3 N_2 adsorption-desorption isotherm (a) and pore size distribution (b) of synthesized SBA-15 with microwave method after hydrothermal stability test.

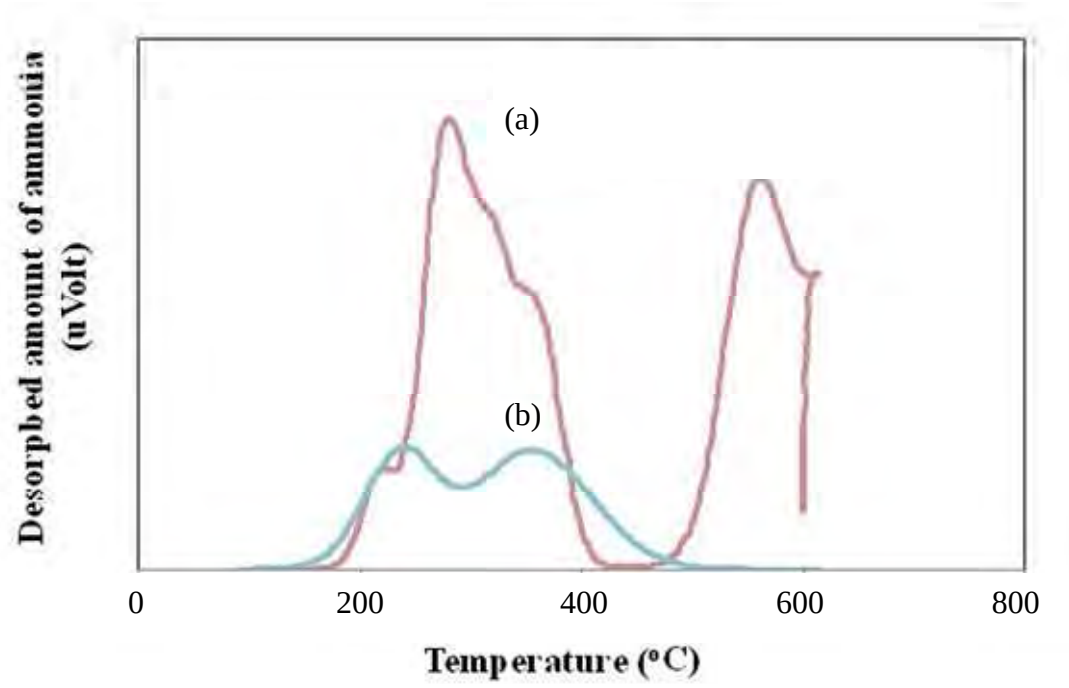

Figure A-4 NH_3-TPD profile of SBA-15-HT-SO_3H (a), SBA-15-MW2-stir-SO_3H (b).

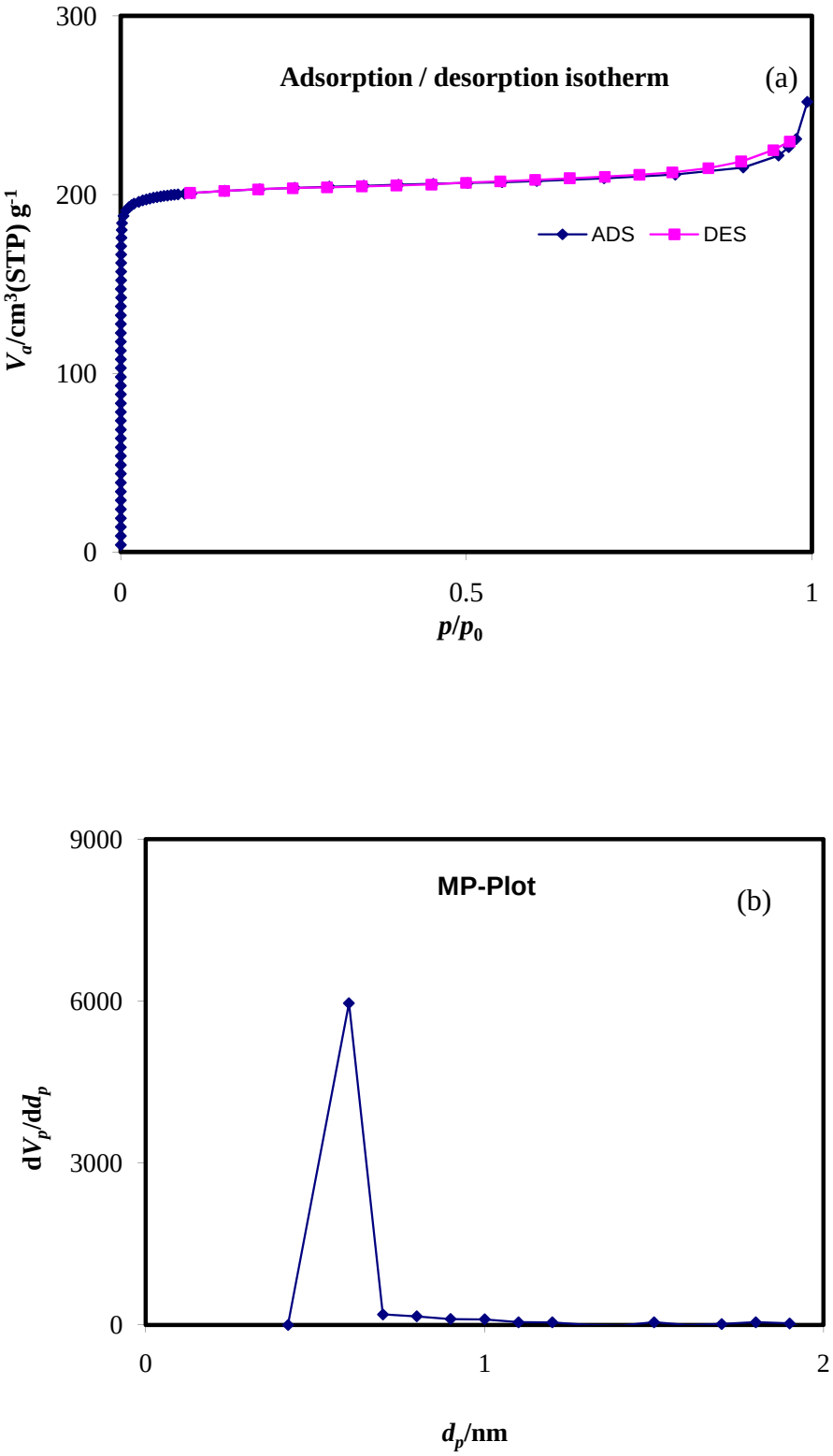

Figure A-5 N_2 adsorption-desorption isotherm (a) and pore size distribution (b) of synthesized Y zeolite with hydrothermal method.

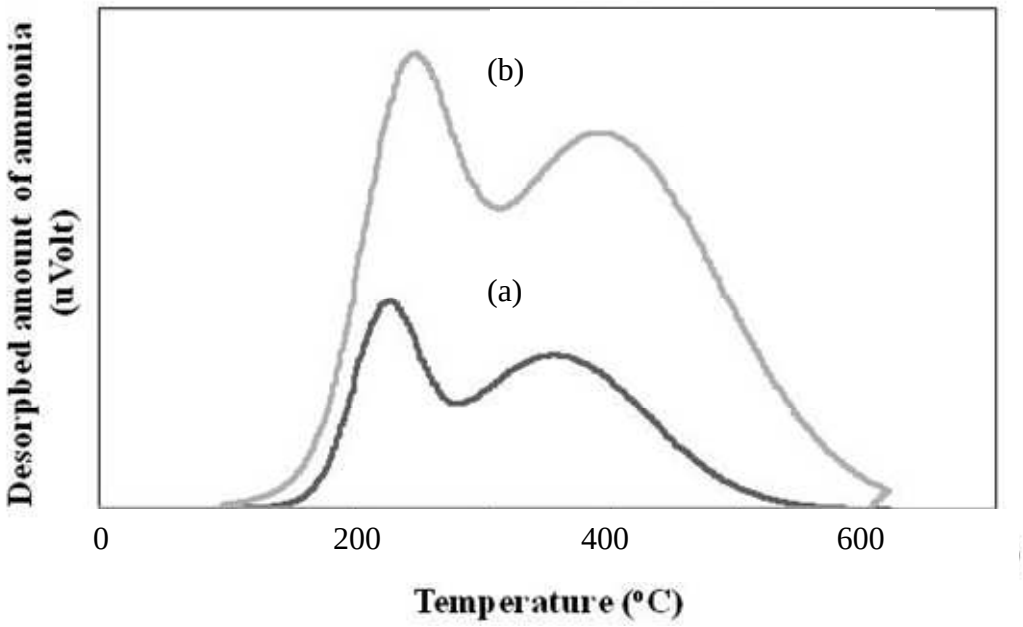

Figure A-6 NH_3-TPD profile of NaY-ART120-SO_3H (a), NaY-AMW2-SO_3H (b).

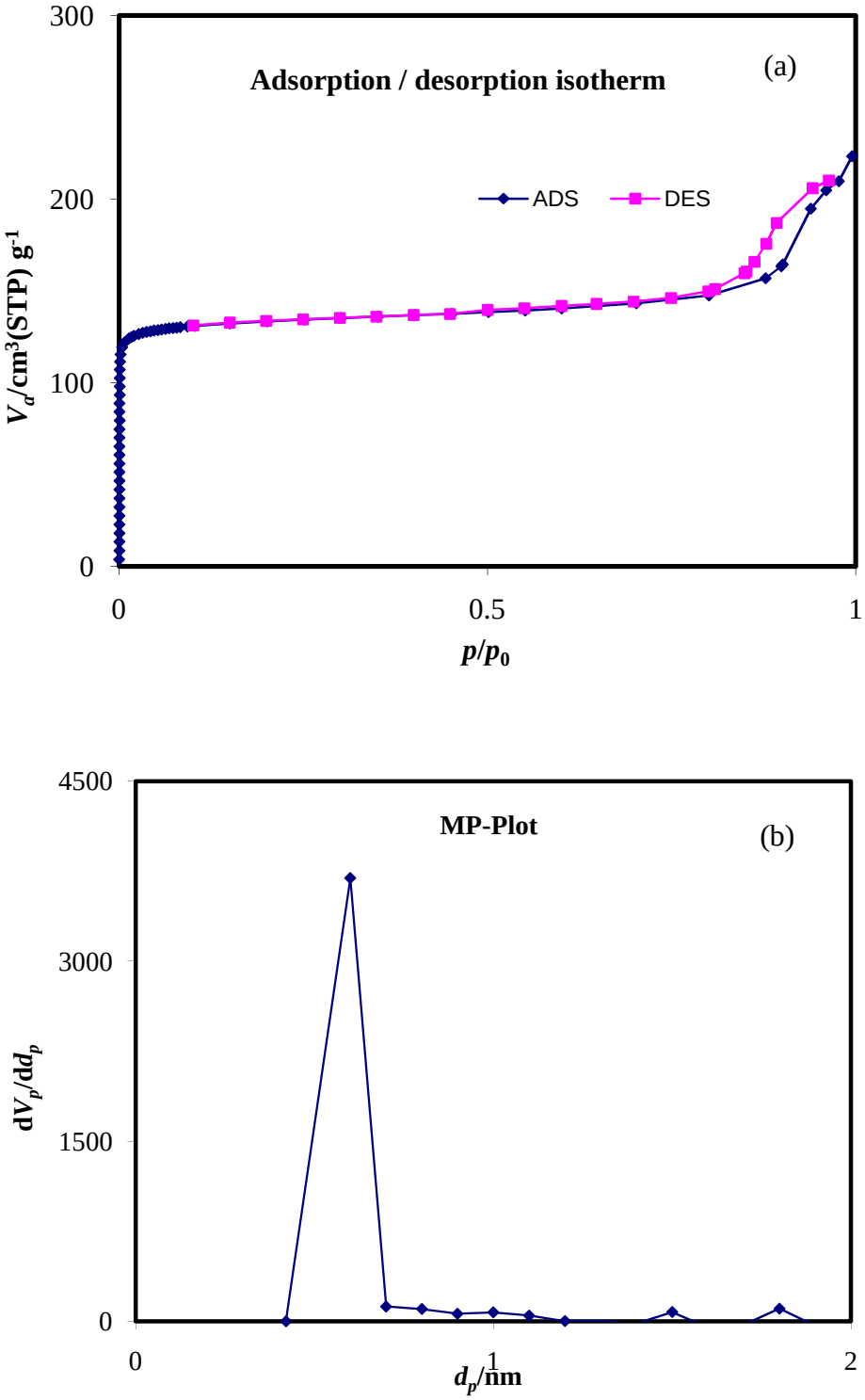

Figure A-7 N_2 adsorption-desorption isotherm (a) and pore size distribution (b) of synthesized X zeolite with hydrothermal method.

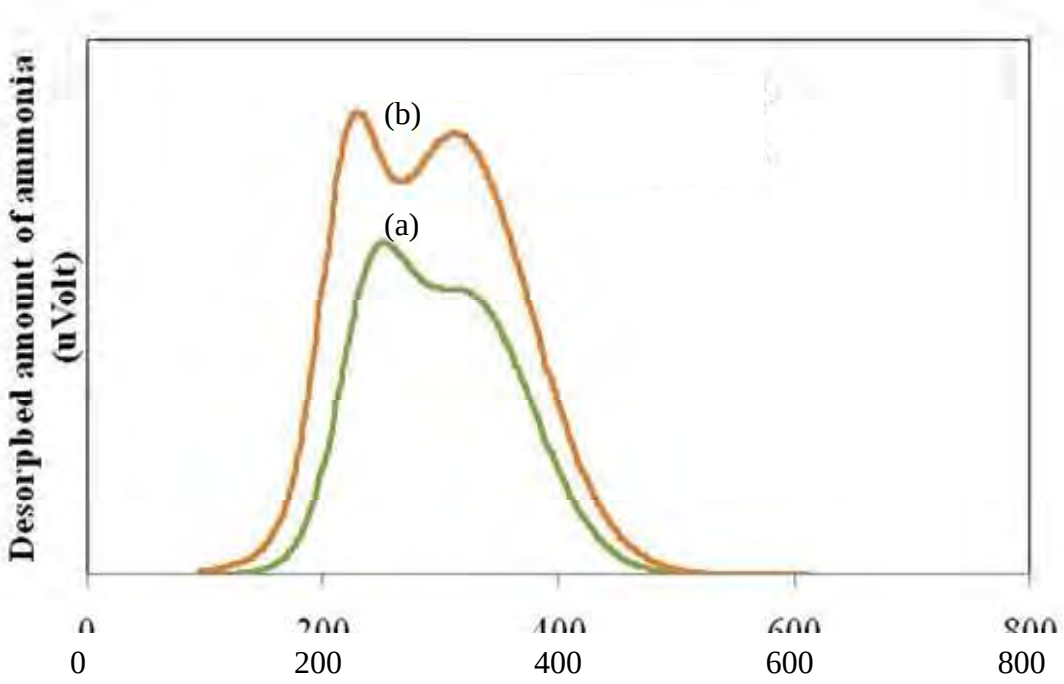

Figure A-8 NH_3-TPD profile of NaX-ART120-SO_3H (a), NaX-AMW0.5-SO_3H (b).

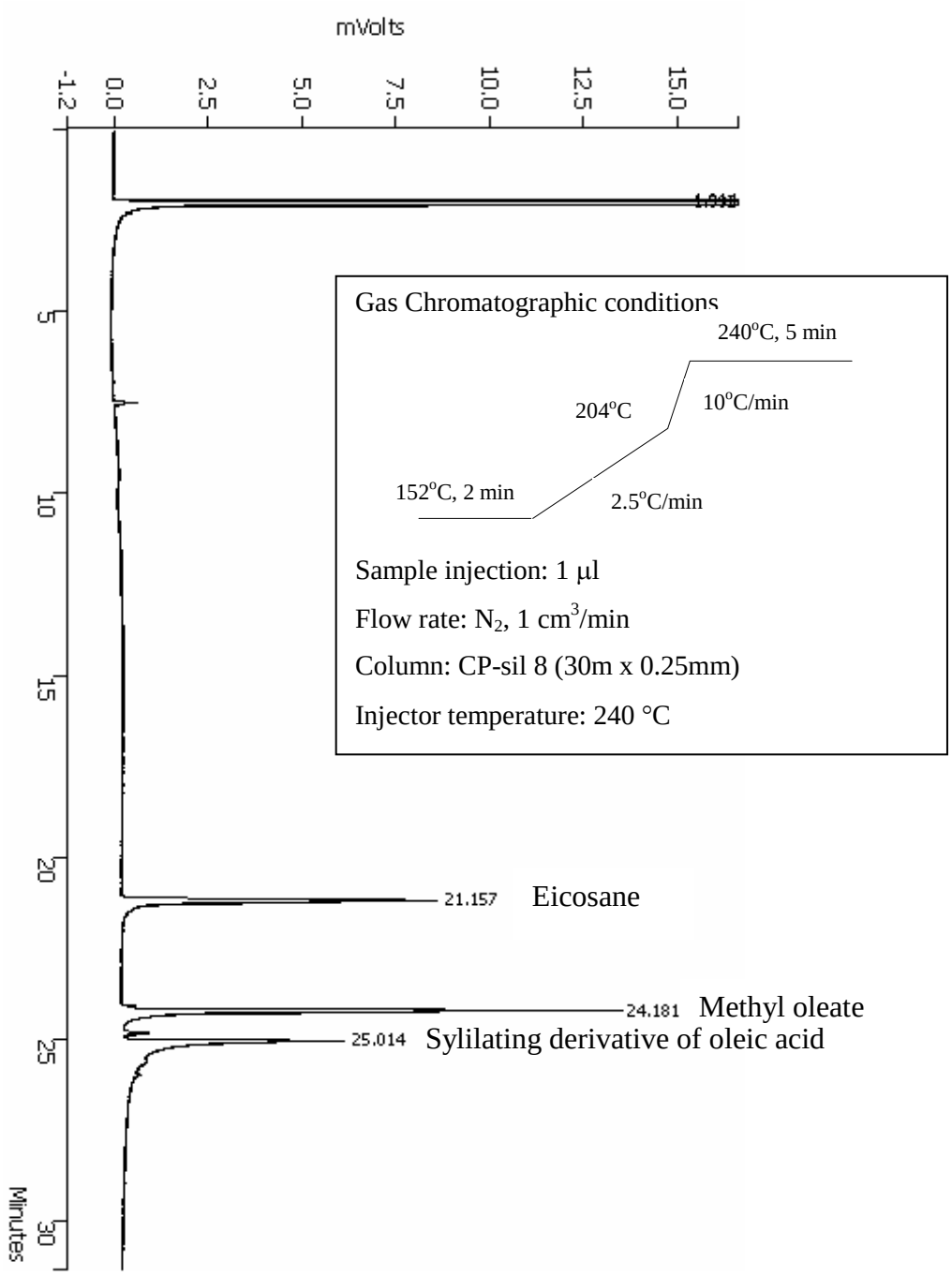

Figure A-9 GC chromatogram of methyl oleate product from esterification reaction**.**

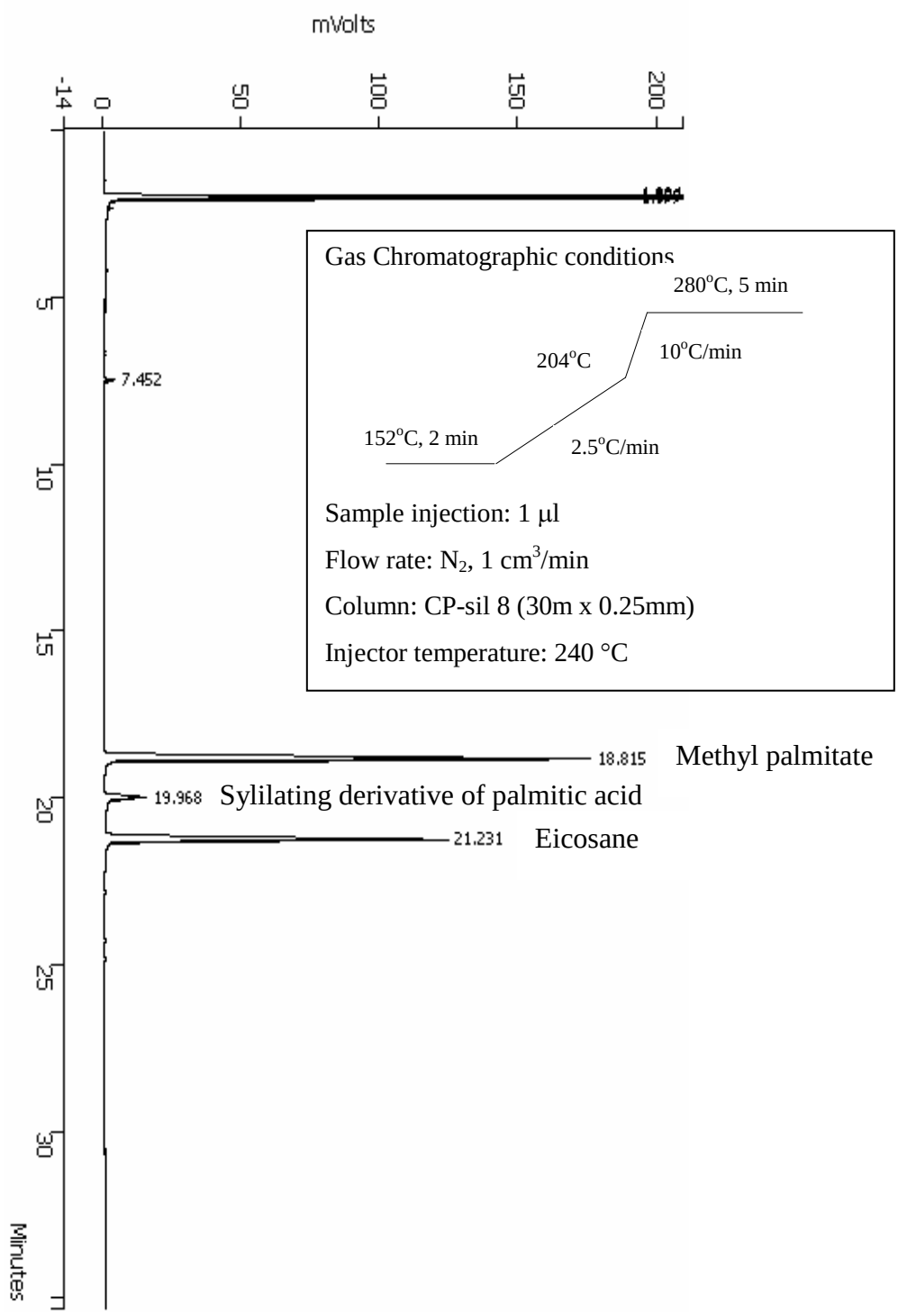

Figure A-10 GC chromatogram of methyl palmitate product from esterification reaction**.**

1. Standard solution and calibration solution

1.1 Methyl oleate standard solution

1.1.1 Stock standard solution 1.0 x 10^{-1} M

A 0.2965 g of methyl oleate was accurately weighed in a 10 mL volumetric flask and made up to the mark with tetrahydrofuran.

1.1.2 Working standard solution (0.05, 0.01, 0.005 and 0.001 M)

The working standard solutions were prepared by dilution of the stock standard solution using a pipette and then made up to the mark with tetrahydrofuran.

1.2 Methyl palmitate standard solution

1.2.1 Stock standard solution 1.0 x 10^{-1} M

A 0.2705 g of methyl palmitate was accurately weighed in a 10 mL volumetric flask and made up to the mark with tetrahydrofuran.

1.2.2 Working standard solution (0.05, 0.01, 0.005 and 0.001 M)

The working standard solutions were prepared by dilution of the stock standard solution using a pipette and then made up to the mark with tetrahydrofuran.

1.3 Standard calibration solution

Five calibration solutions were prepared into a series of vials. The weight 2.5 g of stock and working methyl oleate and methyl palmitate solutions were transferred into the five vials and added 0.5 g of internal standard 1.2 x 10^{-1} M eicosane stock solution to the five standard solutions. Then, a 1 μL of each reaction mixture was analyzed by GC technique under the condition described in Section 3.1.10. Preparation of calibration solution were listed in Table A-1 and A-2

Table A-1 Preparation of standard methyl oleate calibration solution.

Methyl oleate calibration solution	1	2	3	4	5
1.0 x 10^{-1}M (g)	2.50				
5.0 x 10^{-2}M (g)		2.50			
1.0 x 10^{-2}M (g)			2.50		
1.0 x 10^{-3}M (g)				2.50	
5.0 x 10^{-3}M (g)					2.50
Internal standard solution 1.2 x 10^{-1} M (g)	0.50	0.50	0.50	0.50	0.50

Table A-2 Preparation of standard methyl palmitic calibration solution.

Methyl palmitic calibration solution	1	2	3	4	5
1.0 x 10^{-1}M (g)	2.50				
5.0 x 10^{-2}M (g)		2.50			
1.0 x 10^{-2}M (g)			2.50		
1.0 x 10^{-3}M (g)				2.50	
5.0 x 10^{-3}M (g)					2.50
Internal standard solution 1.2 x 10^{-1} M (g)	0.50	0.50	0.50	0.50	0.50

2. Calibration function

The calibration function was given by the following expression, obtained from the experimental data using the linear regression method.

Linear regression equation: $Y = aX + b$

2.1 methyl oleate calibration function

$$M_{MO}/M_{eicosane} = a(A_{MO}/A_{eicosane}) + b$$

M_{MO} = the mass of methyl oleate (g)

$M_{eicosane}$ = the mass of internal standard (eicosane, g)

A_{MO} = the peak area of methyl oleate

$A_{eicosane}$ = the peak area of eicosane

In regression function X was represented by the term of $A_{MO}/A_{eicosane}$ while Y was $M_{MO}/M_{eicosane}$.

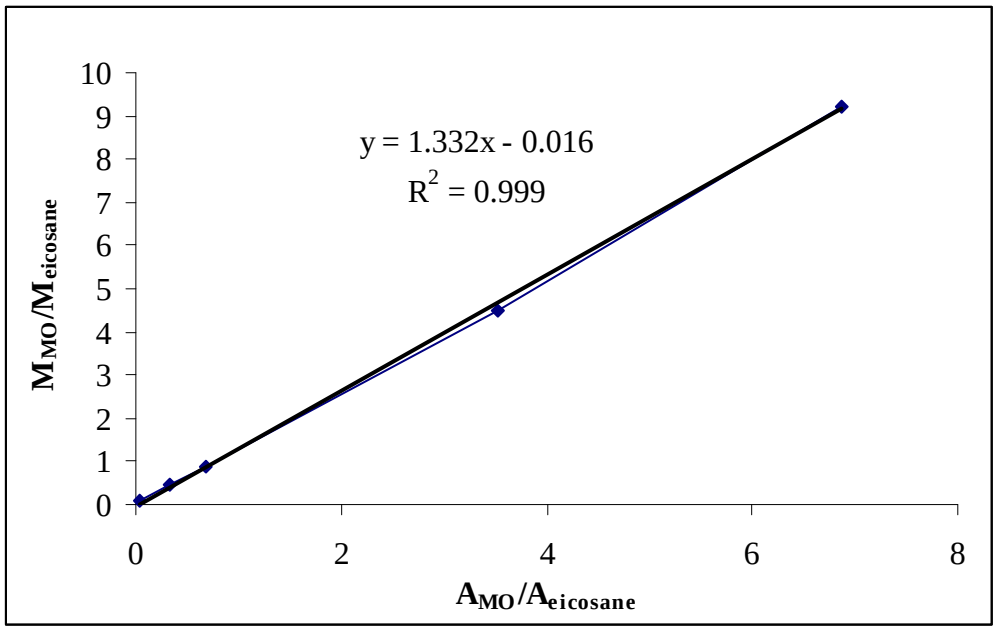

Figure A-11 Calibration curve of methyl oleate.

3. Calibration function

The calibration function was given by the following expression, obtained from the experimental data using the linear regression method.

Linear regression equation: $Y = aX + b$

3.1 methyl oleate calibration function

$$M_{MP}/M_{eicosane} = a(A_{MP}/A_{eicosane}) + b$$

M_{MP} = the mass of methyl palmitate (g)

$M_{eicosane}$ = the mass of internal standard (eicosane, g)

A_{MP} = the peak area of methyl palmitate

$A_{eicosane}$ = the peak area of eicosane

In regression function X was represented by the term of $A_{MP}/A_{eicosane}$ while Y was $M_{MP}/M_{eicosane}$.

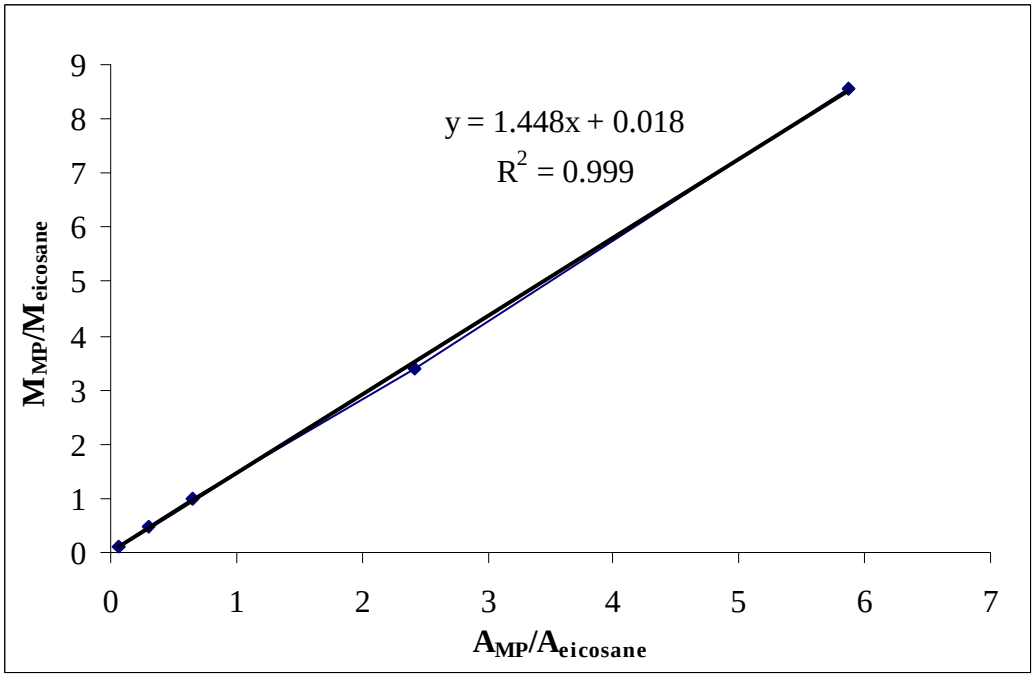

Figure A-12 Calibration curve of methyl palmitate.

VITAE

Miss Pijarin Rakmuang was born on September 25, 1984 in Nakhonsawan, Thailand. She received a Bachelor Degree of Science, major in Industrial Chemistry from King Mongkut's Institute Technology of North Bangkok in 2007. She worked at Modern Technology Component Co., Ltd for 4 months. Since 2008 she has been a graduate student in the program of Petrochemistry and Polymer Science, Faculty of Science, Chulalongkorn University and completed her Master of Science Degree in 2011.

In 5-7 January 2011, she participated in Pure and Applied Chemistry International Conference (PACCON2011) at Miracle Grand Convention Hotel, Bangkok, Thailand which had already been approved by proceeding and poster presentation in the title of "Synthesis of SBA-15 mesoporous material via microwave for esterification of oleic acid".

Her present address is 205/138 Soi. Sripornsawan T. Suanyai A. Muang Nontaburi, Thailand 11000.